POLITECNICO DI MILANO

Scuola di Ingegneria Industriale e dell'informazione
Corso di Laurea Magistrale in Materials Engineering and Nanotechnology
Dipartimento di Chimica, Materiali e Ingegneria Chimica "Giulio Natta"

BIOHYBRID ELECTROSPUN MEMBRANES AS BIOSENSING TOOLS

Relatore: Prof.ssa Chiara Bertarelli

Tesi di Laurea di:
Carlotta Tordelli Matr. 883669

Anno Accademico 2018/2019

Abstract

Biofunctional electrospun membranes show remarkable characteristics, such as high surface to volume ratio, which open to a variety of advanced technologies including biosensing.

In this study, poly(vinyl alcohol) (PVA)/ bovine serum albumin (BSA) nanofibers were produced by means of electrospinning followed by crosslinking with glutaraldehyde (GA) to make them stable when operate in water environment.

The characterization by using scanning electron microscopy (SEM) evidenced homogeneous and defect-free fibers with diameters of about 150 nm. The presence and the quantity of BSA at the fiber surface were determined by analysing the spectra obtained by Fourier Transform Infrared Spectroscopy (FTIR) and by performing the Bradford protein assay. Moreover, the efficient BSA bioactivity was demonstrated in chemical filtration, since this biohybrid membrane allows for binding several chemical species on the fibers surface, including non-steroidal antinfiammatory drugs or vitamins. Here, the immersion of the PVA-BSA membrane in a solution containing Atto 520-Biotin, led to a further decoration of the fibers to develop an optical biosensing platform. Specifically, this highly emissive membrane can be used as a probe for biomolecules, where the variation of the emission intensity could be related to the amount of the target to be detected. Accordingly, Photoluminescence (PL) and photoluminescence-excitation (PLE) spectra of the Biotin-decorated membrane were collected and high fluorescence quantum yields were measured. A preliminary binding test aimed at assessing possible future applications of fluorescent biotin functionalized fibers was carried out.

Abstract (italiano)

Le membrane biofunzionali elettrofilate presentano interessanti caratteristiche, come l'elevato rapporto superficie/volume, che possono essere sfruttate nello sviluppo di tecnologie avanzate, compresa la biosensoristica.

Nel presente studio, sono state prodotte nanofibre di alcool polivinilico (PVA) e sieroalbumina bovina (BSA) tramite la tecnica di electrospinning seguita da una reticolazione con glutaraldeide (GA) per renderle stabili ed adatte ad operare in ambiente acquoso, che è l'ambiente di riferimento in campo medico/biologico.

La caratterizzazione tramite microscopia a scansione elettronica (SEM) ha evidenziato la produzione di fibre omogenee e prive di difetti caratterizzate da diametri di circa 150 nm. La presenza e la quantità di BSA sulla superficie delle fibre sono evidenziate analizzando gli spettri ottenuti tramite spettroscopia infrarossa a trasformata di Fourier (FTIR) ed eseguendo un'analisi colorimetrica tramite il saggio di Bradford.

In particolare, l'efficiente bioattività della BSA è stata dimostrata nella filtrazione chimica: infatti questa membrana bioibrida permette di legare sulla superficie delle fibre un'ampia gamma di specie chimiche, compresi farmaci antinfiammatori non steroidei o vitamine. Nel presente progetto, l'immersione della membrana di PVA-BSA in una soluzione contenente Atto 520-Biotina, ha portato a una ulteriore funzionalizzazione delle fibre che consente di sviluppare una piattaforma per biosensori ottici. Specificatamente, questa membrana molto emissiva può essere utilizzata come sonda per biomolecole, dove la variazione dell'intensità di emissione può essere legata alla quantità di target da individuare. Di conseguenza, gli spettri di fotoluminescenza (PL) e fotoluminescenza eccitata (PLE) della membrana decorata con la Biotina, sono stati registrati e alti valori di efficienza di fluorescenza sono stati

misurati. Infine, un test preliminare volto a valutare possibili future applicazioni delle fibre funzionalizzate con la biotina fluorescente, è stato eseguito.

Table of Contents

List of Figures

List of Tables

Introduction

Nanotechnology is the study of materials at the nanoscale. It is one of the rapidly growing scientific disciplines due to its enormous potential in creating materials suitable for advanced applications. The use of nanotechnology in medicine and biomedical field is a significant example of progress in disease diagnosis, drug design and delivery, discovery of biomarkers, tissues and implants engineering. This requires designing nanotools able to fulfill the gap between the lacks of technological advancements and their possible applications in monitoring, preventing and controlling diseases. Electrospinning has been found to be an effective technique able to partially fill this gap allowing for the continuous production of highly functional polymer nanofibers and membranes with diameters in nanometer range. The relatively simple set-up required for electrospinning and the electrospun fibers properties and morphology make nanofibrous membranes suitable for a wide range of real life applications; among these, biosensing will be considered (Chapter 1).

The present work starts from the production and characterization of biofunctionalized electrospun PVA (polyvinyl alcohol) and bovine serum albumin (BSA) nanofibers by means of SEM analysis (Chapter 2). In order to be employed in filtration of drugs and as biosensing tools for biomedical applications, membranes have to be crosslinked to achieve their water resistance. The immersion in a glutaraldehyde (GA) bath allows to crosslink both PVA and BSA (Chapter 3). The quantity and the presence of BSA on fibers surfaces were investigated performing the Bradford protein assay and FTIR analysis, respectively (Chapter 4).

Particularly, the ability of the spun membrane to interact and bind biomolecules has been tested with a fluorescent vitamin, the Atto 520-Biotin (Vitamin H or B8). The BSA/Biotin interaction allows for the immobilization of the vitamin onto the nanofibers surface by a simple filtration or immersion step and its subsequent quantification by UV-visible absorption spectroscopy (Chapter 5). The peculiar

optical properties of Atto 520-Biotin such as fluorescence emission efficiency, allow to further characterize its presence onto the fibers and determine its possible use in quenching tests. Hence, photoluminescence (PL) and photoluminescence-excitation (PLE) analyses were performed to collect emission and excitation spectra of both BSA and Biotin. In addition, to quantify the fluorescence efficiency of the biohybrid electrospun membranes, quantum yield measurements were registered. Finally, a preliminary application of Biotinylated electrospun nanofibers in a quenching test was investigated in order to assess the possible detection of other proteins or peptide sequences, such as Avidin, Streptavidin and specific epitopes (Chapter 5).

Chapter 1
Nanosensor Technology: Overview and Applications

Nanotechnology and nanomaterial represent a revolutionary opportunity for technological development. The world of nanomaterials (i.e. with at least one submicrometric dimension [1]) offers a wide range of intriguing systems with outstanding physical and chemical properties and characteristics; these materials include zero-dimensional nanoparticles, one-dimensional nanofibers and nanowires and two-dimensional nanolayers.

The development of nanoscale structures, which have unique features with respect to bulk materials, leads to the growth and the breakthrough of many research fields [2]; among these, nanosensing is one of the striking areas under investigation, aimed at the sensitive and selective detection of extremely small quantity of molecules and biomolecules.

Nanosensors are highly improved sensing systems with unique functionalities, which convey information at the nano-level to the macroscopic world. Generally, a nanosensor can be defined as a sensor fulfilling at least one of the following requisites: (i) the spatial confinement of the interaction with the object is on nanoscale, (ii) the sensitivity is in the nanoscale range or (iii) the size of the sensor is at the nanometer scale [3]. Because of the small size of the active nanostructure, nanosensors have higher surface-to-volume ratio (Figure 1.1), which leads to enhanced physical properties, e.g. unprecedented sensitivity, specificity and faster response time if compared to traditional macroscopic sensors. In biosensing, the greater specificity is a consequence of the fact that they operate at a similar scale as the natural biological

processes, where functionalization with chemical and biological molecules allows recognition events that generate detectable physical changes.

Nanosensors can be also integrated in macroscopic sensing device to generate a new class of devices called “intelligent sensors”, which enable simultaneous data processing, storage and analysis. These advanced sensors will provide high accuracy, ultra-high sensitivity, extreme specificity and real-time in vivo information with greater speed, having multiple-analyte options and requiring a smaller quantity of sample [4].

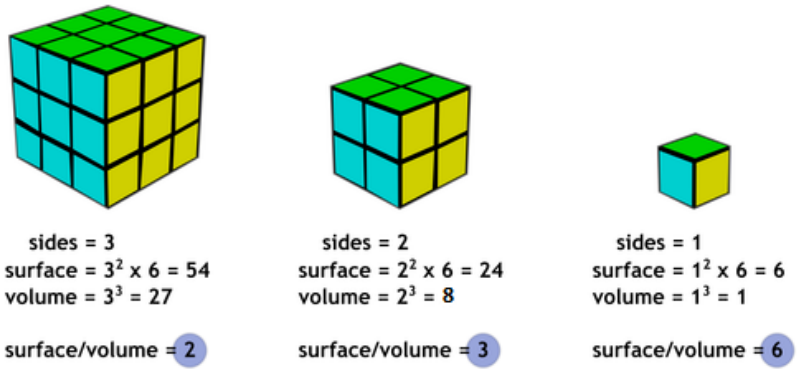

Figure 1.1- As the size of the cube gets smaller, the surface area-to-volume ratio strongly gets larger.

Despite the field of application, nanosensors typically work with electrical output signals: conductimetric nanosensors detect resistance changes in nanomaterials upon interaction or binding with an analyte; mechanical nanosensors work similarly to the electrical ones since they can detect a capacitance variation caused by a physical change; optical nanosensors exploit the sensitivity of fluorescence or changes in color to make quantitative measurements of a target analyte concentration. Biosensors generate a measurable signal proportional to the concentration of a target biocompound [5-8]. The ultimate goal of nanobiosensors is the early diagnosis through the detection of any biochemical species and biophysical event associated with a specific disease, ideally at the level of a single molecule or cell. This technology would revolutionize conventional medical practices by enabling not only early diagnosis of chronic debilitating diseases, but also ultrasensitive detection of

pathogens, and long-term monitoring of patients using biocompatible integrated medical instrumentation [9]. Research in nanobiosensing technologies over the years has opened to possible advancements in biomedicine. In fact, since 1962 (i.e. first generation biosensor by Clark and Lyons [10]), biosensors have been intensively studied and extensively utilized in various applications, ranging from medical diagnostics (Figure 1.2) and environmental monitoring to homeland security and food industry [11-13]. Nevertheless, there are many other fields of application of nanosensors including aerospace, national security, integrated circuits and agriculture.

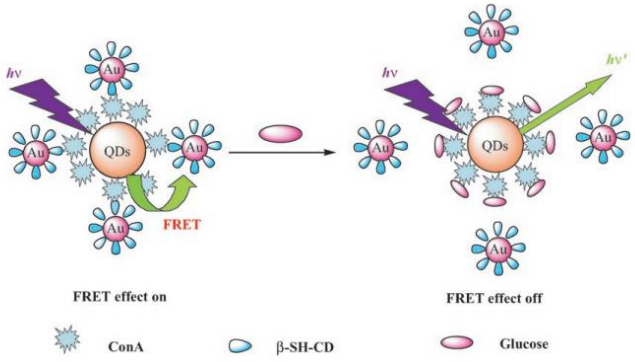

Figure 1.2 - Chemical structure of the QDs-ConA-b-CDs-AuNPs nanobiosensor for diabetes monitoring using glucose sensing and schematic illustration of its FRET-based operating principles [14].

Among all the possible uses and types of nanosensors, bionanosensors applied to biomedicine, especially to early disease diagnosis, are the future goal of the present work.

1.1 Nanobiosensors in Disease Diagnosis

Over the last decade, an increasing number of studies have focused on development of biosensing technology for the detection of several human health-related conditions. More specifically, the ability to detect disease-associated biomolecules, such as disease-specific metabolites, nucleic acids, proteins and cells such as circulating tumor cells, has become essential not only for disease diagnosis in the clinical setting

but also for biomedical research dealing with drug discovery and design. Cancers, cardiovascular diseases, diabetes and infections are some of the most striking challenges under investigation; notably, the growing interest in nanobiosensor technology has led to huge advances in noninvasive and effective early detection of cancer [15] [16]. Monitoring human health for early detection of disease conditions is essential to allow successful treatment and recovery in patients; since many biomolecules help determine the physiological state of a disease condition [17], there is an ongoing need for rapid analysis and active continuous monitoring systems able to detect biomarkers (i.e. RNA products, proteins or other metabolites [18]). Nanobiosensors may fulfill these multiple requirements. Biosensors are generally composed of three elements: the biologically sensitive element, the transducer or detector element and the reader device. The working principle consists of binding bioanalytes of interest onto the bioreceptor, which in turn modulates the physiochemical signal associated with the binding. Afterwards, the transducer converts the physiochemical signal usually into an electrical one. Any variation in signal such as electrical potential, conductance, mass, temperature and intensity of electromagnetic radiation, quantifies the presence or absence of bioagents (Figure 1.3) [19].

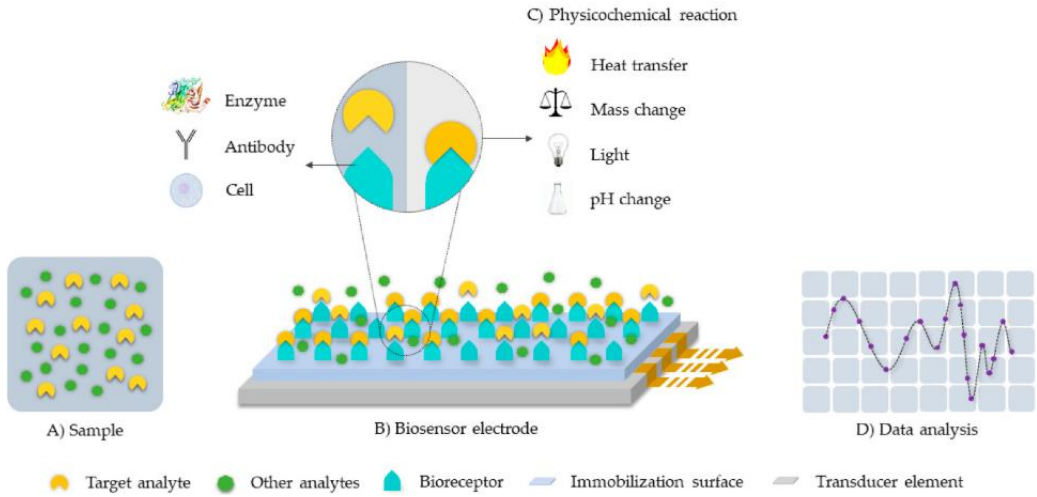

Figure 1.3 – Scheme of a typical biosensor system architecture: A) Sample; B) Biosensor electrode composed by bioreceptor, immobilization surface and the transducer element; C) Physicochemical reaction; D) Data analysis [20].

In order to develop an appropriate biosensor strategy to detect cancer, a specific biomarker or an array of biomarkers (i.e. genes and genetic variations, differences in messenger RNA (mRNA) and/or protein expression, posttranslational modifications of proteins, and metabolite levels [21]) have to be identified to ensure specificity of the device; for this purpose, optimal recognition materials (i.e. antibodies, aptamers, enzymes, nucleic acids and proteins [22]) must be used as receptor molecule [23]. Therefore, nanobiosensors can offer ultrasensitivity and specificity in biomarkers detection, also at low concentrations, which are typical in the early stage of diseases. Different systems have been developed based on a range of transducers, such as optical-based quantum dot (Figure 1.4), fiber biosensors and electrochemical-based biosensors.

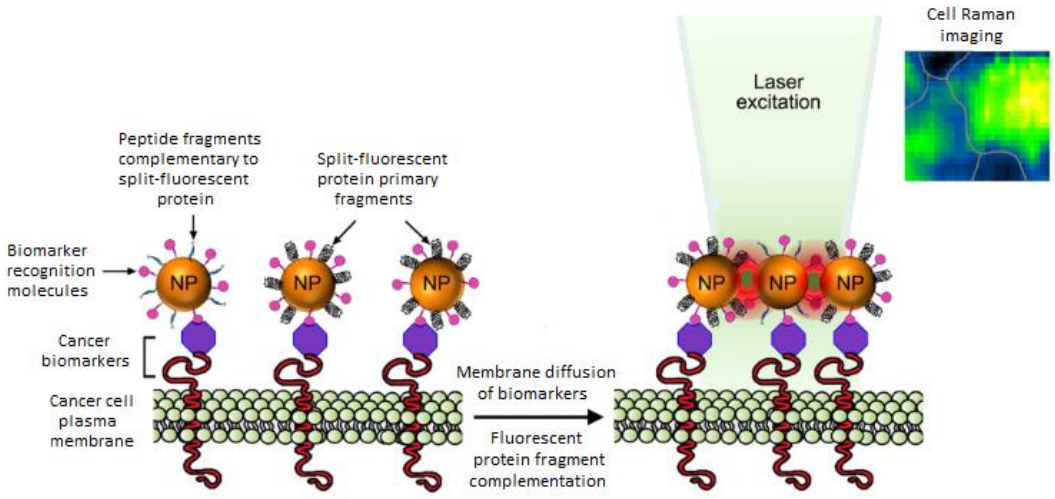

Figure 1.4 – Functionalized nanoparticles as probes for highly selective cancer cells detection over conventional cells by SERS imaging of the fluorescent protein chromophore Raman signature [24].

Further development of these nanosystems and nanoarray devices, the use of novel multi–biomarker sensing and the improved transduction mechanisms will play a significant role in molecular diagnostics by proving early and rapid diagnosis, decreasing the sample volume required and improving the currently available detection methods.

1.2 Fluorescent Biosensors

Fluorescence-based biosensors include a large set of tools, which are useful for fundamental studies as well as for applications in biomedicine, drug discovery and biotechnology. These tools have been designed and engineered over the last decade thanks to the combined efforts of chemists and biologists, and they have been developed hand in hand together with imaging technologies [25]. In particular, the development of genetically-encoded autofluorescent proteins and vitamins and the design of small synthetic probes with exceptional photo-physical properties have pushed the development of fluorescent biosensors that can report on the relative abundance and dynamic behaviour of biomolecules in real-time. Their high-resolution imaging and real-time measurements are expected to improve early cancer detection and to provide better means of determining cancer origin, stage and grade. Hence, although cancer represents the leading cause of death worldwide, its burden could be largely reduced through implementation of diagnostic approaches for early detection and strategies to monitor disease progression and response to treatment [26] [27].

Fluorescent biosensors consist of a peptide, protein or polymeric scaffold, which can recognize a biomolecular target or biomarker and report on this recognition event through measurable variations in fluorescent probes' spectral properties. Specifically, fluorescent probes are genetically, chemically or enzymatically coupled to the scaffold through a receptor which identifies a specific analyte or target, and consequently transduces a measurable and detectable fluorescence signal (Figure 1.5) [28].

(A)

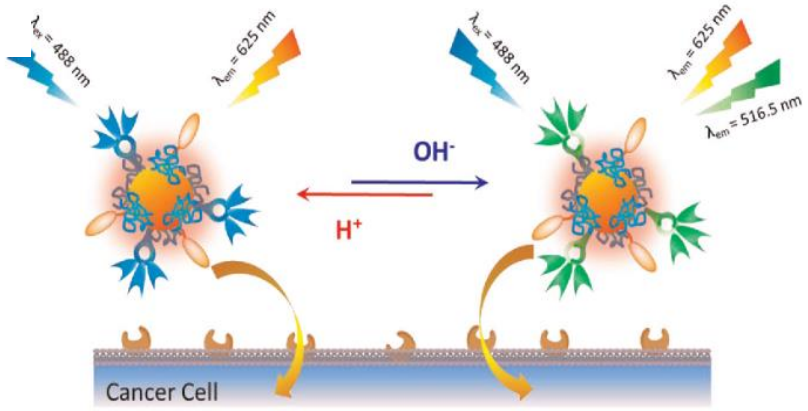

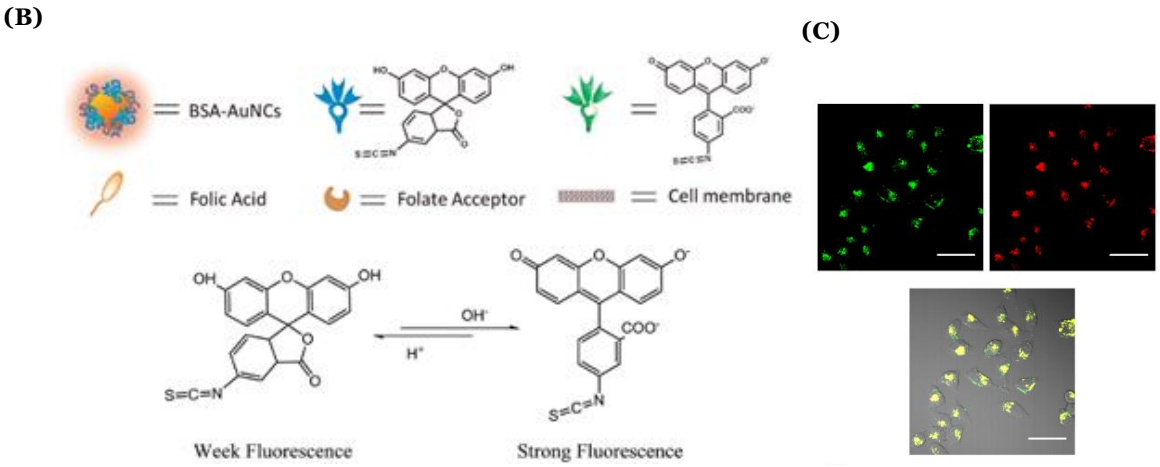

Figure 1.5 – A) Working principle of the developed folic acid-fluorescein-isothiocyanate AuNC fluorescent biosensor for PH detection and cancer cell-targeted imaging; B) Reaction scheme of FITC with H^+ and OH^-; C) Confocal fluorescence image of FGreen (510-550 nm), FRed (580-680 nm) and overlapped fluorescence and bright field image of Hela Cells incubated with FA-FITC-AuNC excited by 488 nm [29].

This fluorescence emission is the result of a three-stage process that occurs in specific molecules called fluorophores or fluorescent dyes (i.e. a fluorescent probe is a fluorophore designed to respond to a specific stimulus). The first step is the excitation: a photon of energy $h\nu_{ex}$ is supplied by an external source and absorbed by the fluorophore, creating an excited electronic singlet state (S1'). The second step concerns the excited-state lifetime: the excited state exists for a finite time (typically 1–10 nanoseconds). During this time, the fluorophore undergoes conformational changes and is also subject to a multitude of possible interactions with the molecular environment. Finally, the third step is the fluorescence emission: a photon of energy $h\nu_{em}$ is emitted, returning the fluorophore to its ground state S_0. Due to energy dissipation during the excited-state lifetime, the energy of this photon is lower, and therefore of longer wavelength, than the excitation photon $h\nu_{ex}$ (Figure 1.6) [30].

The first two steps have important consequences. First, the energy of S_1' is partially dissipated, yielding a relaxed singlet excited state (S_1) from which fluorescence emission originates. Second, not all the molecules initially excited by absorption (Step

1) return to the ground state (S_0) by fluorescence emission. Other processes such as collisional quenching, fluorescence resonance energy transfer (FRET) and intersystem crossing may also depopulate S_1. The fluorescence quantum yield, which is the ratio of the number of fluorescence photons emitted (Step 3) to the number of photons absorbed (Step 1), is a measure of the relative extent to which these processes occur.

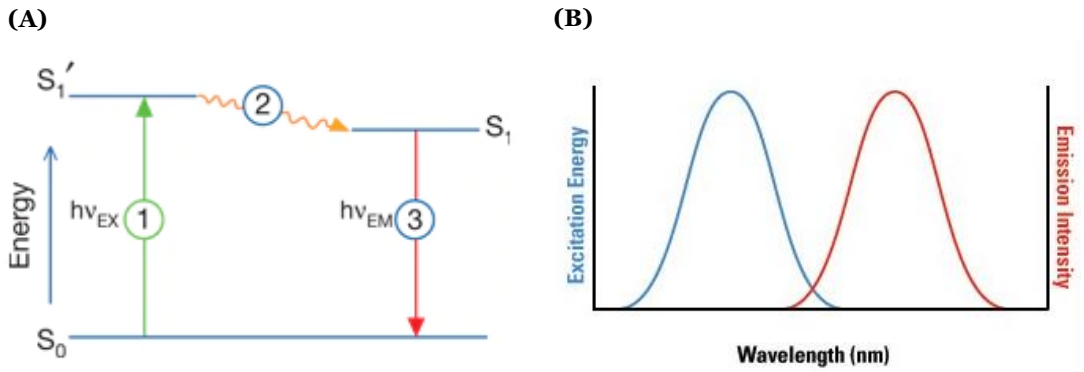

Figure 1.6 – A) Jablonski energy diagram of fluorescence; B) Excitation and emission spectra.

According to this working principle and thanks to the high selectivity provided by ligand-binding biomolecules, fluorescence-based biosensors can probe ions, metabolites and protein biomarkers with great sensitivity. They can also report on the presence, activity or status of the target in complex solutions (i.e. serum, cell extracts). With recent advances in nanomaterials, new strategies are emerging to design novel optical biosensor platforms. These materials can lead to significant improvement in performance of sensors in terms of sensitivity, selectivity, multiplex detection capability and portability [31]. In particular, nanofibers obtained by electrospinning, compared with other nanomaterials, can be applied in optical sensors with several advantages including easy fabrication and functionalization, low cost, easy detection and customized properties, such as chemical composition, structure, morphology, porosity and diameter [32] [33].

1.3 Fibers Production Method: Electrospinning

In the midst of nanomaterials, nanofibers stand out because of their high surface area-to-volume ratio and their enormous potential applications. Nanofibers, which belong to one-dimensional nanomaterials, are characterized by a macroscopic dimension, the length, and by a diameter in the submicrometric range (i.e. from few nanometers up to hundreds of nanometers) [34].

Nanofibers are most commonly produced through electrospinning, which has emerged as a very powerful method combining efficiency, versatility and low cost to elaborate scalable ordered and complex nanofibrous assemblies from a variety of polymers. Hence, electrospinning is a highly adaptable technique used to process solutions into continuous fibers with diameters ranging from few micrometers to few nanometers [35] [36].

The electrospinning set-up consists of four main components: a high voltage power supply, a syringe pump, a metallic needle, which acts as one of the electrodes and a collector (i.e. the counter-electrode). In a typical process, the syringe containing the polymeric solution is placed on an injection pump, which allows its constant flow through the fine metallic needle orifice at a controlled feed rate. Voltage is applied between the droplet of polymer solution held at the end of the capillary tube and the grounded target; as a consequence, the accumulation of electrostatic charge on the surface of the budding polymer droplet induces its geometry shape variation from quasi-spherical to the typical “Taylor cone”. Increasing the charging on the droplet, repulsive electric forces overcome the surface tension of the polymer solution resulting in a fine jet ejection towards the grounded metallic collector fixed at an arbitrary distance (Figure 1.7) [37-39].

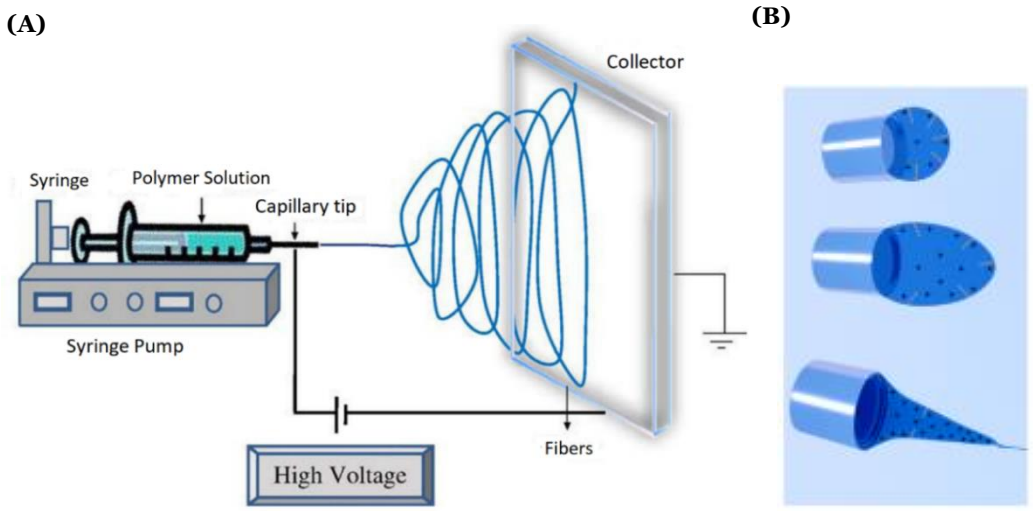

Figure 1.7 – (A) Schematic representation of an electrospinning system in a horizontal configuration; (B) Forces acting on the tip during the formation of the Taylor cone.

Initially, the polymer jet flows straightfully for about 1 cm. Then, during the flight to the collector, it would be influenced by instabilities (i.e. axisymmetric Plateau-Rayleigh instability and the bending or whipping instability [40]). They cause the elongation of the jet with a complex path during which the residual solvent evaporates leaving the charged polymer fiber onto the collector, forming a nonwoven mat.

The experimental parameters set during electrospinning and the solution properties affect the diameter size, the morphology and the composition of deposited nanofibers. Depending on these characteristics and on the versatility of electrospinning, nanofibers and nanomats can be used in a variety of fields and applications such as biomedicine, filtration, nanosensors and electronics [41] [42]; electrospun fiber based not only on polymers but also on metals, ceramics, organic/organic, organic/inorganic as well as inorganic/inorganic composite systems further improve the fields of applications [43].

1.3.1 Relevance of Experimental Parameters in Electrospinning

The morphology of electrospun nanofibers has a key role in their final chemical and physical properties, and it is mainly ruled by the experimental parameters. As a consequence, despite the relatively simple set-up of electrospinning, the production of desired nanofibers requires the appropriate selection and optimization of many operational variables (Table 1.1). It is not always easy to predict and generalize the dependence of nanofibers characteristics on these parameters since they actually depend on the polymer/solvent pairs used and the occurrence of instabilities phenomena during the process.

Environmental Parameters	Process Parameters	Solution Properties
Relative Humidity	Needle Size	Viscosity
Temperature	Applied Voltage	Polymer Mw
Pressure	Feed Rate	Solvent Viscosity
	Collector Distance	Surface Tension
	Collector Type	Concentration
		Conductivity

Table 1.1 – List of the most striking parameters influencing the electrospinning process and nanofibers morphology.

Given a certain polymer, there are several parameters that can affect the resulting fiber morphology, e.g. continuous and defect-free fibers, beaded fibers, circular vs bone-section fibers and porous fibers (Figure 1.8). Therefore, to gain a better understanding of the electrospinning technique and fabrication of polymeric

nanofibers, it is essential to thoroughly understand the effects of these parameters. As reported in Table 1.1, these factors are classified as electrospinning or process parameters, solution and environmental parameters.

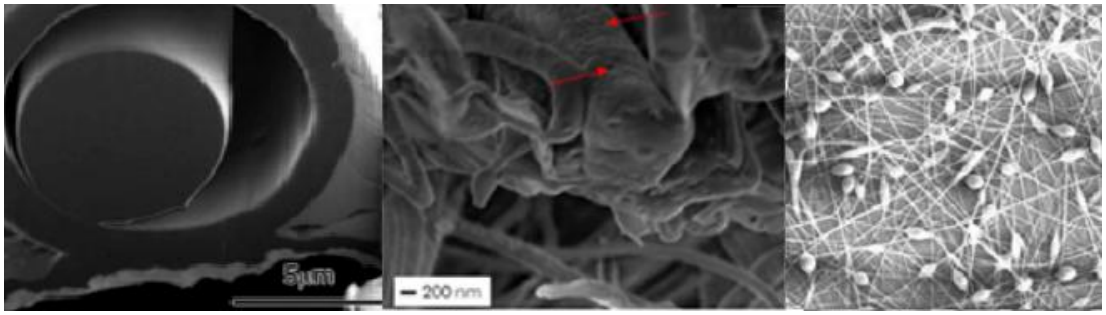

Figure 1.8 – Examples of nanofibers morphologies: core-sheath structure (on the left); porous nanofibers (in the middle) and beaded fibers (on the right) [38].

The flow of current from a high-voltage power supply into a solution causes a spherical droplet deformation into a Taylor cone and the production of ultrafine nanofibers in a critical voltage range. This critical interval varies from polymer to polymer. In electrospinning, the possible formation of smaller-diameter nanofibers with an increase in the applied voltage is due to the stretching of the polymer solution in correlation with the charge repulsion within the polymer jet interacting with the external electric field. On one side, an increase beyond the maximum threshold will result in the formation of beaded nanofibers and the growth of diameters. These consequences are mainly related to the decrease in size of the Taylor cone and the increase in jet length and velocity for the same flow rate. On the other side, a decrease below the critical range hinders the electrospinning. However, its effect on the diameter of electrospun fibers varies, as both expansion and reduction of fibers size with voltage increase have been reported [38] [44].

At the same time, also the flow rate of the polymeric solution through the needle tip determines the morphology of electrospun nanofibers. As in case of applied voltage, uniform beads-free nanofibers could be prepared maintaining the flow rate below a critical value, which depends on the polymer/solvent pair used. In this range, the higher the flow rate, the larger the fiber diameter. Over a threshold value not only

beads are generated due to incomplete drying of the nanofiber jet during the flight towards the collector, but also ribbon-like defects are formed or deposition of unspun droplets can occur.

Similarly to the applied electric field and flow rate, the distance between the metallic needle tip and the collector affects the nanofiber deposition. Since the fibers morphology depends on the deposition time, evaporation rate and whipping or instability interval, a critical distance needs to be maintained. This allows preparing smooth and uniform electrospun nanofibers. Any changes on either side of the threshold distance affect the nanofibers morphology. For instance, when the distance is kept small, defective and large-diameter nanofibers are formed. Whereas, the diameter of the nanofibers decreases as the distance increases up to a tip-to collector distance reaches a threshold value above which the external electric field becomes too weak for the electrospinning to occur. Since the electrospinning procedure relies on the phenomenon of uniaxial stretching of a charged jet, the viscosity of a solution plays a fundamental role in determining its efficiency and the quality of final products. Control of this parameter is generally achieved by changing the polymer concentration or the molecular weight (Mw), since the latter is linked to viscosity through a power law [49]. Once the molecular weight is set, concentration becomes the main governing factor for viscosity. Viscosity of the feed polymer solution is fundamental to obtain a minimum amount of entanglements necessary to have a jet stabilization and beads-free fibers. By examining the total number of entanglements, it is possible to highlight three different regimes [45]:

- Diluted regime, for low concentrations and molecular weight;
- Semidilute/concentrated unentangled regime, for medium/high concentrations and molecular weights;
- Semidilute/concentrated entangled regime, for medium/high concentrations and high molecular weights.

Among these regimes, electrospinning requires the entangled one. In particular, a critical number of entanglements must be achieved in order to avoid formation of defective fibers (Figure 1.9).

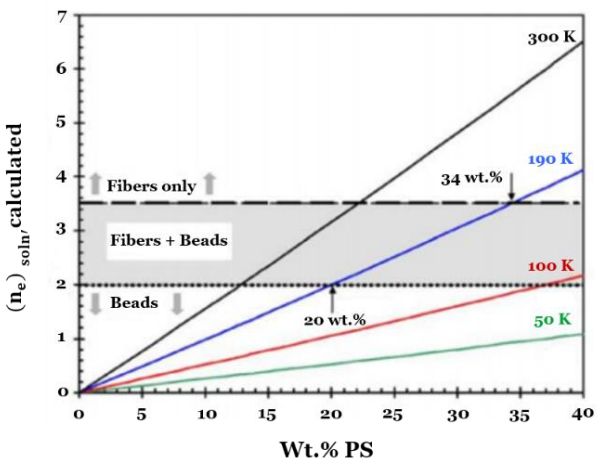

Figure 1.9 – A graph showing the effects of molecular weight and concentration on the morphology of polystyrene fibers, measured by entanglements number [46].

Several other experimental parameters influence the process (Table 1.1), even if their effect is less noteworthy or still not completely understood. Such is the case of the environmental parameters(i.e. relative humidity and temperature), which are usually kept constant. Relative humidity implies the existence of water molecules in vapor phase, which affect the evaporation rate of the solvent from polymeric solutions. In particular, at higher relative humidity the evaporation rate of the solvent decreases and consequently perturbs the ideal jet diameter during the trip to the collector. However, this phenomenon depends on the chemical nature of the polymer. A special case occurs for low boiling point solvent when relative humidity is high: the fast solvent evaporation from the jet during the flight generates a significant decrease of the temperature onto the fiber surface, which causes the condensation of the water vapour as small droplets, which lead to the formation of pores onto the fibers as a fingerprint of their final evaporation. Temperature can cause instead two opposing effects that change the average diameter size: (i) it increases the rate of evaporation of solvent and (iii) decreases the viscosity of the solution; both lead to decrease in the mean fiber diameter [48]. In conclusion, many parameters have to be optimized to achieve the desired outcomes. Moreover, each parameter is often dependent on the others, thus providing a complex system. Hence, a complete control over the process can be quite difficult and time consuming, as evidenced by Coles et al. who performed experiments to investigate the effect of several variables (addition of salt,

concentration, electrostatic potential and collection distance) on polymeric nanofibers [47]. They came to the conclusion that the interplay between variables had a relevant effect on the poly(lactic acid) and poly(vinyl alcohol) fibers spun, with diameters ranging from 0,16 to 5,29 μm, and deposition rate from 7,6 to 298 mg/h.

1.4 Electrospun fibers as Biosensors

As mentioned in previous sections, application of nanotechnology to nanosensors and biosensors gives rise to mainly novel approaches aimed at advancing new features that cannot be achieved exploiting conventional technologies in classic sensors [50]. In particular, nanofibers have become ideal candidates for the fabrication of nanobiosensors with extremely high sensitivity, selectivity and accuracy. These characteristics are due to (i) the interconnected pore network in nanofibrous mats, which allows easy access of the analytes to detection sites, (ii) the high surface-to-area ratio and (iii) the fiber surface functionalization to impart selectivity to chemical recognition. Although electrospun NF-based sensors reported in the literature mostly rely on electrochemical transduction, nanofibers are also suitable for optical biosensors (Figure 1.10).

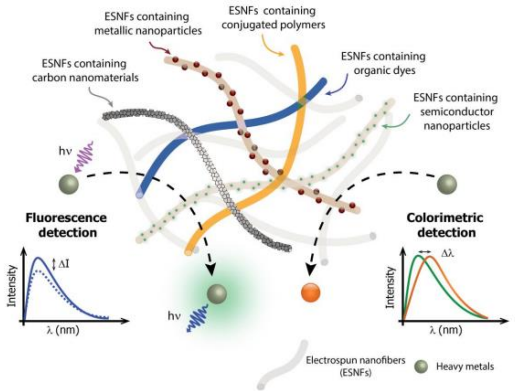

Figure 1.10 – Scheme of electrospun nanofibers (ESNFs) modified by distinct nanomaterials for application in optical sensors for heavy-metal detection. The principles of optical detection by fluorescence quenching (left) or by the color change (right) of the ESNFs in presence of the heavy metal ion are represented [51].

The bioreceptors can be immobilized onto the surface using various strategies, depending on the physical and chemical characteristics of both the recognition elements and the nanofibrous scaffolds, and on their interfacial interactions. The most common methods proposed to generate bioreceptor-NF hybrid assemblies consist in the decoration of biomolecules onto the fiber surface by covalent binding, physical and chemical sorption, cross-linking or entrapment in a membrane. They can be used to immobilize enzymes [52], antibodies [53], proteins and aptamers. Especially, in case of enzyme biosensors, the bioactive molecules can be embedded in NFs by electrospinning a blend of the polymer and enzymes [54]. An efficient immobilization can be achieve providing a favorable and inert environment for the biomolecules, i.e., it should not induce severe modifications in their native structure, which would compromise their biological activity (i.e. recognition capacities, reactivity and/or selectivity). From this point-of-view, hydrophilic polymers such as PVA and PEI are particularly well-suited and have been extensively used in immobilization strategies. However, in both cases polymer is soluble in water, which prevents to use the fibrous membrane in classical water or biological medium. Therefore, the resulting water-soluble NFs must be treated to avoid solubilization in aqueous phase [55]. Several signals can be produced as results of the target/receptor interactions, such as optical fluorescence, commonly used for its extremely low detection limits, fast response and high sensitivity. The peculiar properties of the electrospinning process allow for obtaining fluorescent fibers featuring typically improved optical properties compared to flat thin films, such as enhanced photoluminescence quantum yields and radiative rates, polarized emission and self-waveguiding of the emitted light. These properties, combined with a high surface area to volume ratio, make these nanostructured materials suitable for high performance optical sensing. Fluorescent electrospun fibers can be realized by embedding emissive systems (i.e. quantum dots, fluorescent dyes and bio-chromophores) in optically inert polymer matrices or by using light-emitting conjugated polymers (Figure 1.11) [56] [57].

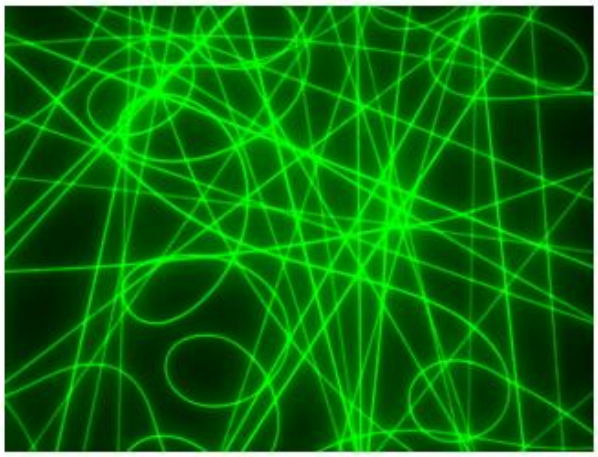

Figure 1.11 – Fluorescence microscope image of poly (ethylene oxazoline) nanofibers containing green fluorescent-labeled albumin molecules.

Electrospun nanofibers have drawn wide attention for optical biosensor development with the aim of rapid and sensitive detection of degenerative diseases such as cancer [58] and purification of water. In particular, the production of cost-effective, portable bioassays can improve the accessibility of health care, and lead towards custom medicine [59].

Chapter 2
Production of Biofunctional Nanofibers

Production of electrospun polymer nanofibers has received much attention because of their potential applications for biomedical devices, tissue engineering and drug delivery carriers. Depending on both the application and the suitable polymer, a process design has to be carefully performed considering solvent, concentration, possible additives and experimental conditions [60]. Not only for biomedical applications but also for any green process, water is the reference choice, as the solvent since it is nontoxic, cheap and easily accessible [48]; in addition, many biological molecules (i.e. B group vitamins, proteins and amino acids) have good solubility in water, which allows for electrospinning without degradation and denaturation [61]. Bioactive molecules can act as receptor in sensing devices. The immobilization of biomolecules onto the nanofibers surface is of great interest for biomedical applications, and it can be achieved by physical adsorption, covalent binding of e-spun membranes, by embedding the biomolecules into the feed polymer solution or by coaxial electrospinning, thus obtaining biofunctional nanofibrous scaffolds [62] [63]. Some examples are listed in Table 2.1.

Polymer	Biomolecule	Solvent	Reference
PEO or PVA	Lipase Enzyme	H2O	[64]
PVA	Alginate	H2O	[65]
PLGA and PLA/ PEG	DNA	DMF	[66]
PCL	BSA	CHCl3/H2O	[67]
PLCL	Heparin/Collagen	HFIP	[68]
PEOX	Albumin	H2O	[57]

Table 2.1 – Examples of electrospun synthetic polymers/biomolecules from the literature.

In addition to biomolecules, biological colloidal particles and other particulates can be also embedded in nanofibers via electrospinning. The encapsulation of biomolecules into a protective polymer matrix is a broadly useful way to preserve them from degradation [57]. When co-axial electrospinning is used, which consists in forming a charged jet from two different solutions, fed from an inner and outer needle, unusual fiber architectures can be obtained, with the active molecules localized onto specific sites, e.g. encapsulated inside the fiber beads or internally in core-sheath fibers [69].

Since any biomolecule has its own characteristics and may interact differently with the chemical environment, the polymer/biomolecule pair has to be carefully selected depending on the post-process treatments of the mat and its possible application. Electrospun fibers with a number of proteins including bovine serum albumin (BSA), green fluorescent protein, casein, silk, lysozyme and eggshell membrane protein have been reported [63]. In the present work, we develop a biohybrid membrane of PVA, containing BSA for biosensing applications.

2.1 Bovine Serum Albumin (BSA)

As the most frequent plasma protein, serum albumin constitutes more than 50% of the serum proteins in the healthy individuals. It has a key role in oncotic pressure maintenance in circulatory system and, unlike the several specialized transport proteins present in plasma, it is known as a versatile protein carrier for various endogenous and exogenous ligands. In particular, it can reversibly bind bilirubin, hormones, vitamins, drugs and fatty acids, keeping the latter ones in a soluble form inside the plasma. Moreover, serum albumin is considered a nobility biomarker for liver function synthesis, and also for several diseases, such as, inflammatory disorders, brain tumors, rheumatoid arthritis, myocardial ischemia, cancer, blood brain barrier (BBB) damage, cerebrovascular disease and cardiovascular risk disease [70] [71]. Since it can be used in a variety of applications, the interest of scientific community in albumin and its interaction with other species has grown over the last 25 years (Figure 2.1).

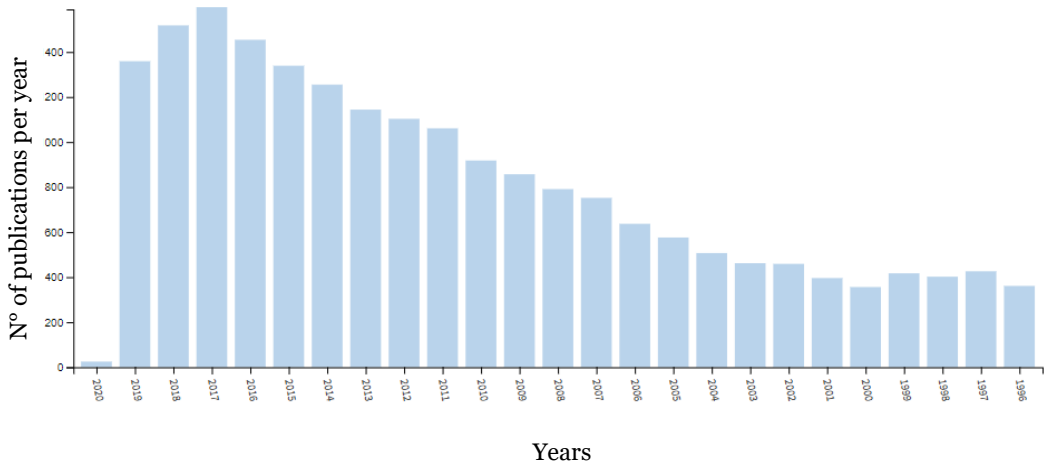

Figure 2.1 – Bar graph of the n° of publications per year in web of science starting from 1996, generated by searching "albumin interaction".

Human Serum Albumin (HSA) and Bovine Serum Albumin (BSA) are the two main types of albumin in existence. BSA and HSA are frequently used in biophysical and

biochemical studies since they have a similar folding, a well-known primary structure, and they have been associated with the binding of many different small molecules [72]. In particular, bovine serum albumin is widely used in research as a generic protein and it is commonly used as a model protein due to its medicinal importance, low cost, ready availability, stability, water solubility and structural similarity with human serum albumin. Indeed, BSA has a molecular weight of 66,430 kDa and contains 583 amino acids residues while, HAS's molecular weight is 69,3 kDa and the amount of amino acids residues is 585 [73] [74]; besides, the two proteins show approximately 76% sequence homology and since few years ago their configuration was assumed to be very similar, although the crystallographic structure of BSA had not been determined yet [75]. However, now it is possible to state that they both adopt a "heart-like" shape (Figure 2.2), composed of three structurally similar domains.

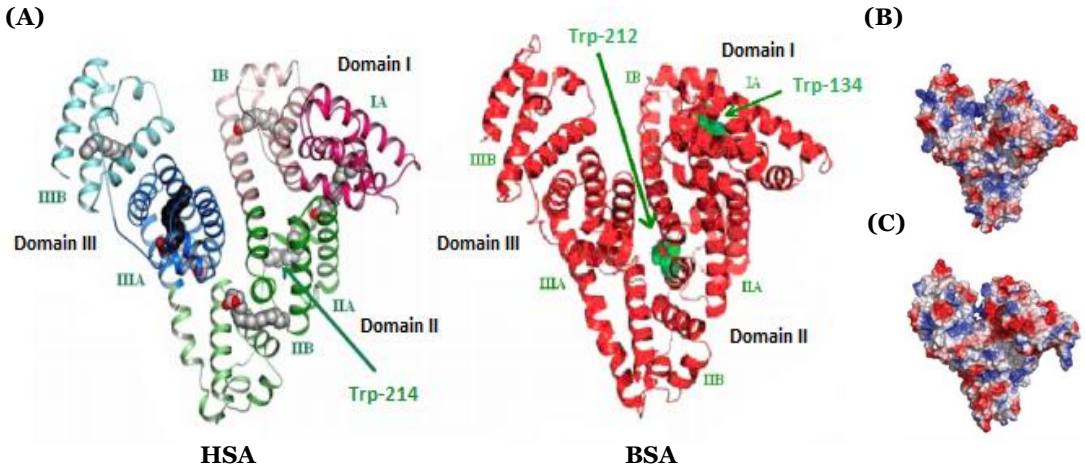

Figure 2.2 – On the left, (A) three-dimensional structures of HSA and BSA with domains and tryptophan residues in green; on the right heart-like shapes of (B) HSA and (C) BSA.

In Figure 2.2 the tryptophan residues of HSA (Trp-214) and BSA (Trp-134 and Trp-212) are also shown since they represent one of the main differences between the two proteins. While Trp-214 of HSA and Trp-212 of BSA are in similar positions, in a hydrophobic binding pocket, the second tryptophan of BSA, Trp-134, is located in proximity of the outer layer of the albumin protein, but buried in hydrophobic pocket of domain I. Despite of this dissimilarity, BSA is widely used in biomedical and

biochemical research instead of HSA [73]. The overall similarity between BSA and HSA has further increased the interest in its possible interaction with biomolecules and drugs such as biotin, ketoprofen, fluorescent probes, aspirin and oxaprozin-E [76] [77].

As for BSA functional fibrous membrane, bovine serum albumin alone has been tentatively electrospun or used to functionalize polymeric nanofibers surface. For example, *Dror et al.* (2008) obtained self -standing mats composed entirely of BSA by electrospinning directly a BSA solution (Figure 2.3) [77]. Control of the spinnability and the mechanical properties of the produced nanofibers, however, was achieved by manipulating the protein conformation, its aggregation and intra/intermolecular disulfide bonds exchange, by means of a complex solution formulation. Due to the strong manipulation of bovine albumin, it is reasonable to suppose that it would not be able to maintain its bioactivity, hence, its interaction with other molecules is reduced.

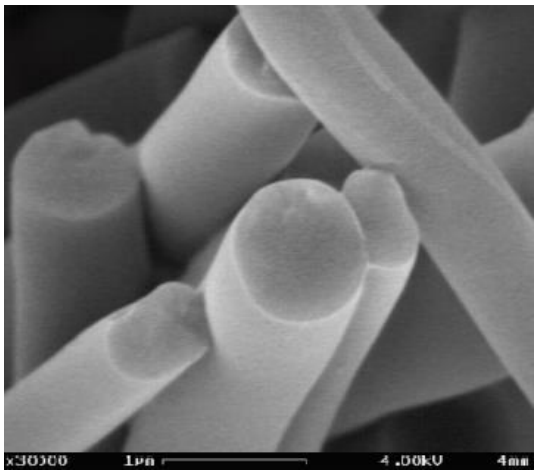

Figure 2.3 – SEM image of the cross-section of electrospun bovine serum albumin (BSA) fibers [77].

On the other side, the co-electrospinning process of two or more materials open very versatile methodology for encapsulation and release of bioactive agents. In particular, the blends of BSA and some polymers (i.e. PVA [78], PLGA [79], PEO [80] and PCL

[67]) have been used in electrospinning since they form quite simple feed solutions and allow to produce fibers with diameters in the range of few hundreds of nanometers (Figure 2.4).

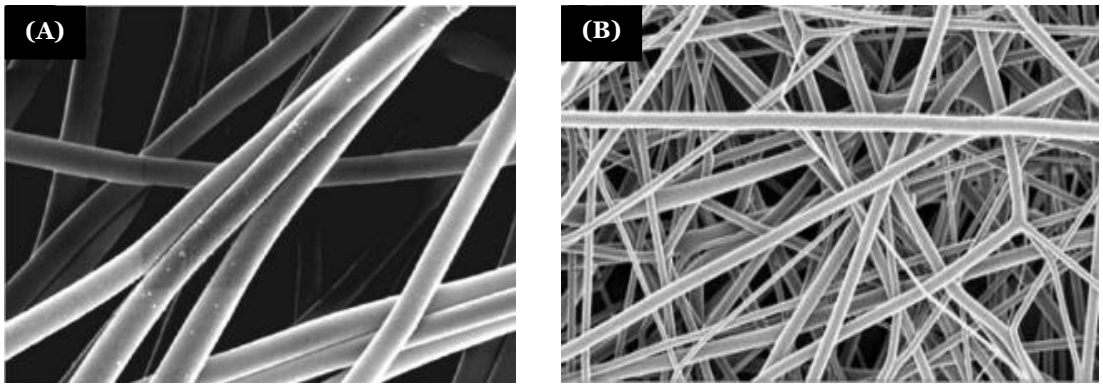

Figure 2.4 – Examples of BSA/polymer electrospun fibers; (A) BSA/PVA [78] and (B) BSA/PLGA [79].

Bovine serum albumin has been chosen in this study, as it is cost-effectiveness, commercially available, it has good stability and solubility in water.

2.2 Poly (vinyl alcohol) (PVA)

Biocompatibility and biodegradability are two of the main parameters that need to be taken into account in biomedical and environmental engineering applications. As a consequence, among all the possible polymers, which have been successfully blended with BSA, poly(vinyl alcohol) (PVA) has been selected. Moreover, PVA, which is a synthetic polymer that has been available for more than nine decades, is nontoxic, water-soluble, harmless, hydrophilic, low cost and inert in body fluids. The presence of hydroxyl groups enhances degradability through hydrolysis [81].

Poly(vinyl alcohol) is usually obtained from the hydrolysis of poly(vinyl acetate) upon the polymerization of vinyl acetate (Figure 2.5), affording polymers at different

hydrolysis degrees, which indicate the percentage of acetate groups that are converted into hydroxyl groups.

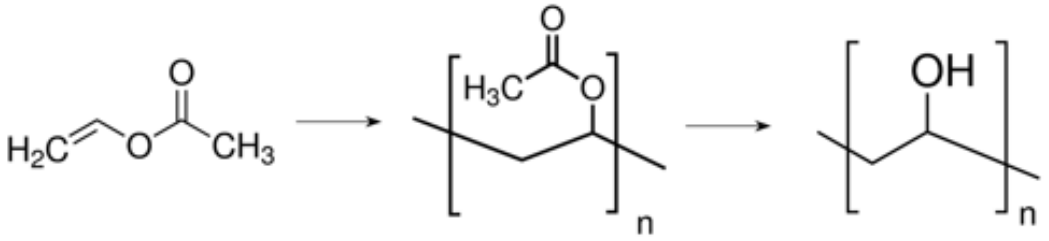

Vinyl Acetate **Poly (vinyl acetate)** **Poly (vinyl alcohol)**

Figure 2.5 – Chemical reactions for the synthesis of PVA: polymerization of vinyl acetate and subsequent hydrolysis of poly (vinyl acetate) to poly (vinyl alcohol).

In terms of hydrolysis degree, the main grades of PVA produced can be classified as fully hydrolyzed with a degree of hydrolysis ≥ 99% or partially hydrolyzed, which can be considered as the mixture of ethylene alcohol and ethylene acetate monomeric units. More specifically, the fully hydrolyzed PVA cannot be easily electrospun, due to the strong hydrogen bonding between intra- and intermolecular hydroxyl groups that greatly decrease its solubility in water [82]. Despite its lower solubility, fully hydrolyzed PVA is preferred over the partially hydrolyzed polymer to attain high degrees of crystallinity, which improve its water resistance [83]. Since PVA is water-soluble, the nanofibers obtained from its electrospinning cannot maintain their morphology when they come into contact with water; in fact, upon contact with an aqueous solution nanofibers and mats shrink and tend to dissolve. Water dissolution of the polymeric nanofibers hinders any possible application of PVA nanofibers in biosensing and filtration in aqueous environments.

Nevertheless, PVA is exploited as polymeric scaffold for BSA. Indeed, there are few examples of PVA/BSA fibers reported in literature [84] [85] [86]. An interesting feature of this blend is that the location of the protein within the fiber can be controlled by carefully selecting the electrospinning solution pH and the applied polarity of the electric field, since the pH affects the net charge on the protein. In particular, at the isoelectric point (i.e. pI) of BSA (pH 4.7-5.2) there is no net charge

on the protein, whereas above and below the isoelectric point, the protein carries a negative / positive charge. Hence, by electrospinning solutions at a pH above or below pI of BSA, the charged protein segregates towards the surface of the fibers, while a pH similar to pI allows to obtain a core-sheath configuration, in which BSA is located at the core of fibers due to electrophoretic forces [78]. Accordingly, the electrospinning from water solution of PVA and BSA is expected to give a surface distribution of the protein, which would maximize the bioactive surface of electrospun fibers [87]. An example of core-sheath architecture is shown in Figure 2.6.

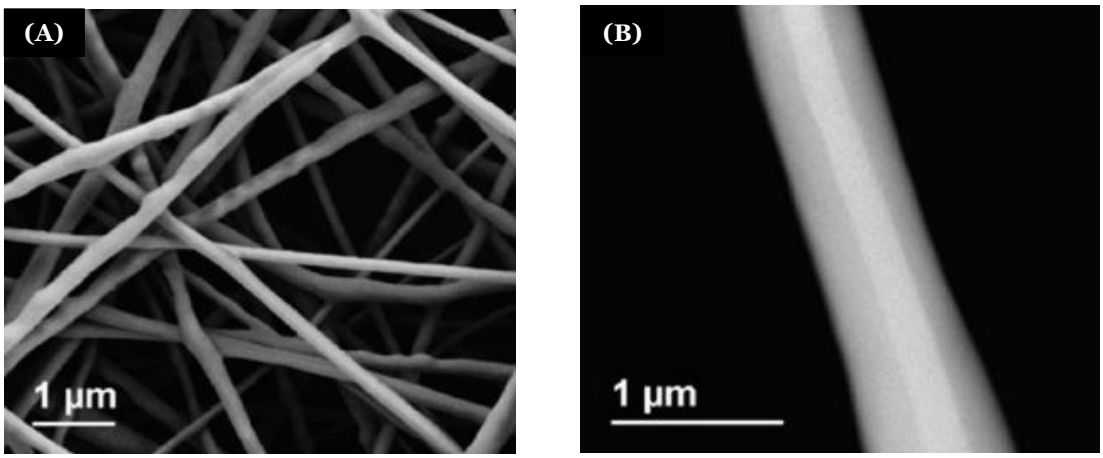

Figure 2.6 – Representative images of core-shell nanofibers obtained by (A) scanning electron microscopy and (B) transmission electron microscopy [88].

2.3 Electrospinning of PVA/BSA nanofibers

In order to maximize the surface-to-volume ratio of the PVA/BSA fibers, which allows to have a higher surface available for interactions with other small molecules, it is necessary to identify the optimal experimental conditions to have defect-free, homogeneous and nanometric fibers. In this work, fully hydrolyzed poly(vinyl alcohol) (weight average molecular weight, Mw = 89,000 – 98,000) was dissolved

into distilled water without any additives in order to avoid possible interferences with BSA, in the functionalized PVA nanofibers. As reported in Section 2.2, the fully hydrolyzed PVA does not easily dissolve in water due to the hydrogen bonds between hydroxyl groups [82]. Hence, at room temperature, it is hard to afford a homogeneous feed solution. As a consequence, the solution of PVA and distilled water has to be heated up to achieve complete polymer dissolution. This can take some time depending on the concentration of PVA, the stirring efficiency and the temperature. A wide range of temperatures (i.e. from 65°C [89] up to 95°C [90]) and times (i.e. form 1,5 h [90] up to 12 h [91]) have been employed for the total dissolution of PVA in water. The correct heating step of the solution not only allowed for the complete dissolution of PVA but, it also reduced the probability of gel formation. Thus, an efficient method, which led to total dissolution of the polymer in short time and prevents the gel development, was applied.

The weighted polymer powder is carefully added to distilled water under stirring to inhibit the formation of aggregates, which are thought to be the main cause for gelation; subsequently, the solution was heated up to 95°C inside the oil bath and left stirring for 1 h at approximately 120 rpm. After that, it was left to slowly cool down to room temperature to avoid gel formation.

By running this simple process, it was possible to obtain homogeneous and viscous solutions of fully hydrolyzed PVA in relatively short times: 1 hrs of heating and 1 hrs of cooling.

In order to obtain electrospun PVA/BSA nanofibers or mats, it was necessary to add BSA to PVA solutions. Since bovine serum albumin undergoes irreversible denaturation at temperatures over 50°C, it could not be added directly at the beginning with PVA to be dissolved together. In particular, unfolding of BSA induced by heating of aqueous solutions of the protein causes its aggregation [92]; the rate of heat-induced aggregation of BSA depends not only on temperature, but also on pH values, protein concentration and incubation time [93]. Therefore, BSA was separately dissolved in distilled water at room temperature and aliquots were added to the PVA solution to achieve the desired PVA/BSA in the feed solution to be electrospun. Dissolution of BSA in water could be attained through weak stirring or

absence of stirring since vigorous stirring causes protein denaturation, which was visible as foaming of the solution (Figure 2.7).

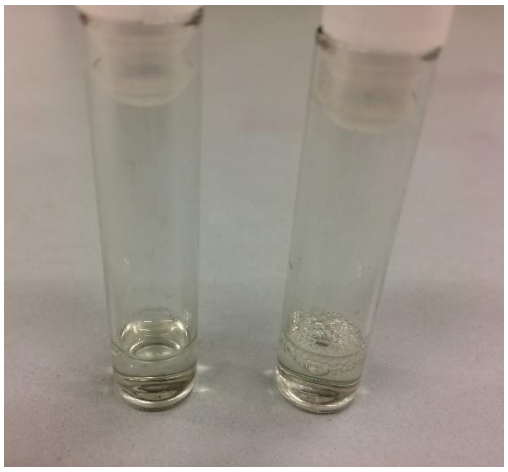

Figure 2.7 – BSA aqueous solutions (10% loading). On the left clear solution and on the right foaming of the solution.

To reach the set total solvent volume (i.e. 2 mL of dH2O) upon BSA addition and, consequently, the desired concentration, PVA solutions were prepared with higher concentrations. The addition of BSA into the poly(vinyl alcohol) solutions was done at about 25°C under weak stirring. Since BSA has to be stored at 4°C, the batch solutions as well as the electrospinning feed solutions were maintained at that temperature to ensure stability of the protein.

Electrospinning of pure PVA and PVA/BSA solutions were carried out with a horizontal setup using a syringe with a 22-gauge needle (Figure 2.8); the electrospun fibers were collected on either microscope glass or silicon substrates fixed to the metal collector at a defined distance from the tip, with an aluminum tape. Fibers on glass and self-standing mats were employed for optical analysis and to perform any chemical post-processing treatment, while fibers collected on Si substrates were analyzed using scanning electron microscopy (SEM) for the characterization of fibers diameters.

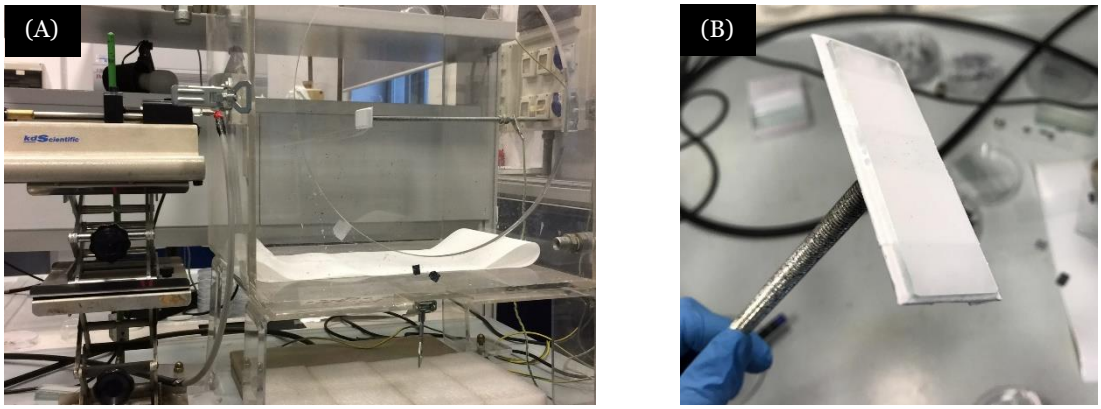

Figure 2.8 – Images of (A) electrospinning horizontal setup and (B) fibers deposited onto a microscope glass fixed to the metal collector.

PVA/BSA solutions were prepared with two main PVA concentrations (i.e. wt.%, defined as mass of PVA per mass of total solution) and different protein loadings (i.e. a percentage of weight of BSA over weight of PVA) aimed at producing beaded-free nanofibers. The two PVA concentrations selected are the result of an extensive investigation regarding the electrospinning of pure PVA solutions and the optimization of experimental parameters such as solution concentration, applied voltage, tip-to-collector distance and feed rate to attain high efficiency of the process (Table 2.2).

Concentration (wt.%)	Voltage (kV)	Feed Rate (ml/h)	Distance (cm)
10	12-24	0,1-0,4	18-25
12	15-21	0,05-0,1	20-30
14	15-18	0,05-0,2	25-28
15	15-19	0,1-0,3	12-18
16	15-17	0,2	13-18

Table 2.2 – Experimental parameters tested to electrospin PVA.

In particular, starting from the 12 wt.% mark, increasingly defect-free nanofibers were formed from aqueous PVA solutions (i.e. slightly beaded fibers in case of 12 wt.% and homogeneous fibers with occasional beads in case of 14 wt.%). Moreover, as the concentration of the feed solution increases, also the average diameter grows up, as evidenced in Table 2.3.

Concentration (wt.%)	**$d_{average}$ (nm)**
12	284± 52
14	481 ±80
15	634 ±86

Table 2.3 – Concentrations of electrospun samples with respective average diameters computed from SEM images.

As the final aim was to obtain membranes with high surface area-to-volume ratio, defect-free fibers with small diameters were required. Thus, solutions and optimized experimental parameters of either 12 wt.% or 14 wt.% of PVA were used as starting point for PVA/BSA feed solutions preparation. Both to investigate the role of BSA in the electrospinning of PVA and to achieve the highest efficiency of the process and the desired fibers characteristics, many tests were performed using the previously selected concentrations of PVA (i.e. 12 wt.% and 14 wt.%), by varying the protein loading inside the solutions and some experimental parameters. Results are summarized in Table 2.4.

PVA (wt.%)	BSA load (%)	Voltage (kV)	Feed Rate (ml/h)	Distance (cm)
12	10-50	16-18	0,3	18
14	10-50	16-18	0,3	18

Table 2.4 – Experimental parameters tested to electrospin PVA/BSA blends.

As can be seen in Table 2.4, the voltage used to produce PVA/BSA fibers is slightly lower compared to the one set in PVA electrospinning, in order to hinder occasional discharges, which would affect the process. Moreover, its value is tuned depending on the environmental conditions (i.e. temperature and relative humidity) in the electrospinning chamber. By analyzing optical microscope images (Figure 2.9) of the fibers obtained from electrospinning of either 12 wt.% or 14 wt.% of PVA with 10% BSA loading, small morphological differences between the two samples can be noticed, even when the BSA content is varied.

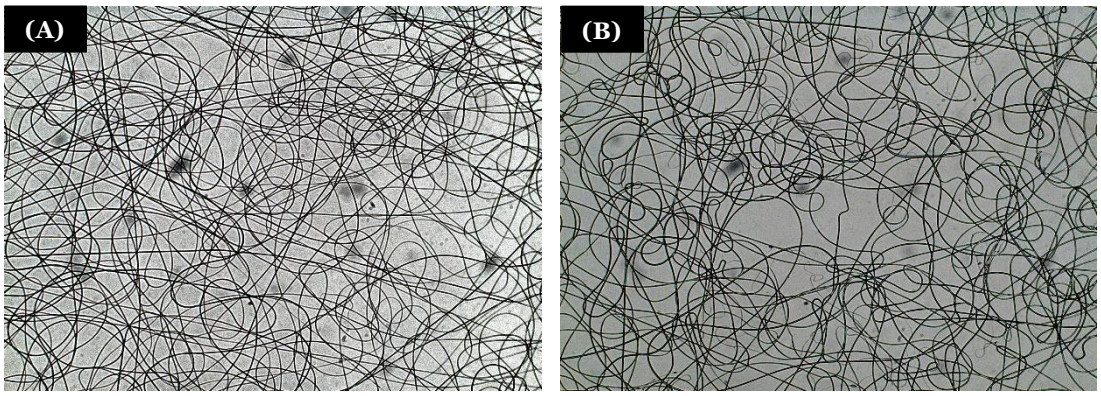

Figure 2.9 – Optical microscope images of PVA/BSA fibers: (A) PVA at 12 wt.% and 10% BSA load; (B) PVA at 14 wt.% and 10% BSA load.

However, the addition of bovine serum albumin to poly(vinyl alcohol) led to a significant increase in the fiber production, as it can be demonstrated comparing two electrospun mats (i.e. one with BSA and one without BSA) of PVA obtained employing

the same experimental conditions and deposition times. The aftermaths of BSA incorporation into PVA solutions were also studied by *Tang et al.* (2012). They showed that the addition of BSA slightly increased solution viscosity at polymer concentrations required to electrospin, due to PVA and protein interactions (i.e. polar interactions) [78]. Despite this, they stated that the slight growth of viscosity did not bring to changes in the overall spinnability between the pure PVA solutions and the PVA/BSA blends.

Here, the positive effect of BSA on the ability of PVA to be electrospun was ascribed to the net negative charge formation onto the protein as a consequence that the aqueous solution has a pH higher than the BSA isoelectric point (i.e. pH 4.7-5.2). Since the protein carries a net negative charge, the electrical conductivity of the feed solution increases and, consequently, improves the spinnability of PVA/BSA and fiber production. Higher conductivity, also, usually allows to obtain a significant drop in the diameter of electrospun nanofibers as the jet carries more charges and experiences an higher stretching by the applied electric field [48] [94] [95]; both effects, i.e. higher productivity and lower fiber size, were herein noticed after addition of BSA. Accordingly, it can be possible to understand why the previously used PVA concentration of 12 wt.%, which gave some beads and slightly defective fibers, now, provides a defect-free nanofibrous mat with incredibly small diameters ($d_{average}$ = 144 ± 28 nm) after 10% BSA loading. The absence of defects can also be noticed upon 15% and 20% BSA loadings (Figure 2.10).

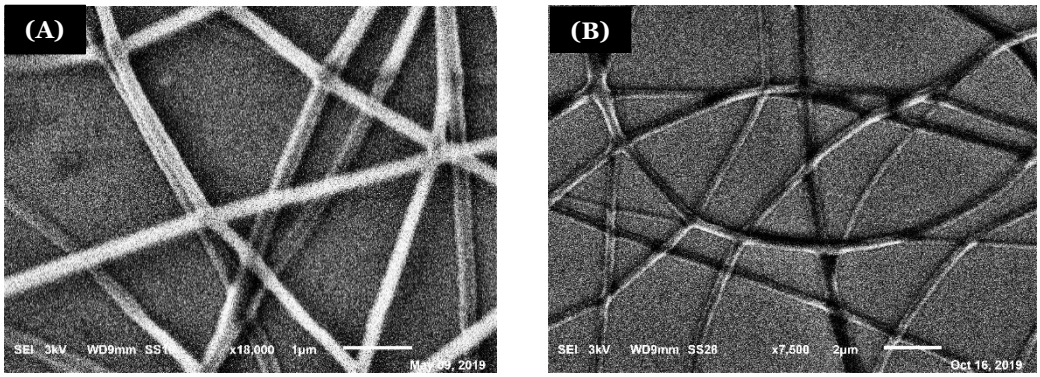

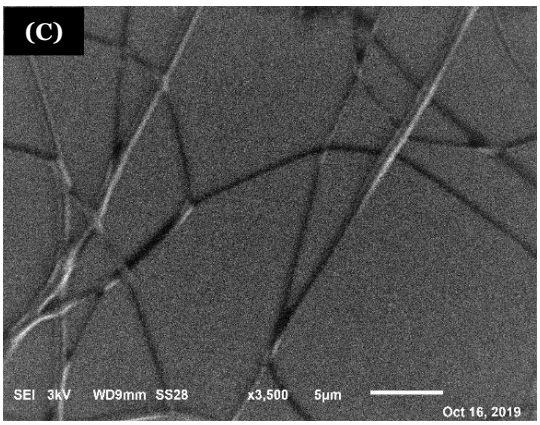

Figure 2.10 – SEM images of electrospun nanofibers of: (A) 12 wt.% PVA and 10% BSA loading; (B) 12 wt.% PVA and 15% BSA loading and (C) 12 wt.% and 20% BSA loading.

Also by increasing the BSA content while keeping constant the PVA concentration (i.e. 12 wt.%), the diameters increase as reported in Figure 2.11. From the examination of electrospun nanofibers, it is additionally possible to observe how the BSA load affects the homogeneity of diameters distribution. In particular, rising the protein load, the variation of diameter from fiber to fiber, within the same sample, grows (i.e. 10% BSA load: 144±28 nm; 15% BSA load: 190±60 nm and 20% BSA load: 300±90 nm).

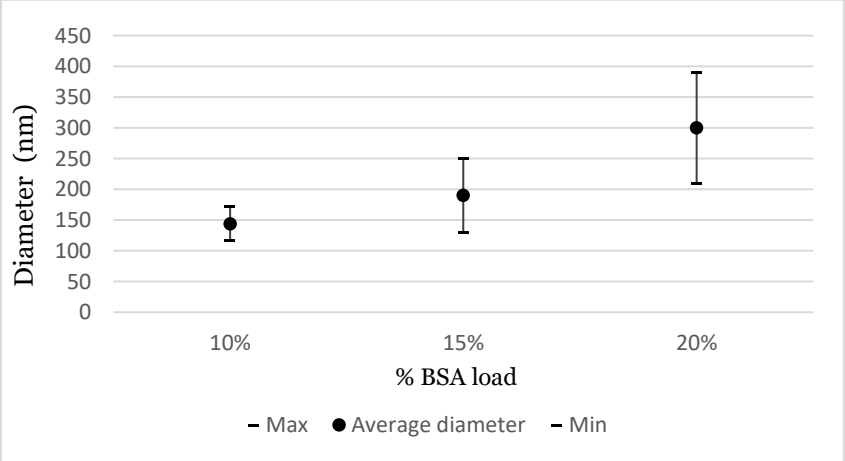

Figure 2.11 – Diameters analysis of different PVA/BSA samples spun from solutions having 12 wt.% PVA and different BSA loading.

According to all the morphological data acquired through electron microscopy, mats having 10% BSA loading and 12 wt.% PVA concentration were selected for the next step of this study, as they combined a stable electrospinning, high yield of deposition and the lowest fiber diameter. Indeed, thick and self-standing mats were produced in a relatively short time, with high surface area (Figure 2.12).

Figure 2.12 – Example of a self-standing nanofibrous mat electrospun from a solution containing 12 wt.% PVA and 10% BSA loading after detachment from a glass substrate.

Chapter 3
Stabilization of fibers against Dissolution in Water

As mentioned in Chapter 2, since PVA is soluble in water and, consequently fibers dissolve in water in a short time, the PVA/BSA electrospun mat cannot work in aqueous environment [91] [96] [97]. Although the solubility of PVA as a bulk polymer is achieved at relatively high temperatures, the high surface area of the electrospun nanofibrous mat enhances the hydrophilicity and in general favors solvation due to the large surface of interaction with the solvent molecules, leading to a fast dissolution upon contact with water [86]. In fact, all the samples that have been produced showed this behaviour in aqueous solutions and a partial dissolution just in presence of moisture (Figure 3.1).

Figure 3.1 – A PVA/BSA mat (A) before and (B) after water interaction. An imminent severe shrinking was noticed.

Consequently, a post-process to make the PVA/BSA nanofibers water-resistant was required. This allowed to enable any possible application in aqueous or moist

environments. To improve water resistance of PVA several methods have been devised (Table 3.1). Despite a physical crosslinking in methanol that was herein tested giving unsuccessful results, crosslinking of PVA can be divided into two main categories: (i) photocrosslinking, which is activated by UV radiations and (ii) chemical crosslinking, which makes use of co-reactant that bind the –OH groups forming a bridge. Examples of chemical crosslinking of PVA are reported by *Gohil et al.*, who successfully crosslinked PVA by heat treatment using maleic acid or by *Ding et al.*, who crosslinked electrospun PVA/glyoxal fibers by heat treatment [98].

Stabilization methods	**References**	
Photocrosslinking	[82] [98] [99] [100] [101] [102]	
Chemical crosslinking	[64] [82] [83] [84] [85] [103]	
	PROs	**CONs**
Photocrosslinking	No chemicals involved after electrospinning	Irradiation damage, need of a sensitizer
Chemical crosslinking	High efficiency and homogeneity	Appropriate selection of solvent and reagent

Table 3.1 – Crosslinking methods reported in literature with advantages and disadvantages.

At first glimpse, photocrosslinking seems to be an attractive method, since it requires a simple irradiation step, which lasts from few minutes down to few seconds [99] and can be performed *in situ* [100] without additional chemical treatments. However, it necessitates either an *a priori* functionalization of PVA polymeric chain (Figure 3.2) [101] or the addition of a sensitizer [102] to be effective. In case of the former choice, it would mean not only to add a further synthesis step but also to perform a new full optimization of the electrospinning

process to attain defect-free fibers. Whereas, in case of the latter choice, any possible interaction of the sensitizer with BSA under UV irradiation would have to be considered.

So far, there have been no studies carried out specifically on the photocrosslinking of PVA/BSA mats; this can suggest the probable degradation of the protein caused by UV radiations. Therefore, our attention was focused on chemical treatments, more specifically on crosslinking by means of glutaraldehyde, which is highly effective also at room temperature.

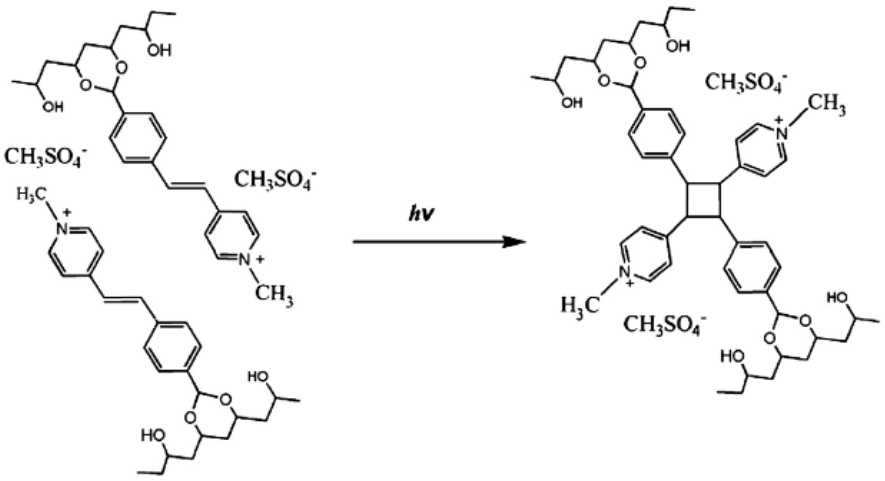

Figure 3.2 – Example of structural modification of UV-induced PVA crosslinking [98].

3.1 Chemical crosslinking with glutaraldehyde

Glutaraldehyde possesses unique characteristics that make it the most popular bis-aldehyde homobifunctional crosslinker in use today as crosslinking reagent. It is a linear 5-carbon dialdehyde characterized by high solubility, in water and alcohol, in all proportions, as well as in organic solvents [104] (Figure 3.3).

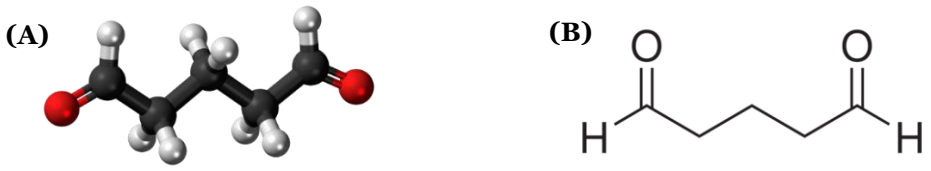

Figure 3.3 – On the left: (A) Ball-and-stick model of the glutaraldehyde molecule, with oxygen atoms in red, carbon atoms in black and hydrogen atoms in white. On the right: (B) chemical structure of glutaraldehyde.

Glutaraldehyde has been widely used to crosslink PVA fibers and blends of PVA with a multiplicity of biomolecules [62] [84] [85] because of its powerful affinity towards hydroxyl groups (Figure 3.4 (A)) [83]. Among all the existing protein crosslinking agents, it has undoubtedly found the widest application in a variety of fields such as enzyme technology [84], biomedical and pharmaceutical sciences (Figure 3.4 (B)). This is due to its rapid reaction with amine groups and its higher efficiency with respect to other aldehydes in generating chemically stable crosslinks [104].

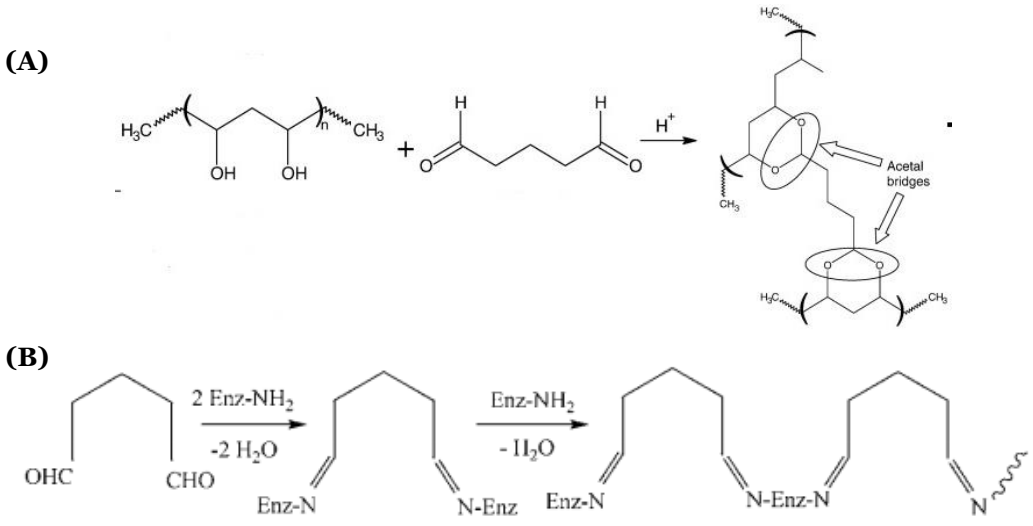

Figure 3.4 – Reactions of glutaraldehyde with (A) PVA and (B) amine groups of enzymes [103].

As reported by *Tang et al.* (2009), water insoluble PVA nanofibers can be generated performing a single step reactive electrospinning. In particular,

poly(vinyl alcohol) and glutaraldehyde (GA) as crosslinker, with addition of hydrochloric acid (HCl) as a catalyst, were electrospun using a conventional setup. Such a mechanism allowed the fibers to cross-link during the deposition process, thereby avoiding any chemical post-treatment [103]. At first glance, it seems to be a suitable method to crosslink PVA, but when a PVA/BSA system is considered, the addition of GA to the electrospinning feed solution modifies its pH and, consequently, the BSA distribution onto the fibers. Nevertheless, a successful crosslinking of PVA/BSA blends by means of glutaraldehyde is mentioned by *Moradzadegan et al.* [85]. They produced PVA nanofibers functionalized with BSA and the acetylcholinesterase enzyme. Actually, the crosslinking reported in this work was run only by using glutaraldehyde vapors and lasted for 12 hours.

Herein, crosslinking as a single immersion step of the PVA/BSA spun membrane in glutaraldehyde solution was preferred to increase PVA/BSA nanofibers water resistance.

Nanofibers collected on either glass or Si substrates were immersed into an acetone bath containing glutaraldehyde (0,15 M) and hydrochloric acid (0,05 M) for 1 h treatment, as stated for pure PVA fibers [98]. Then, the samples were washed in distilled water for 1 h to remove excess of crosslinker possibly adsorbed to the fibers surface and dried by gentle solvent evaporation for several hours. The evidence of the process effectiveness is shown in Figure 3.5.

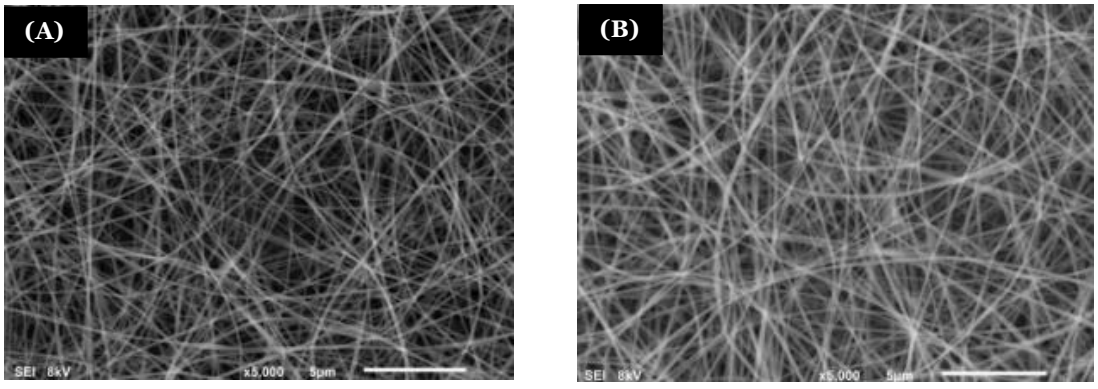

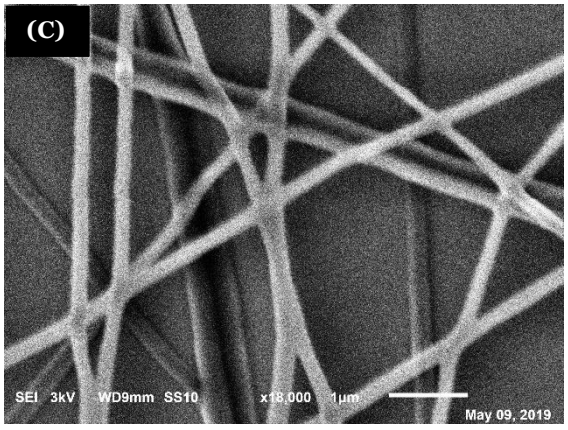

Figure 3.5 – SEM images of 12 wt.% PVA and 10% BSA load electrospun fibers (A) before crosslinking and (B) after crosslinking and immersion in water; (C) zoom on fibers after crosslinking.

As we can see from Figure 3.5, the treatment with GA is highly effective and it allows to retain fibers morphology even after water immersion: the diameters before crosslinking are almost 130±15 nm, while after crosslinking and water immersion are almost 144±28. Thus, it was adopted as the standard treatment for the production of insoluble PVA/BSA nanofibers.

The nanostructure of the resulting mats will be further investigated using Fourier Transform Infrared Spectroscopy (FTIR) in Chapter 4, underling the characteristic bands of the crosslinking agent and BSA protein.

Chapter 4
Analysis of Protein Content

The functionalization of nanofibers is a fundamental step to obtain bioactive fibers able to work as biosensors. Hence, once the crosslinking of PVA/BSA nanofibers was performed, the presence of active bovine serum albumin (BSA) protein onto the fibers surface was probed. The quantification and the investigation of BSA enable a complete characterization of produced nanofibers, both before and after crosslinking. In particular, we had to quantify the amount of BSA in the as-spun BSA/PVA membranes and its possible release from fibers upon immersion in crosslinking solution. In the former case, because of the electrostatic nature of the force acting on the solution throughout the process, an uneven electric field distribution can lead to a more effective spinning of one of the two components of the blend, resulting in a different PVA/BSA ratio if compared to the initial one. In the latter case, instead, BSA leaking could occur during the crosslinking, which was performed by immersion in a water solution; in addition, it was also worth to determine if BSA is released also from the crosslinked mat during the working life, which would be ascribed to weak interaction with the polymeric scaffold. Obviously, both situations must be avoided as they mean losing part of the bioactive component from the system. In order to assess the actual amount of protein, many procedures have been devised. The choice of an adequate method to quantify the protein present in a sample, is a fundamental step and depends on the nature of the protein, on the required sensitivity and accuracy, on the purity of the sample and on the measurement times [105]. In literature, the most widely utilized methods for the analysis of protein contents are the assays of Biuret, Bradford, Lowry, Smith and Warburg-Christian. Nonetheless, many authors recommend the Bradford assay (1976)

because of its advantages if compared with the other methods [106] [107]. In particular, the most striking ones are: (i) the quickness of the assay (i.e. 5 min), (ii) the high stability of protein-dye complex, (iii) the use of visible light to measure the absorbance, (iv) the detection of protein amounts as small as 1 to 20 μg and (v) the high reproducibility. Hence, among all the procedures, this simple, fast and inexpensive method has been selected to quantify the BSA amount. In addition, infrared spectroscopy, which is generally used to determine the chemical functional groups in a sample, was herein exploited to investigate the presence of BSA both after and before crosslinking [108] [109].

4.1 Bradford Protein Assay

The Bradford assay is a colorimetric test based on the absorbance shift from 465 nm to 595 nm of the Coomassie Brilliant Blue G-250 (Figure 4.1) dye upon its addition to a known volume of protein solution.

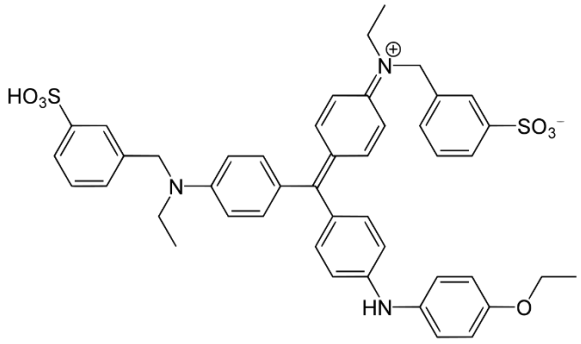

Figure 4.1 – Coomassie Brilliant Blue G-250 dye structure.

More precisely, when added to the protein solution, the dye binds to the protein resulting in a color change from a reddish brown to blue depending on the protein concentration. The dye has been assumed to bind to protein via electrostatic interaction of the dye sulfonic groups to the protein. The bound sites are primarily arginine residues, but the dye also binds to a lesser degree of lysine, histidine,

tyrosine, tryptophan and phenylalanine [110]. The consequent protein-dye complex (Figure 4.2) has a high extinction coefficient and remains dispersed in solution for a relatively long time [108].

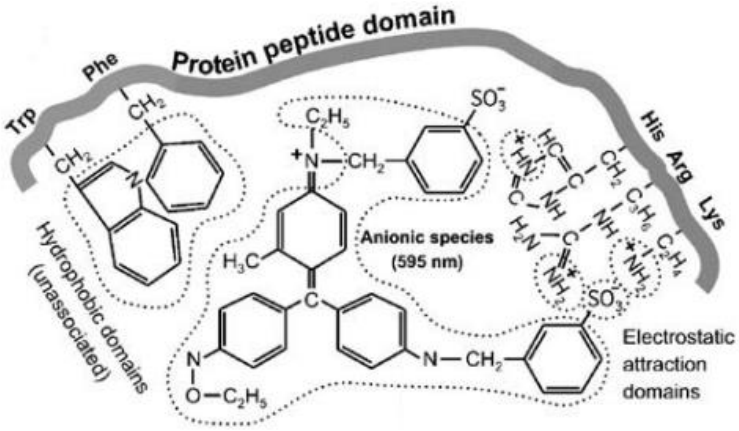

Figure 4.2 – Mechanism of Coomassie Brilliant Blue G-250 binding to proteins [110].

The Bradford test has been extensively used for BSA evaluation, both in terms of standard reference for comparison to other proteins [111] and direct quantification of BSA release [85] [112]. There are two main approaches to achieve a quantitative interpretation of the test (Figure 4.3):

- by measuring the shift in absorbance at 595 nm, which will be proportional to the amount of protein bound to the dye (direct test);
- by measuring the shift in absorbance at 465 nm, which will be proportional to the unbound dye remaining in solution (indirect test).

(A)

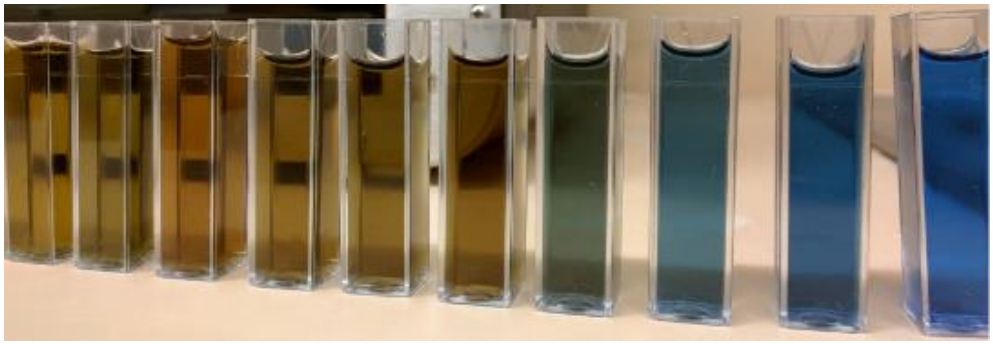

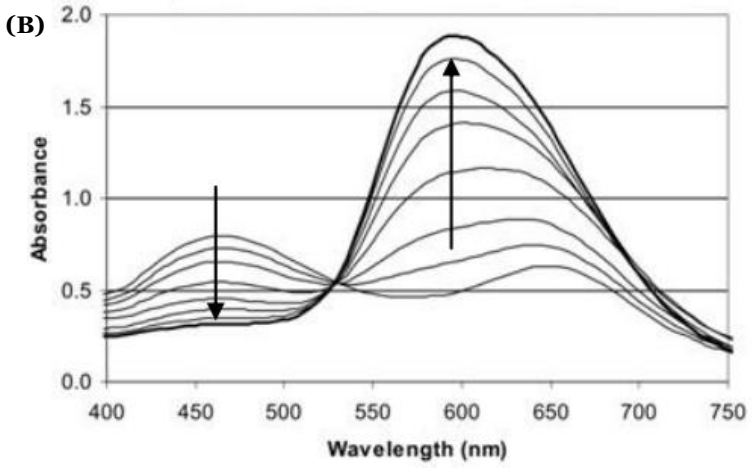

Figure 4.3 – (A) Growing protein content in solution with CBB from brownish towards blue and (B) shifts in UV-visible absorption spectrum, decreasing at 465 nm and increasing at 595 nm.

In both cases, the quantification of BSA present in solution can be attained taking into consideration a previously computed calibration curve, which works as reference curve. Consequently, the modus operandi for the Bradford protein assay herein used, started with the evaluation of calibration curves for both the direct and indirect tests. In order to assess the calibration in direct test, aqueous solutions of known BSA concentrations were prepared. Specifically, 250 µL of such solutions were picked up and mixed with 1,25 mL of CBB, left to react for 5 minutes and subsequently probed at 595 nm in a spectrophotometer using CBB as baseline. For the indirect test, instead, after the same 5 minutes required for the reaction stabilization, samples were centrifuged for 2 minutes at 1500 rpm, in order to precipitate dye-protein complexes which can interfere with the measurement. Then, the solutions were tested at 465 nm using water as baseline [107] [111].

By repeating this procedure three times for each concentration and each type of test, it was possible to obtain the calibration curves shown in Figure 4.4 (direct test) and Figure 4.5 (indirect test).

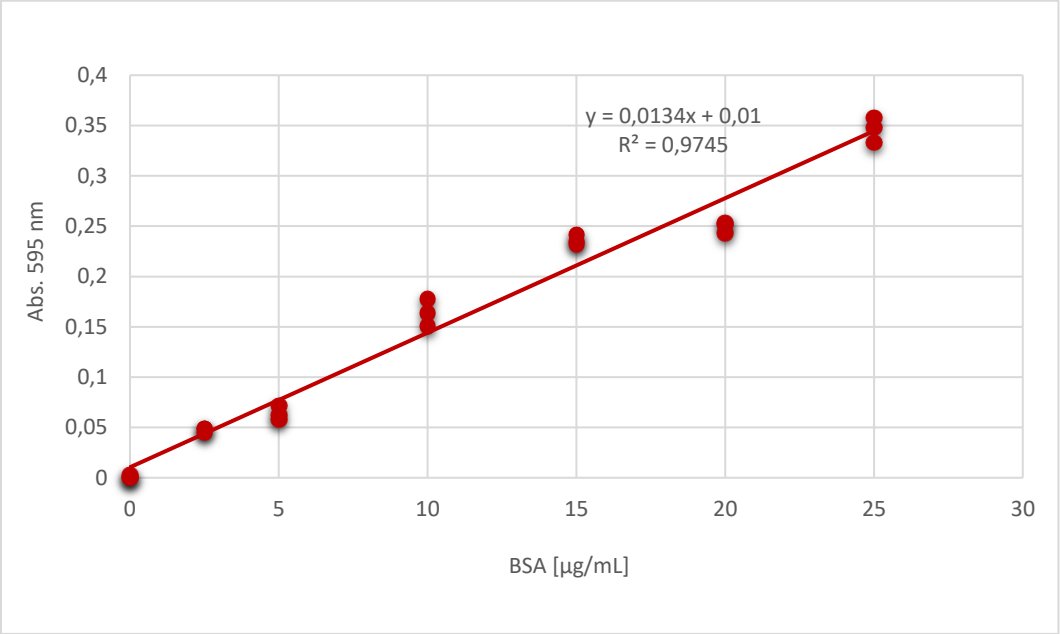

Figure 4.4 – Calibration curve obtained for direct protein quantification; equation and coefficient of determination (R^2) *are shown.*

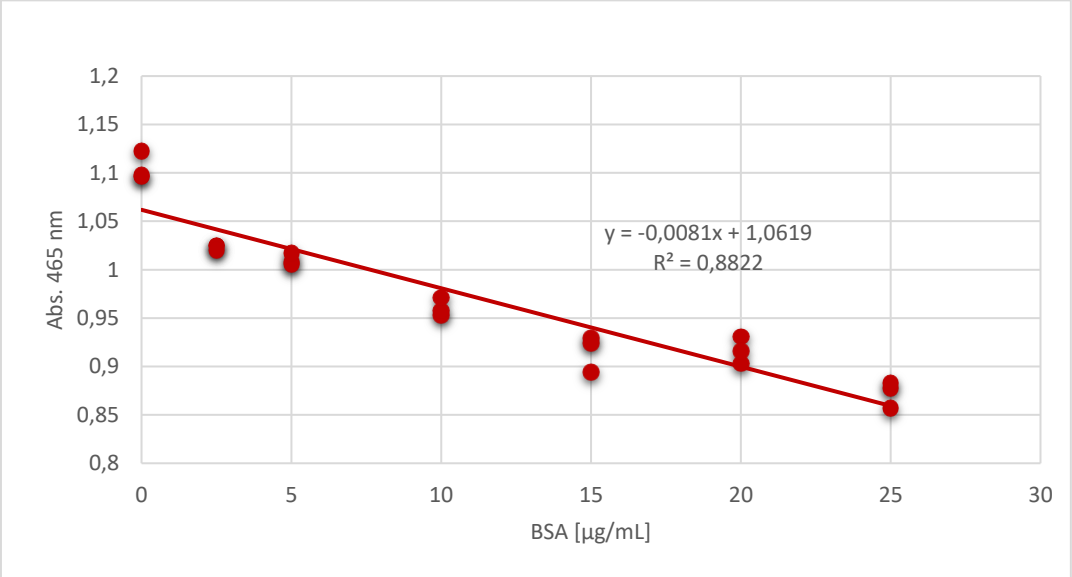

Figure 4.5 – Calibration curve obtained for indirect protein quantification; equation and coefficient of determination are shown.

In the equations of lines shown in Figure 4.4 and Figure 4.5, "y" represents the measured absorbance, while "x" states for the concentration of protein expressed in μg/ml of the volume probed. Looking more closely at the values of R^2, it can be deduced that the regression prediction, in direct measurements ($R^2 = 0{,}9745$), approximates better the real data than the one in indirect measurements ($R^2 = 0{,}8822$). Since the absorbance of the dye at 595 nm presents a sharper increase by varying the concentration of BSA in solution than the reduction experienced at 465 nm, the direct method is thought to be more sensitive to protein concentration variations. Despite of this, we run both tests to have a more detailed characterization of the system under analysis. Hence, once obtained the calibration curves, two procedures have been designed to quantify BSA content:

- **Procedure 1** (quantification of BSA content in soluble mats): e-spun membranes of known mass and characterized by 10% nominal BSA loading were dissolved in distilled water. Subsequently, the solutions obtained were probed with the previously described protocols to quantify their BSA content. In order to reach a better quantification, the same PVA/BSA feed solution was used to prepare spincoated films, which are then tested for their protein content and compared to fiber mats.

- **Procedure 2** (quantification of BSA leaking from crosslinked samples): previously electrospun and crosslinked mats of 12 wt.% PVA and 10% BSA load were immersed in distilled water for approximately 1 h. The water is consequently tested to check any possible protein release.

Apart from the analysis of PVA/BSA blends containing 10% and 30% BSA loads, pure PVA mats have been also tested as reference values. The acquired outcomes can be easily summarized as average values of multiple runs of measurement done carried out at 465 nm and 595 nm, as shown in Table 4.1.

Sample (nominal BSA%)	Estimated BSA loading (%)	Estimated leaking (%)
Procedure 1 (loading)		
(E) 0% (PVA)	0%	-
(E) 10%	9,32%	-
(S) 10%	9,74%	-
Procedure 2 (leaking)		
(E) 0% (PVA)	-	0%
(E) 10%	-	0,20%
(E) 30%	-	1,20%

Table 4.1 – Summary of Bradford test results. The theoretical BSA loading (%) follows the letter (E), which indicates an electrospun sample and the letter (S), which indicates a spincoated sample.

Looking at table 4.1, two relevant aspects rise from the examinations. Firstly, considering the experimental error, the amount of BSA in solution is very close to the value found in the membrane, both in electrospun and spincoated samples. Thus, the protein loss and the possible change in composition caused by the electric field throughout the production step were ruled out. Secondly, the leaking of protein from the mats, markedly at 10% loading, is negligible. Consequently, the bioactive component in the crosslinked mats remains available even after immersion in water. Moreover, by using the Coomassie Brilliant Blue, the BSA available onto the fiber surface has been determined. In fact, upon immersion of the white colored crosslinked PVA/BSA mat into a solution containing CBB, the specimen turned blue. Therefore, the availability of BSA and its superficial distribution in fibers were confirmed. In case of homogeneous distribution only 19% of BSA is at the surface, while in case of complete surface distribution the

amount of BSA is equal to $3.2*10^{16}$ (see Annex 1.1). The possible release of BSA from nanofibrous mats during the crosslinking can be further investigated by using Fourier transform infrared spectroscopy (FTIR).

4.2 FTIR analysis

Fourier Transform Infrared (FTIR) spectroscopy can be used to measure surface properties and composition (in ATR mode), allowing the characterization of specific chemical groups present in the samples at solid state. As anticipated at the beginning of Chapter 4, the main purpose in employing this analysis was to identify the presence of BSA both before and after crosslinking and to study the potential effects of glutaraldehyde bath on its structure and bioactivity.

The acquisition of the membranes spectra was achieved after the detachment of a portion of the specimen from the glass substrate, which was subsequently placed onto the sample holder and analyzed with a crystal tip with a refractive index higher than that of the sample. Then, the specimen was tested upon collecting an air background. When needed, spectra were taken after the deposition of few drops onto a zinc selenide substrate and analyzed in transmission after gentle solvent evaporation. All measurements, apart from those of solutions, are obtained using ATR mode, in the range of wavenumber from 3500 to 600 cm^{-1} during 128 scans, with 4 cm^{-1} resolution. However, the spectra below have been attained through ATR correction (Crystal: Si, angle of incidence: 53, number of bounces: 1 and sample refractive index: 1,50) allowing a direct comparison with those obtained in transmission.

Firstly, the spectra of electrospun PVA and BSA at solid state were collected and compared, as evidenced in Figure 4.6.

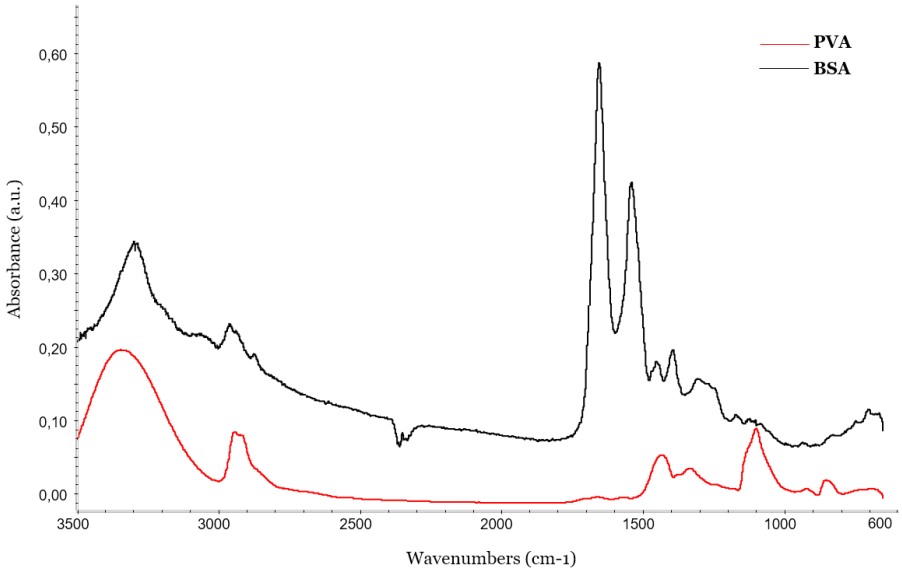

Figure 4.6 – Spectra of pure PVA obtained from electrospinning (red line) and BSA at solid state (black line); intensities are offset to better visualize the differences and similarities in the spectra.

As can be seen, bands of PVA and BSA overlap throughout all the spectral range. However, in BSA spectrum two intense peaks are clearly visible: the Amide I and Amide II bands, which are commonly characteristic in many protein systems. The Amide I vibration, absorbing near $1650 cm^{-1}$, arises mainly from the C=O stretching vibration with minor contributions from the out-of-phase CN stretching vibration, the CCN deformation and the NH in-plane bend. Whereas, the Amide II mode, absorbing at ~ 1550 cm^{-1}, is the out-of-phase combination of the NH in plane bend and the CN stretching vibration with smaller contributions from the CO in-plane blend and the CC and NC stretching vibrations [87] [113]. Considering the PVA spectrum instead, no large signals were registered in this region since the PVA herein employed is fully hydrolyzed. If the PVA were not completely hydrolyzed, it would exhibit the C=O stretching vibration typical of acetate groups close to the Amide I band. As a consequence of the intense peaks of protein amino groups, the presence of BSA could be easily confirmed by looking at the Amide bands in nanofibers spectra. In order to assign the exact position of the peculiar bands of BSA and PVA under investigation, we referred to the literature (see Table 4.2).

Range (cm^{-1})	Normal mode	References
	BSA	
~3300	Amide A	[96][113]
3030-3100	Amide B	[96][113]
1651-1660	Amide I	[96][97][114][115]
1541-1550	Amide II	[96][114][115]
1241	Amide III	[96]
570-710	Sulfide (ν(C-S))	[96]
	PVA	
3315-3387	ν(-OH)	[91] [96] [97][103][117]
2930-2944	ν(C-H)	[97][86][87][117]
1735-1750	ν(C=O) of residual acetates	[87][117]
1433-1448	δ(CH-OH)	[116][87]
1248-1254	ω(C-H)	[116][87]
1093-1097	ν(C-O)	[96][87][116][103]
847-849	ν(C-C)	[116][87]

Table 4.2 – Wavenumber range and principal normal modes of PVA and BSA according to literature.

On the basis of the spectrum obtained analyzing solid BSA, the dependence of the intensity of Amide I and Amide II bands on the protein concentration was examined. As can be noticed looking at Figure 4.7, increasing the protein content in the PVA/BSA samples (i.e. from 10% load to 30% load), the bands intensity rises, as expected. Then, FTIR was performed to study the influence of chemical crosslinking, by means of glutaraldehyde, on the chemical structure of pure PVA (Figure 4.8) and PVA/BSA electrospun mats.

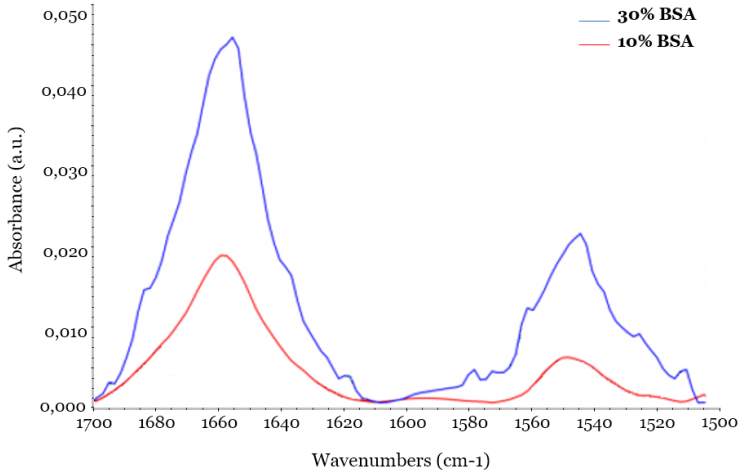

Figure 4.7 – FTIR spectra of electrospun mats containing 10% (red line) and 30% (blue line) BSA loading in common scale, underling the Amide I and Amide II in the 1700-1500 cm^{-1}region.

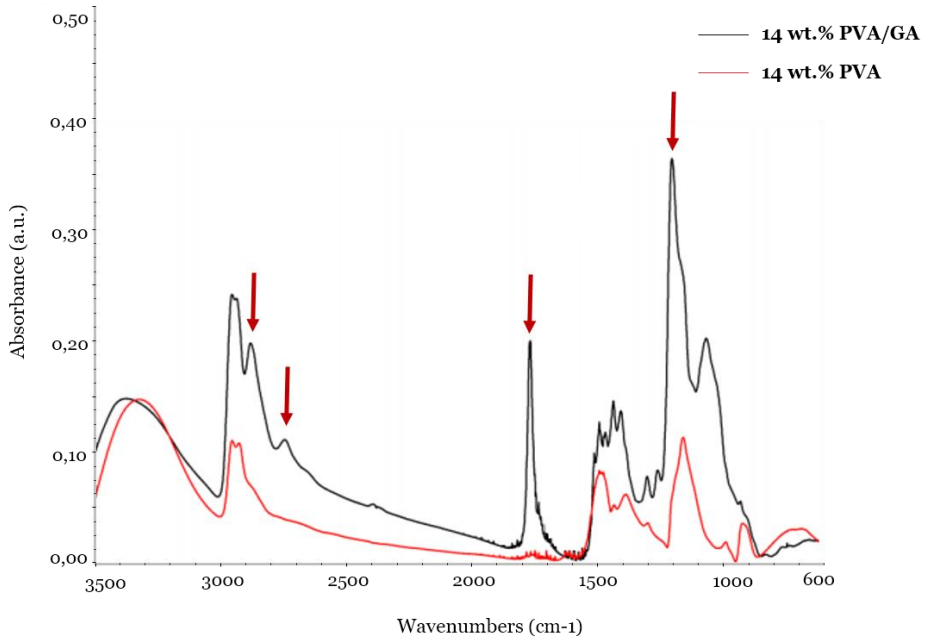

Figure 4.8 – Spectra of electrospun mats of pure 14 wt.% PVA before (line) and after (line) crosslinking with glutaraldehyde. Arrows indicate the bands characteristic of crosslinking process.

In particular, the effect of glutaraldehyde crosslinking on PVA hydrogels was previously investigated by *Mansur et al.* (2008) [117]. The reaction of PVA with GA was distinctly monitored by the decrease of the intensity of O-H peak at 3315-3387 $cm^{-1}$and a shift towards higher wavenumbers. Moreover, the FTIR spectra of PVA/GA samples revealed two important bands at $\nu = 2830\ and\ 2695\ cm^{-1}$of C-H stretching related to aldehydes, a duplet absorption with peaks attributed to the alkyl chain. Finally, a residual band from carbonyl group (C=O) was evidenced at $\nu = 1720 - 1740\ cm^{-1}$,probably related to glutaraldehyde, which reacted only at one of the two available sites (Figure 4.9). The most important and characteristic bands of PVA crosslinked with GA and their assignment are reported in Table 4.3 [117].

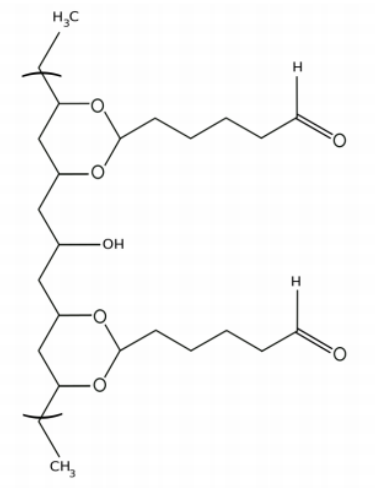

Figure 4.9 – Scheme of partially reacted glutaraldehyde, which is probably the cause of the signal at ~ 1720 cm^{-1} assigned to the stretching of C=O group.

Sample	Chemical Group	Wavenumbers (cm-1)
PVA + GA	O-H from the intermolecular and intramolecular hydrogen bonds	ν 3550-3200
PVA + GA	C-H from aldehyde	Two peaks in ν 2830-2695
PVA + GA	C=O	ν 1750-1735
PVA + GA	C-O-C	ν 1150-1085

Table 4.3 – Vibration modes and band frequencies in PVA crosslinked with glutaraldehyde [117].

By comparing the spectra obtained by *Mansur et al.* with the spectra reported in Figure 4.8, it was possible to observe the same bands of PVA after crosslinking with glutaraldehyde. Hence, the vibration modes and the band frequencies reported in Table 4.3 from the *Mansur et al.* research are also valid for the electrospun mats, indicating that the crosslinking reaction occurs with the same mechanism as for bulk PVA.

The same analysis was applied on the spectra obtained from PVA/BSA electrospun mats (Figure 4.10), identifying:

- the presence of a sharp peak at ~ 1145 $cm^{-1}$and a decrease in intensity of O-H band, underling a successful crosslinking reaction;
- the existence of a sharp peak at ~ 1720cm^{-1}, indicating the partially reacted glutaraldehyde;
- the presence of two bands in the range 2830 – 2695cm^{-1}, representing C-H stretching related to aldehydes.

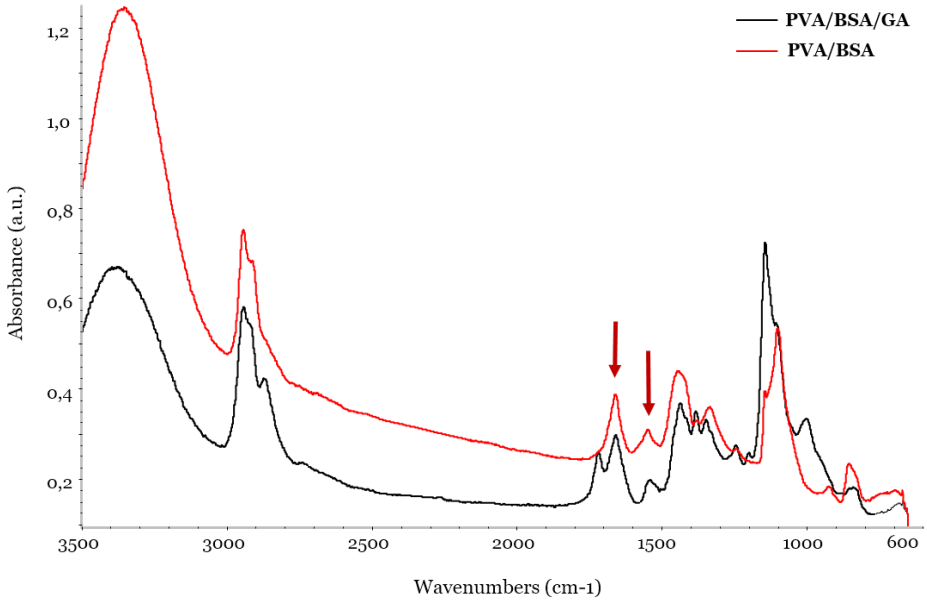

Figure 4.10 – Spectra of 12 wt. % PVA and 10% BSA loading electrospun mats before (red line) and after (black line) crosslinking shown in common scale. Arrows indicate the unshifted Amide I and Amide II bands at 1659 $cm^{-1}$and 1548 cm^{-1}.

Looking more deeply at Figure 4.10, we can also notice the unshifted Amide I and Amide II bands at 1659 and 1548 cm^{-1}respectively, given by the BSA. Since glutaraldehyde reacts not only with OH groups of PVA but also with the NH2 of the protein, the unshifted existence of Amide bands clearly indicate that unmodified BSA was available on the nanofibers, even after crosslinking. Generally, these specific signals are highly sensitive to changes in secondary structures of proteins [113].

Spectra of crosslinked mats before and after immersion in distilled water (i.e. for 1 h) have been also collected to assess whether BSA was released or not (Figure 4.11). The Amide I and Amide II are clearly visible even after water immersion, demonstrating that the crosslinking process was highly effective and the BSA was not released.

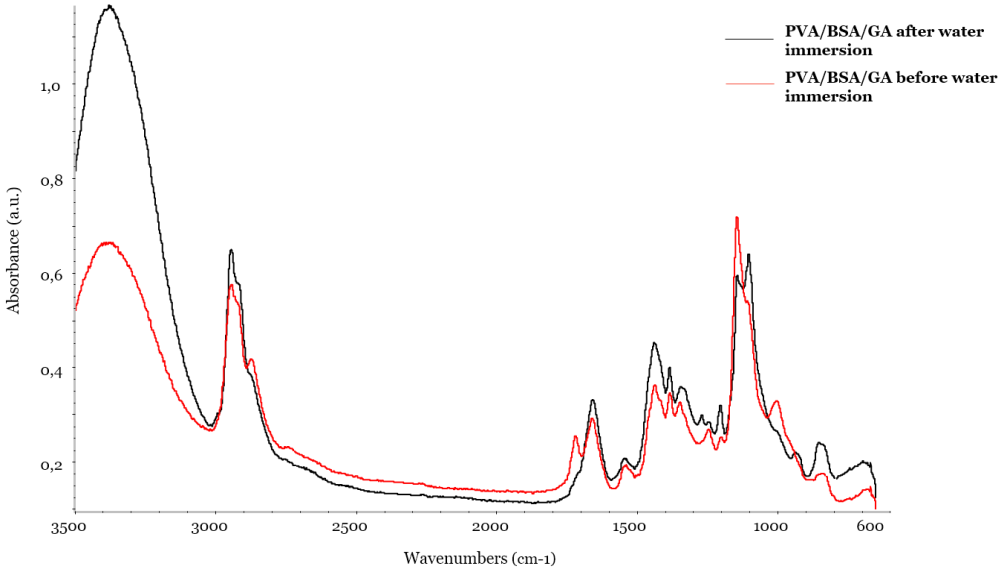

Figure 4.11 – Spectra of 12 wt.% PVA and 10% BSA load mats before (red line) and after (black line) immersion in dH_2O for 1 h. Amide I and Amide II bands still be present at 1659 and 1548 cm^{-1}respectively.

Finally, the crosslinking bath (concentrated solution) was examined after immersion of mats to have a further check for possible leaking of protein in solution (Figure 4.12). The lack of Amide bands in the spectra suggested that protein release during the crosslinking treatment was negligible, as hypothesized in Chapter 3 upon the analysis of fiber diameter.

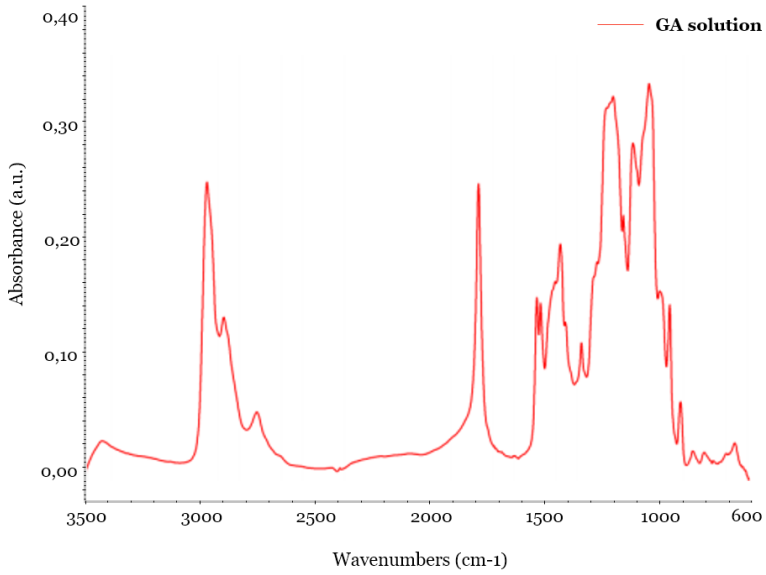

Figure 4.12 – Spectrum of the crosslinking solution after nanofiber treatment, showing the characteristic peaks of GA but no Amide bands from the BSA.

Thanks to the analysis carried out onto the mats and the resulting spectra, we can state that the electrospun PVA/BSA mats are stable against dissolution in water and, consequently, no loss or alteration of protein occur throughout the overall production of the sensing membrane. Starting from these data, a further investigation, regarding the electrospun mats as biosensing tools, is advanced (see Chapter 5).

Chapter 5
Electrospun Membranes for Biosensing

In order to explore the possible use of PVA/BSA nanofibrous mats in biosensing, they have to be further functionalized with a secondary small biomolecule, which is the bioreceptor for the fibrous sensing platform. The bioreceptor has to strongly and stably bind with BSA. This is fundamental to provide reliable outcomes [27]. Biotin, commonly known as vitamin B7, represents an attractive choice. It is widely used in biomedical field, since it easily forms strong non-covalent bonding and it is highly selective towards proteins such as Avidin and Streptavidin and towards chemically synthetized peptides due to their tryptophan residues. In the chemical structure, biotin presents condensed imidazole and thiophene ring, to which a side chain of valeric acid is bound (Figure 5.1).

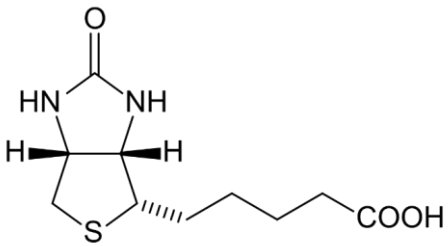

Figure 5.1 – Chemical structure of a non-labeled Biotin.

The crosslinked and fully characterized PVA/BSA membranes were immersed into an aqueous solution of biotin to be immobilized, as the bioreceptor, onto the fiber surface. Before considering the potential and future applications of the electrospun functionalized mats with biotin, it is particularly important to

identify a suitable quantification technique of the Biotin, which would be absorbed by PVA/BSA nanofibers. The fluorescence analysis of electrospun PVA/BSA mats could not be used, since BSA undergoes photobleaching during time (Figure 5.2) due to UV irradiation [118]. In sensing, a fundamental requirement for the active layer is to generate a stable base signal over time. Therefore, BSA emission was not a reliable method to quantify the presence of any type of immobilized target onto PVA/BSA mats including Biotin.

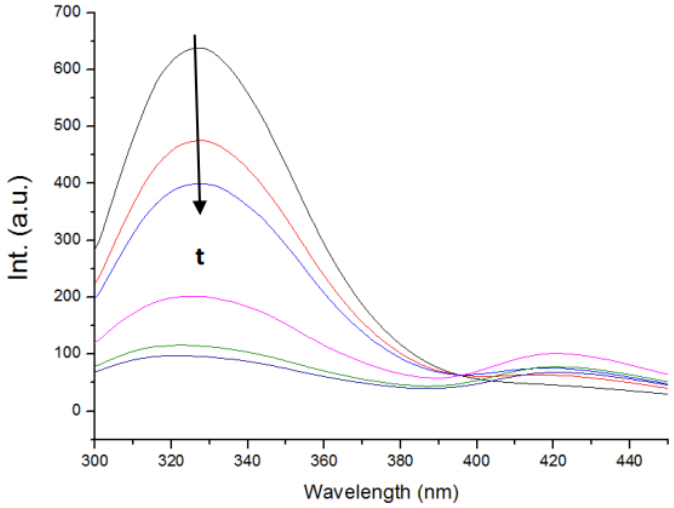

Figure 5.2 – Fluorescence signal from an electrospun mat with 10% BSA loading at different irradiation times (from 1 to 100 minutes) [118].

Hence, in order to determine the amount of biotin immobilized onto the PVA/BSA fibers, we measured the residual biotin remained in the solution after the immersion of the nanofibrous PVA/BSA membrane. This can be accomplished using the UV-visible spectroscopy, as it will be described in the following section. Moreover, we referred to *Wang et al.* who studied the interaction of biotin with bovine serum albumin in solution [119]. They synthetized the biotin-modified BSA by a carbodiimide coupling process and analyzed their chemical interaction by FTIR analysis, highlighting that biotin-BSA coupling occurred due to the binding of carboxyl groups of biotin with the primary amino group of BSA. However, in this study no biotin quantification had been performed.

5.1 Quantification of Atto 520-Biotin

As a preliminary investigation, a fluorescently labeled biotin, the Atto 520-biotin (Figure 5.3 (A)), was tested and analyzed in its potential binding to an electrospun mat of PVA/BSA with 10% protein loading. The idea was to quantify the general immobilization of a pristine biotin using the specific absorption and emission features of this functionalized Atto 520-Biotin. In particular, the Atto 520-Biotin has a characteristic pinkish to reddish color in water, and presents a sharp absorption band at ~ 520 nm and a sharp emission band at ~540 nm (Figure 5.3 (B)).

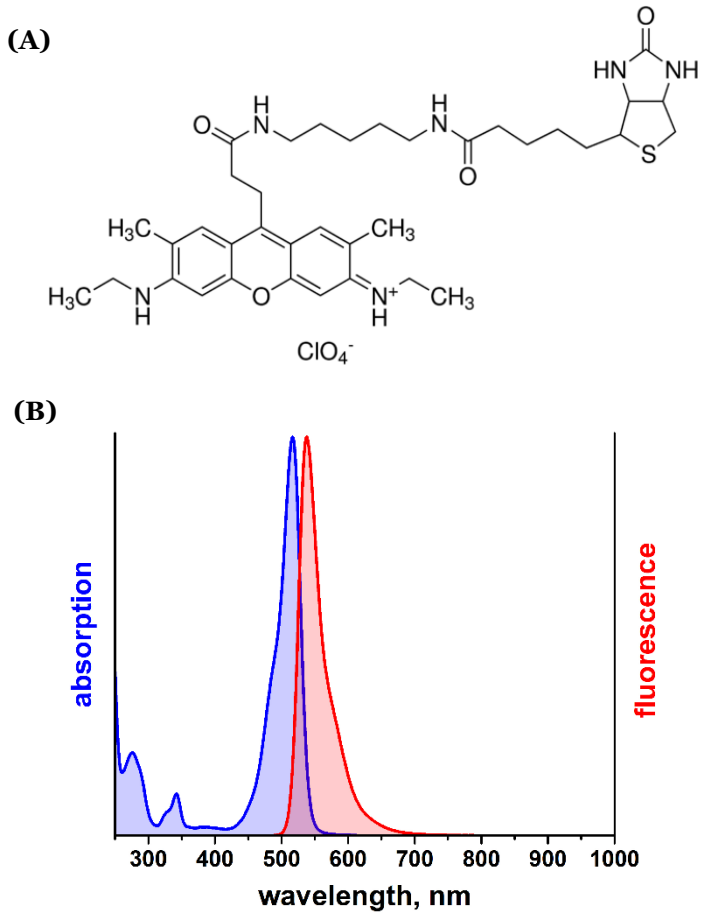

Figure 5.3 – (A) Chemical structure of Atto 520-biotin; (B) absorption and emission spectra of Atto 520-Biotin.

The immobilization of the functionalized biotin onto the PVA/BSA membrane was performed by (i) filtering a solution containing a known content of the target through the nanofibrous membrane, or (ii) upon immersion of the nanofibrous membrane into the solution. The weighted content of Atto 520-Biotin in the solution was related to the absorbance of the solution at λ ~ 520 nm through the well-known Lambert-Beer law:

$$A = \varepsilon \cdot l \cdot [C] \qquad \textbf{(Eq. 5.1)}$$

where "A" states for the absorbance of the sample, "l" for the optical path, "[C]" for the concentration of the analyte and ε for its molar extinction coefficient or molar absorption coefficient. The correct method requires the preparation of a number of solutions at different known concentration and the measurement of the related absorbance. The interpolation of the data as a straight line allows to determine the absorption coefficient ($1{,}1 \cdot 10^5 \cdot l \cdot mol^{-1} \cdot cm^{-1}$[120]), and to determine the calibration curve. Equation 5.1 is valid over the whole spectrum in a given concentration range and for a given solvent, but it is usually employed at the absorbance maximum. Hence, the calibration curve is then applied to determine any unknown concentration of analyte in a solution.

Here, the filtration experiments were performed by means of a custom setup, consisting in a 10 ml syringe with a filtering module attached in place of the needle. The filtering module was in turn made up of two distinct parts: (i) a metallic holder, which is fixed to the syringe tip and can be opened to place fibrous mats, and (ii) a set of Teflon O-rings to hold the film in place. The self-standing PVA/BSA fibrous mat was folded and put in the paper filter slot (Figure 5.4).

Electrospun membranes were produced with 10% BSA loading and were weighed after electrospinning, in order to have a precise quantification of the total protein content. Subsequently, a biotin aqueous solution ($7{,}3 \cdot 10^{-6} M$), prepared by diluted solutions from a mother solution ($6{,}43 \cdot 10^{-5} M$), was analyzed with a UV-visible spectrometer to determine the intensity of the absorption peak before filtration. Then, a known volume (i.e. 4 mL) of such solution was loaded in the syringe, filtered through the electrospun membrane and the filtrate collected to be analyzed. Hence, the quantity

of the residual unbound biotin was measured, i.e. the quantity of biotin immobilized onto the fibrous membrane was determined as the subtraction between the quantity of biotin in the solution before and after filtration. Specifically, known the molar absorption coefficient, the weight of the mat and the volume of the interacting solution, the quantity of biotin filtered by the mat was computed and normalized on the mat weight. In particular, by knowing the BSA content and the mass of filtered biotin, it is also possible to calculate the number of target molecules catched by each protein. This evaluation was done both in case of a complete availability of the protein at the mat surface and in case of a homogeneous distribution of the protein throughout the fiber volume (see Appendix I for the mathematical analysis).

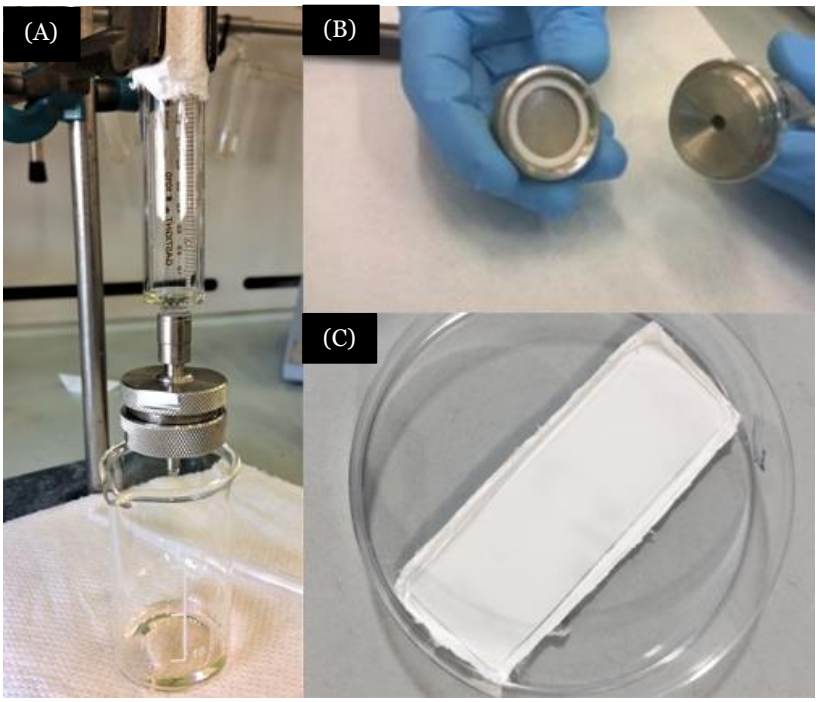

Figure 5.4 – The above images represent: (A) the experimental setup for filtration; (B) the empty filtering module and (C) an example of a self-standing mat containing 10% of BSA used in filtration.

Filtration experiments were performed both for pure PVA membranes, which work as an inactive filtering media to be used as standard reference value, and for different PVA/BSA mats of different thickness (i.e. weight). During the first filtration of

aqueous biotin solution through a PVA/BSA mat, a drop in the absorption peak intensity was experienced, which means that a certain amount of the target was absorbed by nanofibers. In the case of a bare PVA mats instead, no filtration of biotin occurred. An analogous result was obtained for immobilization of the target upon immersion of membrane or cast films into the biotin solution. In fact, there were no visible differences in the absorption peaks of the vitamin before and after immersion of the bare PVA mats. This demonstrates that PVA is not able to bind biotin, and the decoration with a biofunctional species (i.e. BSA) is required to enable the target catching. Multiple filtration measurements have been carried out, and results are reported in Table 5.1 as averages. A scheme of the process for two specific samples (i.e. pure PVA and PVA/BSA mats) is also reported in Figure 5.5.

Membrane type	Mass of Biotin per gram of membrane [µg/g]	Molecules of Biotin per BSA unit (surface distribution)	Molecules of Biotin per BSA unit (homogeneous distribution)
PVA	0	0	0
PVA/BSA	132 ± 28,5	2,7 ± 0,4	14,2 ± 1,5

Table 5.1 – Amount of biotin immobilized from single filtration tests

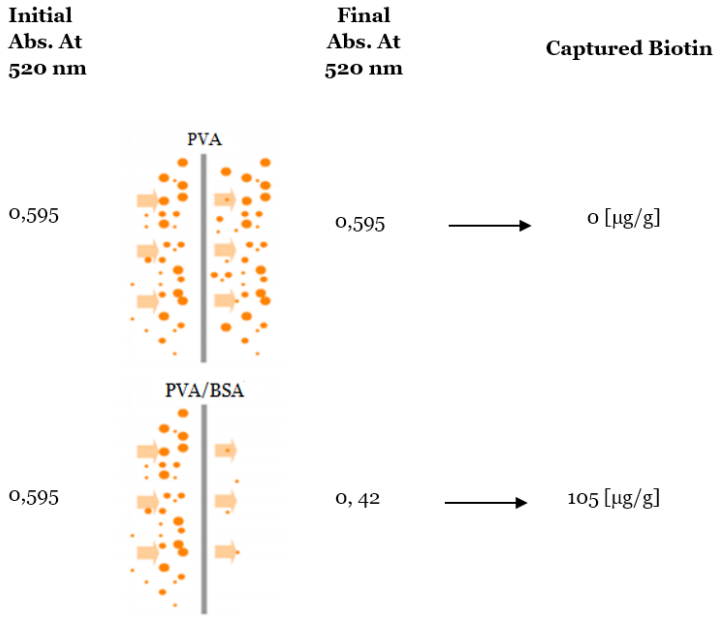

Figure 5.5 – Filtration tests by using: a bare PVA mat (on top) and a PVA/BSA mat (at the bottom). The different filtration efficiencies are reported.

In order to further characterize the bioactivity of nanofibers towards biotin, more filtration steps have been performed:

- The solution used in first filtration was collected and further filtered twice employing the same starting membrane without any rinsing step;
- Afterwards, a cleaning step by means of distilled water was carried out, enabling the removal of free biotin, which derives from its weak interaction with the BSA;
- A new solution with concentration $7{,}3 \cdot 10^{-6} M$ was driven through the regenerated filter and probed in the UV-visible spectrophotometer.

A schematic representation of the steps above described is presented in Figure 5.6.

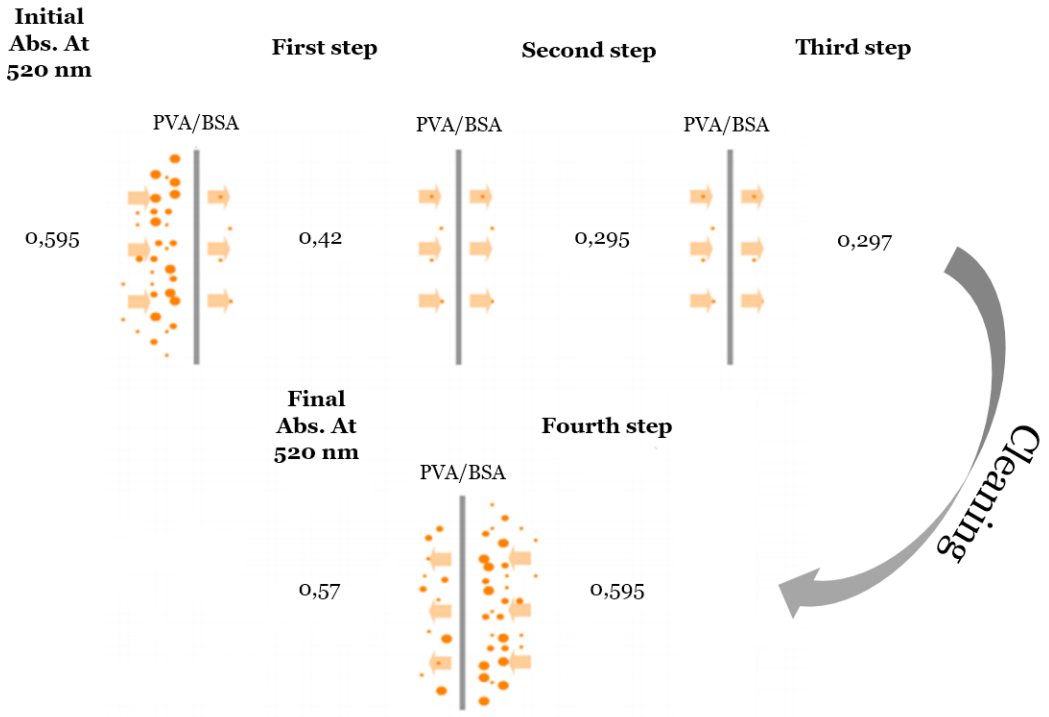

Figure 5.6 – Results obtained using the same nanofibrous mat with complete filtration run.

As we can see from the results, even after the first filtration run a measurable variation of the absorption peak intensity was experienced. Moreover, the value reached with the second filtration run can be approximately achieved in one filtration step, leading to 160 [μg/g] of biotin per mass of mat (Figure 5.7). After the second filtration run,

the absorption peak remained constant or grew a little, proving that in a maximum of two filtration steps the mat reaches its highest absorption capacity; consequently, no further reduction of biotin concentration is experienced in later runs.

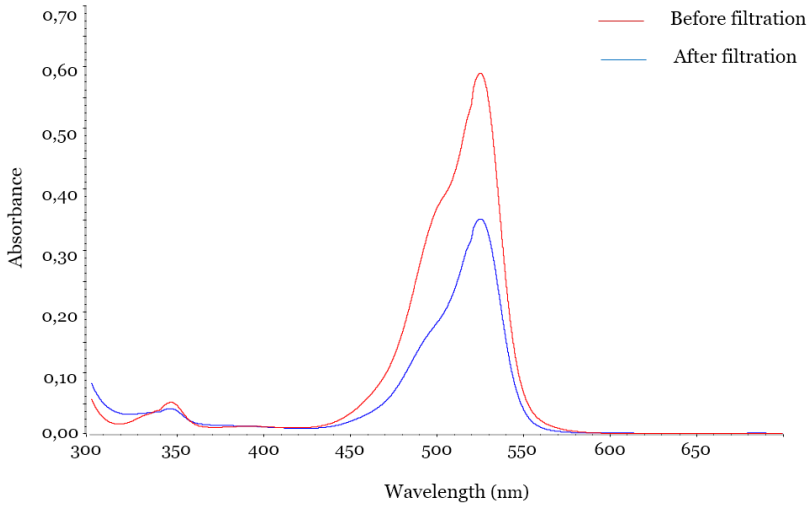

Figure 5.7 – UV-visible spectra showing the absorption bands of an Atto 520-Biotin solution bath before (red line) and after (blue line) first filtration step by a PVA/BSA membrane.

The stability of the immobilization of the biotin derivative onto PVA/BSA membranes have been also investigated. A stable binding means that the biotin can be used as a receptor site to probe relevant biomarkers, thus developing a fluorescence platform for biosensing. On the contrary, a reversibility of the biotin catching process, makes the PVA/BSA membranes reusable filtering media. The membrane regeneration test was performed upon immersion of the PVA/BSA/biotin mat in distilled water followed by a new filtration run of a freshly prepared biotin solution. A decrease in intensity of the absorption band of the biotin solution was noticed after filtration, underling that the membrane was still active by the regeneration process (13,6 micrograms of biotin per gram of mats are immobilized). However, the catching of the biotin by the regenerated membrane was much weaker than the one obtained with the first test, indicating that the regeneration process was not complete. This demonstrates that some biotin molecules (ca.90%) strongly bind BSA leading to irreversible immobilization onto the fiber surface.

The ability of electrospun nanofibers to immobilize biotin on their surfaces was further confirmed performing long immersion tests. Mats with various BSA content were immersed in a set volume of biotin aqueous solution (i.e. 4 mL) for at least 4 h. Once dried, the nanofibers are rinsed in distilled water for 1 h, which is analysed by UV-vis spectroscopy (Figure 5.8). As highlighted in case of filtration, it is possible to notice a sharp decrease in the absorption peak after immersion of a PVA/BSA membrane in biotin bath and a very low absorption of water solution upon rinsing. This means that the system is able to permanently incorporate the biotin (almost 90%), even after immersion in distilled water. The Atto 520-Biotin immobilized during the first immersion was quantified by means of the Lambert-Beer law. 710±5 micrograms of biotin per gram of mat without rinsing in water have been calculated.

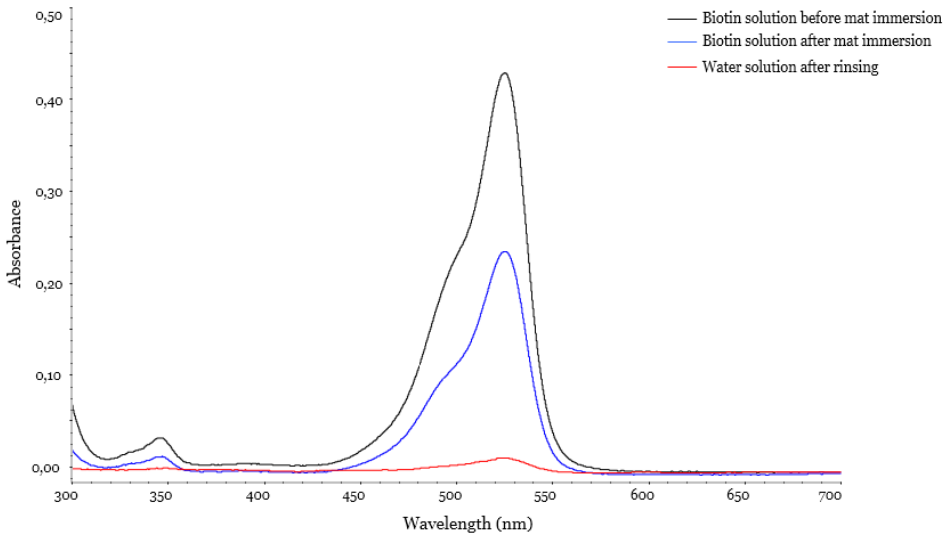

Figure 5.8 – Spectra of a biotin solution before PVA/BSA mat immersion (Black line), after PVA/BSA mat immersion (Blue line) and water solution after rinsing of a PVA/BSA/Biotin mat (red line).

To sum up, we have demonstrated a biohybrid functional platform with fibers stably decorated with a fluorescent biotin, which can be used as receptor in biosensing, where the variation of the Atto 520-Biotin fluorescence can be potentially exploited to quantify a specific target of biological relevance in biomedical diagnosis.

5.2 Fluorescence Analysis

Fluorescence was used to probe the presence of biotin in the PVA/BSA electrospun mats. Specifically, a quantitative analysis of the fluorescence efficiency was carried out by measuring the quantum yields of PVA/BSA mats after their immersion in aqueous Atto 520-biotin solutions and to quantify the possible biotin leaking in water. As previously reported, the selected biotin is labeled with the Atto 520 dye, which presents an emission band at ~ 540 nm. This cationic dye has a pinkish color in aqueous solutions and a yellowish emission upon illumination with light in the visible range (Figure 5.9). Atto 520 is a recent fluorescent label derived from the well-known Rhodamine 6G. Characteristic features of the label are strong absorption, high fluorescence quantum yield, poor intersystem crossing, high thermal and photo-stability. These characteristics make it very suitable for fluorescence analysis.

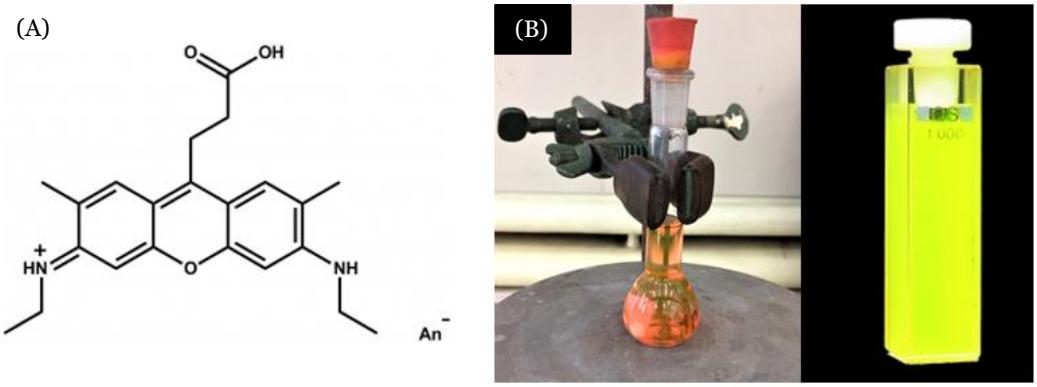

Figure 5.9 – (A) Chemical structure of Atto 520 dye responsible for Biotin derivative fluorescence and (B) aqueous solution containing tagged biotin before (pink) and after illumination with light in the visible range (yellow).

In order to have a precise insight of biotin fluorescence, we have to consider that also bovine serum albumin is a fluorescent protein, which can undergo quenching interacting with chemical and biochemical species. In particular, protein fluorescence is usually related to the existence of phenylalanine (Phe), tyrosine (Tyr) and tryptophan (Trp) residues belonging to its amino acid sequence. However, the

contributions of Tyr and Phe to the intrinsic fluorescence is almost negligible: Phenylalanine has a small absorption coefficient, while Tyrosine has a low fluorescence quantum yield due to different quenching mechanisms with the peptide chain of the protein or by energy transfer [121]. Therefore, BSA fluorescence is mainly caused by tryptophan (Figure 5.10), namely Trp-212, which is located in a cleft of the second domain and Trp-134, close to the surface of the protein (see Chapter 2 for the structure of BSA).

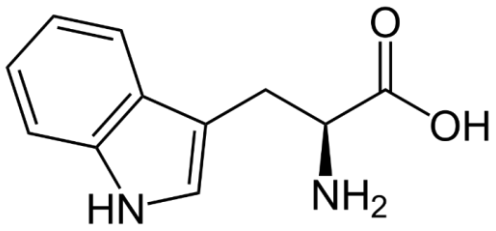

Figure 5.10 – Chemical formula of tryptophan residue responsible for BSA fluorescence.

Once defined the chemical species involved in fluorescence of biotin and BSA, samples preparation procedures for photoluminescence (PL), photoluminescence-excitation (PLE) analyses and subsequent quantum yields evaluation are discussed in the following sections.

5.2.1 PL and PLE analyses

Photoluminescence (PL) and Photoluminescence-Excitation (PLE) measurements were performed to check the position of BSA extinction and emission bands and to find the best excitation wavelength for biotin, which results in its most intense fluorescence. All the excitation and emission spectra below reported were recorded with the spectrofluorometer shown in Figure 5.11 characterized by a Xenon lamp 400W as continuous light source. It is provided with a photomultiplier tube and a charge coupled detector. The first one is used to detect excitation spectra recording wavelength by wavelength; instead, the second one is employed for photoluminescence spectra, recording the whole wavelength range concurrently. Moreover, two monochromators are present, one for emission and one for excitation.

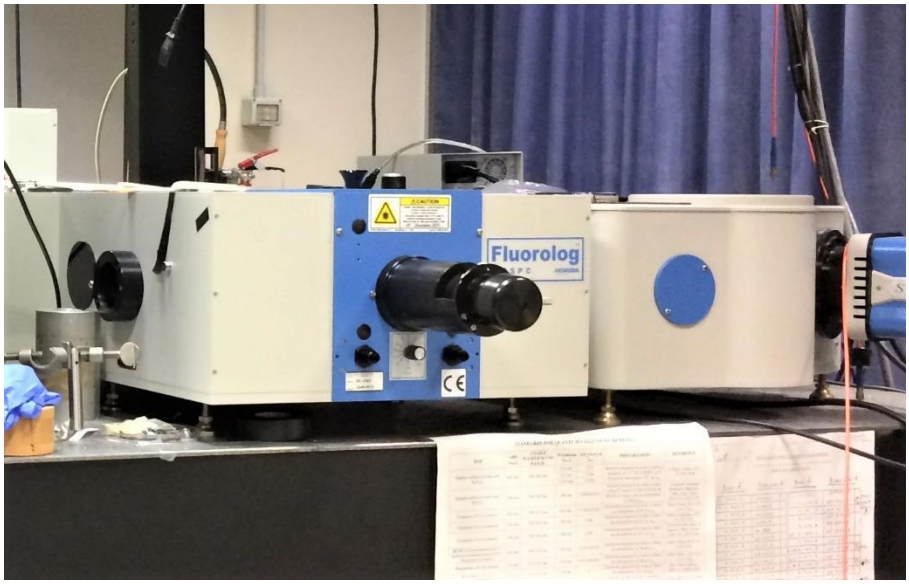

Figure 5.11 – Spectrofluorometer Fluorolog HORIBA used to record the PL and PLE spectra.

Two specific samples were prepared: a PVA/BSA membrane free from biotin and a PVA/BSA/Biotin mat. The latter was obtained starting from an electrospun and crosslinked PVA/BSA mat characterized by 10% protein loading, which was detached from its glass substrate and subsequently immersed in a aqueous solution containing the tagged biotin ($7{,}3 \cdot 10^{-6} M$) for at least 4 hrs. Afterwards, it was removed from the solution and left to dry for several hours, without rinsing in water. Once dried, the mat was a self-standing mat and that can be analyzed in the spectrofluorometer. In particular, both the samples were fixed on the sample holder and illuminated with different excitation wavelengths. The excitation wavelengths and the resulting spectra are reported in Table 5.2 and shown in Figure 5.12, respectively.

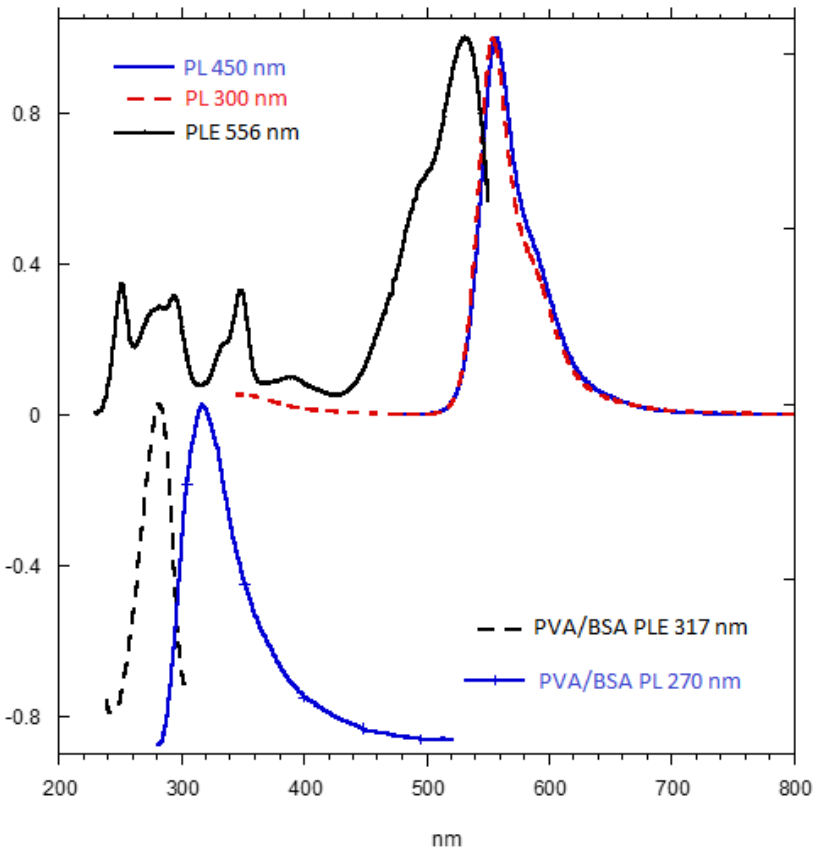

Figure 5.12 – Absorption and emission spectra of PVA/BSA and PVA/BSA/Biotin mats obtained with different excitation wavelength.

Sample	Excitation wavelength	PL maximum	PLE maximum
PVA/BSA mat	270 nm	317 nm	-
PVA/BSA mat	317 nm	-	280 nm
PVA/BSA/biotin mat	450 nm	556 nm	-
PVA/BSA/biotin mat	300 nm	556 nm	-
PVA/BSA/biotin mat	556 nm	-	520 nm

Table 5. 2 – Summary of the excitation wavelengths and respective PL and PLE maximum obtained analyzing two samples: (A) PVA/BSA mat and (B) PVA/BSA/Biotin.

On the basis of the data collected, we decided to use 510 nm as the main excitation wavelength to perform the following fluorescence quantum yield analyses.

5.2.2 Fluorescence Quantum yield measurement

The procedure employed to produce the samples used in PL and PLE analyses is followed for different PVA/BSA mats containing 10% and 15% BSA loads, having circular or rectangular shapes and functionalized with Atto 520-biotin by immersion. In this case, the immersion took place in a set volume of biotin in order to find a correlation between the amount of immobilized biotin, which is tested by UV-visible analysis (see Chapter 4) and the fluorescence intensity. Once the immersion ended and the mats were dried, they were tested using an adapted Labsphere IS-060 shown in Figure 5.13.

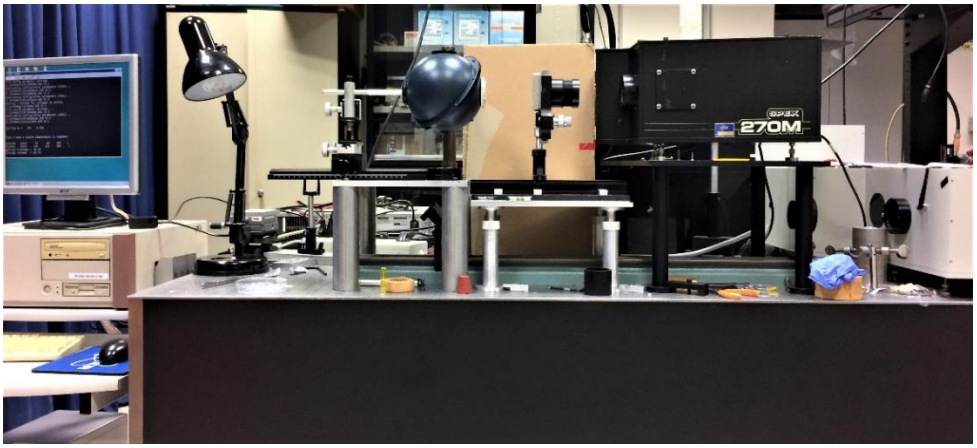

Figure 5.13 – Image of Labsphere IS-060 used to measure fluorescence quantum yield.

The evaluation of the fluorescence quantum yield (see definition in Appendix I) of the self-standing electrospun mats, was done by performing three different measurements per each sample:

- **Measure a** – sample holder without the specimen is inside the sphere;
- **Measure b** – sample holder with the specimen inside the sphere and the light does not directly hit the sample;
- **Measure c** – the light hits the sample inside the sphere.

Consequently, three emission spectra per each sample were collected (Figure 5.14) and used to obtain a precise measurement of quantum yields (see mathematical analysis in Appendix I). The integrating sphere employed is a fundamental optical component consisting of a hollow spherical cavity with its interior covered with a diffuse white reflective coating, with small slits that allow the entrance and exit of the samples and the passage of the light rays. Thanks to the internal reflective surface, light incident on any point is equally distributed by multiple scattering reflections. This is the reason why even in measure "b", the emission spectra of samples presented a peak related to biotin fluorescence.

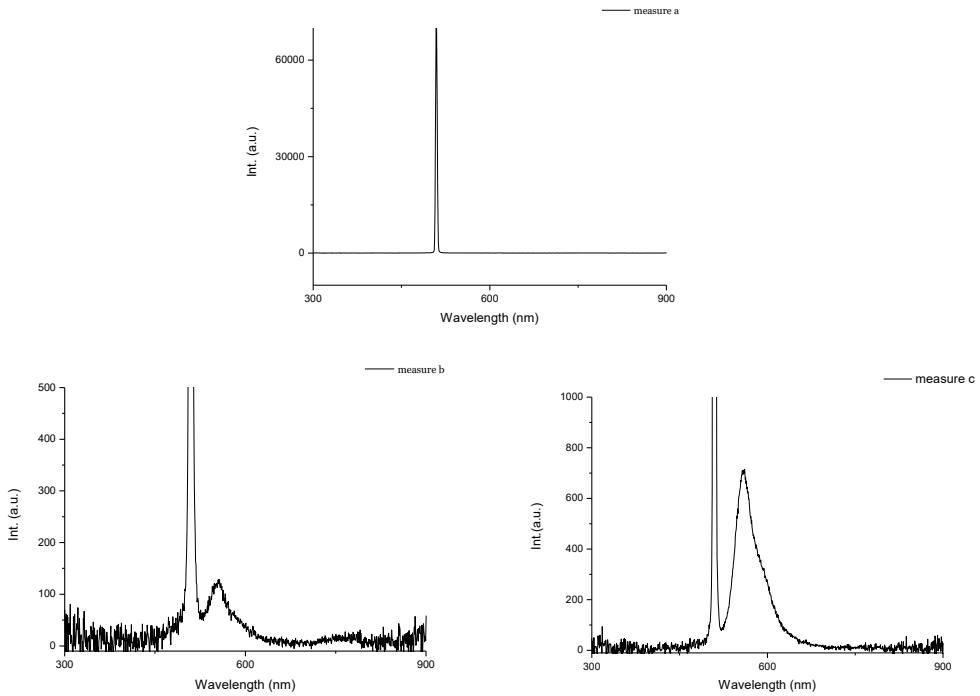

Figure 5.14 – Example of spectra obtained from the analysis of a PVA/BSA/Biotin electrospun mat: measure "a" and measure "b" (on top) and measure "c" (at the bottom).

The same electrospun mats previously analysed immediately after immersion in a biotinylated solution, were then immersed in distilled water for at least 1 h and tested following the same procedure. By looking at the measure "c" spectrum (Figure 5.15) recorded after rinsing in water the same PVA/BSA/Atto 520-Biotin mat of the spectra in Figure 5.14, it can be seen that a slight increase in fluorescence intensity occurred. Hence, the emission in measure "c" after rinsing was higher than that one obtained just upon immersion in a biotinylated solution and dried. Moreover, the maximum moved towards shorter wavelength. This trend was further confirmed looking at the quantum yields of all the analysed mats. In fact, they increase upon rinsing in water, as reported in Table 5.3 for two specific samples: 12wt.% PVA/10% BSA load/Atto 520-Biotin (Sample 1) and 12wt.% PVA/15% BSA load/Atto 520-Biotin (Sample 2).

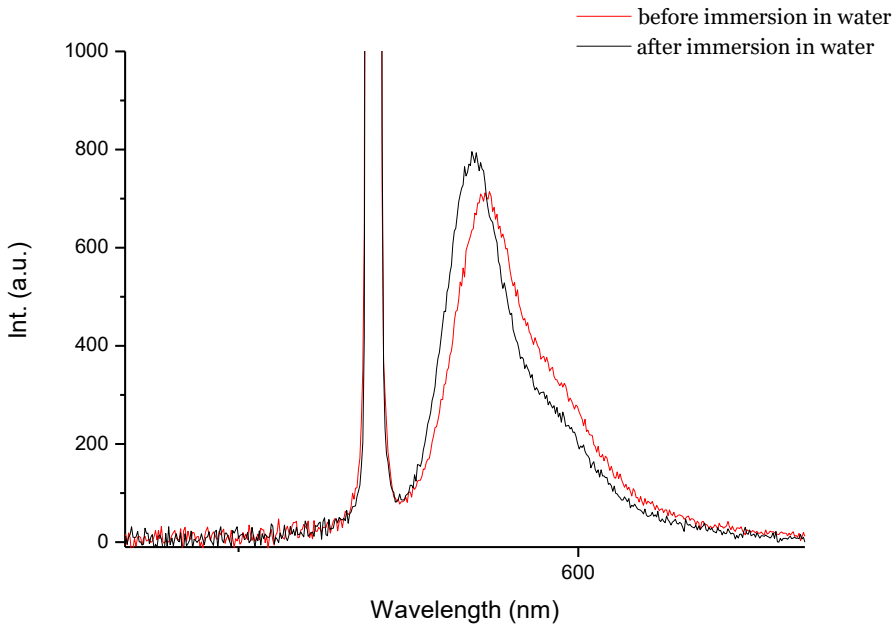

Figure 5.15 – Spectra of a PVA/BSA/Biotin mat resulting from measure "c" before (red line) and after (black line) immersion in water.

	Sample1 (Before immersion in dH2O)	Sample1 (After immersion in dH2O)	Sample 2 (Before immersion in dH2O)	Sample 2 (After immersion in dH2O)
La	254979,6	239789	237771,8	242987
Lb	249852	244449	236445	236785
Lc	167722,9	192557	115489,6	144551
La*λ	129880,8	122171	121118,8	123797
Pb*	1776	1548	3635	3184
Pc*	21543	20587	37558	35764
$\frac{\text{TauP}}{\text{tauL}}$	1	1	1	1
A	0,33	0,21	0,51	0,39
Abs	0,173	0,104	0,311	0,214
QY	0,48	0,75	0,58	0,7

Table 5.3 – Summary of QY and absorbance obtained from the analysis of Sample 1 and Sample 2 before and after immersion in water.

In order to explain the variation of emission intensities in our samples, i.e. of fluorescence quantum yields, we considered the possibility of aggregates formation in solid-state materials. In fact, as stated by *Banerjee et al. [122]* the photophysical behaviour of an aggregated solid-state material can be very different from its solvated molecule in diluted solution (i.e. Atto 520 $QY_{solution}$ = 90%). Different structural arrangement and intermolecular interaction in solid-state material can lead to changes in the optical features. Fluorescence quenching and red shift in absorption and emission spectra are examples of optical changes related to aggregates formation [123]. Since in the spectrum before immersion in water, we measured a lower intensity and a red shift (red line in Figure 5.16) compared to the rinsed sample, we can state that this behaviour is related to solid state interactions. Hence, rinsing allows to remove weakly interacting Atto 520-Biotin from the PVA/BSA fiber surface, leading to better disperse immobilized fluorescent biotin with a consequent increase in quantum yield. The high fluorescence efficiency of Atto 520-Biotin experienced in PVA/BSA mats is an extremely promising outcome. It can be exploited to develop bioprobes for the detection of tumor markers (i.e. anti-p53 autoantibody), proteolytic

enzymes and proteins (i.e. Streptavidin), since they contain tryptophan residues that work as quenching agents. To confirm this hypothesis, preliminary and qualitative tests were performed.

5.2.3 Qualitative Quenching Test

Understanding the dependence of spectroscopic properties of fluorescent dyes on their microenvironment conditions and external agents is crucial for the development of new fluorescence-based assays. Many fluorescent dyes can be used as sensors to probe their local environments in biological and analytical applications. For example, rhodamine and oxazine dyes are known to be efficiently quenched by the nucleobase guanosine and the aromatic amino acid tryptophan (Trp) [124]. Indeed, the most powerful fluorescence quenchers among the natural amino acids are Methionine (Met) and Histidine (His), while among the aromatic amino acids are Tryptophan (Trp), Tyrosine (Tyr) and Phenylananine (Phe).
The effect of tryptophan, as well as of other target molecules, on the fluorescence quenching at different concentrations can be quantified trough the Stern-Volmer equation:

$$\frac{F_0}{F} = 1 + K_s[Q] = K_{q,s}\tau_0[Q] \qquad \textbf{Eq. 5.2}$$

Where τ_0 and F_0 are the fluorescence lifetime and intensity in the absence of a quencher, τ and F are instead the fluorescence lifetime and intensity in the presence of the quencher Q with concentration [Q]. Finally, K_s is the static constant [125].
Motivated by these considerations and referring to the study conducted by *Marmè et al.* [125], we run a qualitative quenching test using DL-tryptophan as quenching agent for the Atto 520-Biotin. The preparation of a suitable sample for the quenching test required few steps: crosslinking of an electrospun mat (12wt.% PVA and 10% BSA load); mat immersion in an aqueous biotin solution ($7{,}3 * 10^{-6}M$) for 4 hrs; rinsing of the mat in distilled water for 1 h and, a subsequently immersion in tryptophan

solution for another hour. Particularly, as stated by *Marmè et al.,* aqueous solutions containing tryptophan (i.e. 30 mM and 6 mM) were prepared. Since the isoelectric point of tryptophan is 5.9, basic solutions were needed to reach its complete dissolution. Hence, in case of the 30 mM concentration, an addition of 100 µL of ammonium hydroxide solution to distilled water was required. Whereas, in case of the 6 mM concentration, the weighed tryptophan powder was directly added to distilled water and stirred at 40°C for 1 h. Consequently, transparent solutions were obtained (Figure 5.16).

Figure 5.16 – Tryptophan solutions with 6mM concentration (on the left) and 30mM concentration (on the right)

Once the immersion in tryptophan solution was completed, the mat was left drying. In order to highlight the difference between quenched and non-quenched samples, three different specimens were prepared and analysed: (i) a PVA/BSA/Atto 520-Biotin after rinsing in water (sample 1), (ii) a PVA/BSA/Atto 520-Biotin after rinsing and immersion in tryptophan solution (sample 2) and (iii) a PVA/BSA/Atto 520-Biotin without rinsing in water (sample 3). The resulting photoluminescence (PL) spectra are shown in Figure 5.17. As expected, the sample 2 and sample 3 have a lower fluorescence emission intensity than sample 1. This because in sample 3 and sample 2, we have aggregates formation (see Section 5.2.2) and tryptophan that cause Atto 520 fluorescence quenching, respectively.

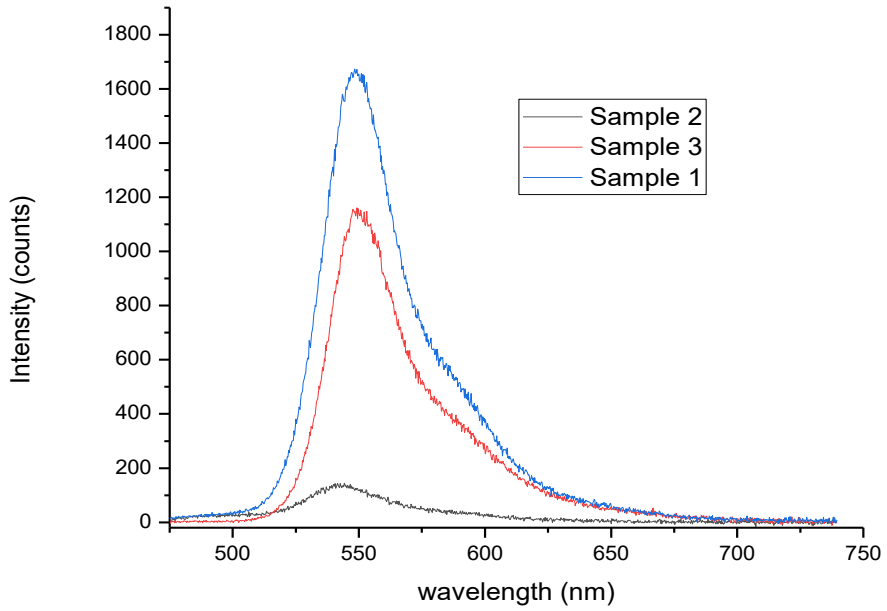

Figure 5.17 – Spectra of a PVA/BSA/biotin mat after rinsing in water (blue line), a PVA/BSA/biotin mat after rinsing and immersion in water (black line) and a PVA/BSA/biotin mat without rinsing in water.

The effective result found confirms that the electrospun membranes herein produced can be used to detect anti-p53 autoantibodies (tumor markers), proteolytic enzymes and Streptavidin. Since gene mutation in p53 – the guardian of the genome –is the most frequently found abnormality in human cancer and often triggers the immune system to produce antibodies directed against the nuclear tumor suppressor protein p53 (i.e. the DNA transcript of the p53 gene), they can be used as promising fluorescence-based bioassays for early-stage cancer diagnosis [126] [127]. In fact, the presence of p53-autoantibodies in human serum validates a malignant disease (i.e. lung and breast cancers) with a specificity of 100% if autoimmune diseases are neglected [127].

In order to detect the anti-p53 autoantibody, a short peptide epitope derived from the antibody recognition sequence of p53 has to be synthetized: a sequence of 14 amino acids containing one tryptophan residue, which causes fluorescence quenching [126]. Then, this sequence is able to bind to the anti-p53 autoantibody. The effectiveness of

the binding between peptide sequence and anti-p53 autoantibody can be in theory confirmed by using a secondary antibody labeled with a fluorophore.

The fluorescence quenching by means of tryptophan can be further exploited to investigate the Biotin-Streptavidin binding. Indeed, each hydrophobic binding pocket of streptavidin contains four tryptophan residues that are involved in strong biotin binding (Figure 5.18).

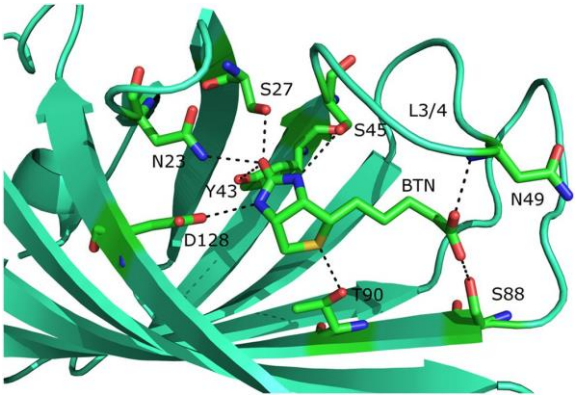

Figure 5.18 – Binding of biotin to the wild-type streptavidin. Hydrogen bonds are marked as dashed lines.

The binding between biotin and Streptavidin can be further characterized by using a labeled Streptavidin with horseradish Peroxidase (HRP). In fact, in presence of tetramethylbenzidine (TMB) substrate and H_2O_2, it becomes blue. The blue color develops in proportion to the amount of analyte present in the sample. Already existing studies exploit the HRP-streptavidin pair such as the ELISA assay (Figure 5.19). Hence, fluorescence and UV-vis analyses can be potentially used to investigate and quantify the biotin-streptavidin binding.

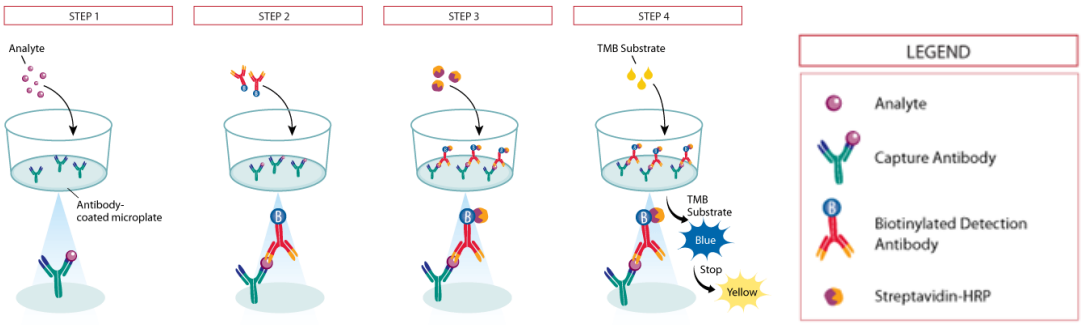

Figure 5.19 – Example of an ELISA assay. Step 3 and step 4 highlight the biotin-streptavidin interaction and the use of HRP labeled streptavidin.

Conclusions

In the present work, we have developed nanofibrous biofunctionalized mats suitable for biosensing applications.

Homogeneous and defect free nanofibrous membranes with extremely small diameters ($d_{average}$ = 144±28 nm) were produced from a feed solution of poly(vinyl alcohol) and bovine serum albumin (PVA/BSA blend) by means of electrospinning. In order to achieve water resistance, enabling their use in aqueous and moist environments, the electrospun membranes were chemically crosslinked by a fast immersion in a glutaraldehyde bath. The nanostructured morphology kept unchanged and stable throughout the overall production process and also in all working life of the biofunctional membranes.

The characterization of PVA/BSA mats, both before and after crosslinking and upon their immersion in water, was performed by FTIR and Bradford protein assay. The resulting outcomes demonstrate that BSA does not undergo significant changes in any of the processing steps. Afterward, the bioactivity of BSA functionalized membranes was tested in filtration experiments of a molecular target (i.e. Biotin). During the process, the target interacts with specific sites of the immobilized protein, leading to the immobilization of 132±28,5 micrograms of biotin for each gram of mat. Even after an extensive rinsing step, almost 90 % of this value remained stable and immobilized within the fibers. The ability of the system to permanently bind Atto 520-Biotin was further investigated with long rinsing tests.

In order to further characterize the biotin/BSA biohybrid platform as a fluorescence sensor of biomolecules, we performed fluorescence analyses, exploiting the peculiar optical properties of Atto 520-Biotin conjugate. Firstly, photoluminescence (PL) and photoluminescence-excitation (PLE) analyses were performed to find the best excitation wavelength, which allows achieving the highest emission intensity of this emissive biotin. The most suitable wavelength resulting from these analyses (510 nm)

was used for the quantification of mats (PVA/BSA/Biotin) fluorescence quantum yields before and after immersion in water. Quantum yield of water-rinsed PVA/BSA/Atto 520-Biotin turned out to be very high, which makes this fibrous mat a promising platform for biosensing.

Finally, a preliminary analysis of Biotin fluorescence quenching induced by tryptophan was performed with good results, opening the way for using this sensing platform to detect proteins (i.e. Streptavidin and Avidin), tumor markers (i.e. anti-p53 autoantibody) or proteolytic enzymes that are involved in tumor progression and metastasis.

Appendix I
Mathematical Analysis

A.1.1 Estimation of BSA at the surface of homogeneous fibers

We considered a section of nanofiber, represented by a cylinder with an arbitrary length (L) of 100 nm and a base diameter (D) equal to the mean diameter of the fibers, so approximately 140 nm. The total volume of this structure can be easily evaluated:

$$V_{tot} = \frac{\pi D^2 L}{4} = 1{,}54 * 10^6\ nm^3 \qquad \textbf{(Eq. A.1)}$$

Knowing the density of PVA (ρ_{PVA} = 1, 19 g/cm^3), we can compute the total mass (m_{fib}) of the fiber, neglecting the influence of BSA on density:

$$m_{fib} = \rho_{PVA} * V_{tot} = 1{,}83 * 10^{-15}\ g \qquad \textbf{(Eq. A.2)}$$

With a protein content of 10%, the mass of BSA (m_{BSA}) in the total volume will be $1{,}83 * 10^{-16}\ g$; this value corresponds to 1660 albumin particles (N_{BSA}^{tot}), evenly distributed throughout the volume, with an equivalent particle density of:

$$\rho_{BSA}^{particles} = \frac{m_{BSA} * N_{avogadro}}{Mw_{BSA} * V_{tot}} = 1{,}08 * 10^{-3} particles/nm^3 \qquad \textbf{(Eq. A.3)}$$

We now only consider part of the total volume, namely the annular section with inner diameter (D_{inner}) equal to the diameter of the cylinder minus twice the diameter of a BSA particle (~ 7 nm), which will approximately contain all of the BSA particles exposed to the surface of the fiber (Figure A.1).

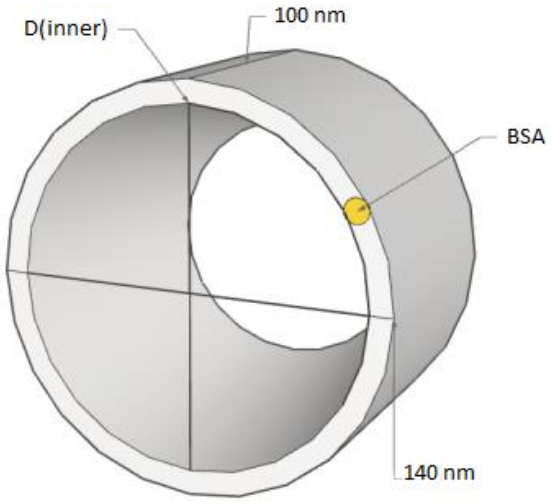

Figure A.1 – Representation of the annular section considered for the computation of surface-available BSA.

The volume occupied by this section can be computed:

$$V_{shell} = V_{tot} - \frac{\pi D_{inner}^2 L}{4} = 2{,}93 * 10^5\ nm^3 \qquad \textbf{(Eq. A.4)}$$

The number of BSA particles in this shell are given by:

$$N_{BSA}^{shell} = V_{shell} * \rho_{BSA}^{particles} = 316\ particles \qquad \textbf{(Eq. A.5)}$$

This means that assuming a homogeneous distribution, only 19 % of the overall BSA particles will be found at the surface:

$$Ratio(\%) = \frac{N_{BSA}^{shell}}{N_{BSA}^{tot}} * 100 = 19\ \% \quad \textbf{(Eq. A.6)}$$

Knowledge of the total mass of the mat used in filtration tests (m_{mat}) allows for the determination of the total content of BSA particles in membranes having a BSA loading (mass of PVA/ mass of BSA) of 10%:

$$N_{BSA}^{mat} = m_{mat} * \frac{0{,}1 * N_{avogadro}}{1{,}1 * Mw_{BSA}} \quad \textbf{(Eq. A.7)}$$

For the case of a complete surface distribution, this value will correspond to the number of BSA particles interacting with biotin (since biotin can only bind to the BSA at the surface). For the case of a homogeneous distribution, instead, we will have to introduce a correction factor (K):

$$K = \left(\frac{Ratio(\%)}{100}\right)^{-1} = 5{,}26 \quad \textbf{(Eq. A.8)}$$

By measuring the average quantity of target immobilized per gram of fibers by means of the Lambert-Beer law, we can therefore compute the number of biotin molecules bound to each BSA molecule in both cases:

$$\frac{N_{biotin}}{N_{BSA}^{surface}} = K * \frac{\frac{g_{biotin}}{g_{mat}} 10^{-6} * \frac{N_{avogadro}}{Mw_{biotin}}}{N_{BSA}^{mat}} \quad \textbf{(Eq. A.9)}$$

The correction factor will range from 1 (core/sheath configuration) to 5,36 (homogeneous distribution), thus allowing for the computation of 2,7 ± 0,4 molecules

of biotin per BSA unit in the first case, and 14,2 ± 1,5 molecules of biotin per BSA unit in the second.

In the real case of PVA/BSA nanofibers, where a preferential protein distribution at the surface can be assumed but, a true core/sheath structure could not be proven by TEM imaging, this correction factor (and therefore the number of molecules) will be in between the two values.

A.1.2 Determination of Fluorescence Quantum Yield

The fluorescence quantum yield (QY) of a dye is the fraction of photons absorbed resulting in emission of fluorescence:

$$Qy = \frac{\#\ photons\ emitted}{\#\ photons\ absorbed} = \frac{k_f}{\sum k_i} \qquad \textbf{(Eq. A.10)}$$

Where k_f is the fluorescence rate constant and k_i denotes the rate constants of all the decay processes from the first excited state of the fluorophore ($k_i = k_r + k_{nr}$).

The fluorescence QY can be evaluated depending on the sample physical state in which the fluorophore is:

- **QY measurement in solutions**

The QY of a fluorophore in solution is determined relative to a reference compound of known QY:

$$QY = QYRif\left(\frac{1-10^{-A_{rif}}}{1-10^{-A}}\right)\left(\frac{n^2}{n_{rif}}\right)\frac{AreaPL}{AreaPL_{rif}} \qquad \textbf{(Eq. A.11)}$$

Where QY_{rif} is the quantum yield of the reference compound, n is the refraction index, Area PL is the area under the peak obtained in the spectrum and has to be multiplied by λ and A is the absorbance at the excitation wavelength. The absorbance at the excitation wavelength is optimally kept in between 0.1 < A < 0.2 in case of 1 cm cell.

- **QY measurement in solids using integrating sphere**

In case of QY evaluation in solids, the use of integrating spheres with a laser as excitation source is generally required to collect the emitted light. In order to compute the QY, three different spectral scans per sample must be picked up:

i. Emission spectrum obtained when the sample holder, without the specimen, is inside the sphere (Measure "a").
ii. Emission spectrum obtained when the sample holder, with the specimen, is inside the sphere and the laser does not hit the sample (Measure "b").
iii. Emission spectrum obtained when the laser hits the sample inside the sphere (Measure "c").

Once all the spectra are acquired and the areas of luminescence ("P") and lamp ("L") are known and multiplied by λ, absorbance and QY can be determined:

$$QY = \frac{P_c^* - (1 - A)P_b^*}{A * L_a} \qquad \textbf{(Eq. A.12)}$$

$$P_{b/c}^* = P_{c/b} - \frac{L_{c/b}}{L_a} P_a \qquad A = 1 - \frac{L_c}{L_b}$$

Appendix II
Experimental Section

A.2.1 Branched-polyethylenimine (b-PEI) fibers

Fibers functionalization is a fundamental step to obtain a bioactive substrate, which can be exploited in biosensing. A good functionalization was achieved in few steps leading to a simpler and faster process. Accordingly, we tried to electrospun the branched-polyethylenimine instead of the poly (vinyl alcohol) (PVA)/ bovine serum albumin (BSA) blend, in which the addition of BSA is carried out to functionalize the surface of PVA electrospun nanofibers. In particular, the protein located at the surface of the fibers allows the binding with other small molecules such as biotin, which is commonly known as vitamin H. The reason why biotin binds easily to the protein is the presence of a primary amino group in BSA molecules. Since the b-PEI contains primary, secondary and tertiary amino groups at the estimated ratio of 1:2:1, it was selected as a valid alternative of BSA and preferred over the linear polyethylenimine (l-PEI), which contains mainly secondary amino groups (Figure A.1).

(A) **(B)**

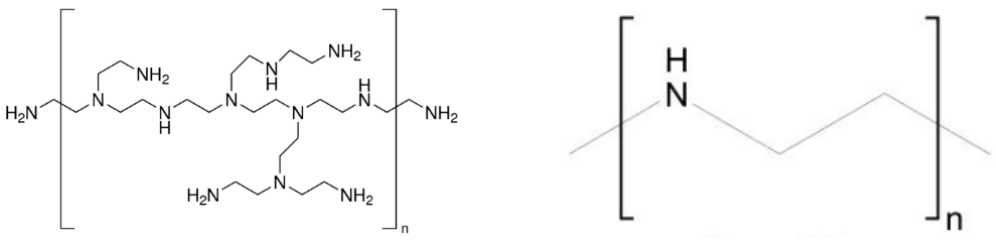

(C)

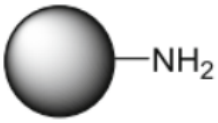

Figure A.1 – Chemical structures of (A) Branched-PEI and (B) Linear-PEI. (C) Schematic representation of a BSA molecule.

This can be further confirmed taking into consideration the study by *Zeng et al.* (2009). They analyzed the interaction between biotin and primary amino group of b-PEI [A] in solution to produce a potential targeting gene vector. More precisely, biotin was linked to a 25 kDa b-PEI using EDC (Figure A.2) and the resulting product was further purified to remove the residues of solvent and the free biotin.

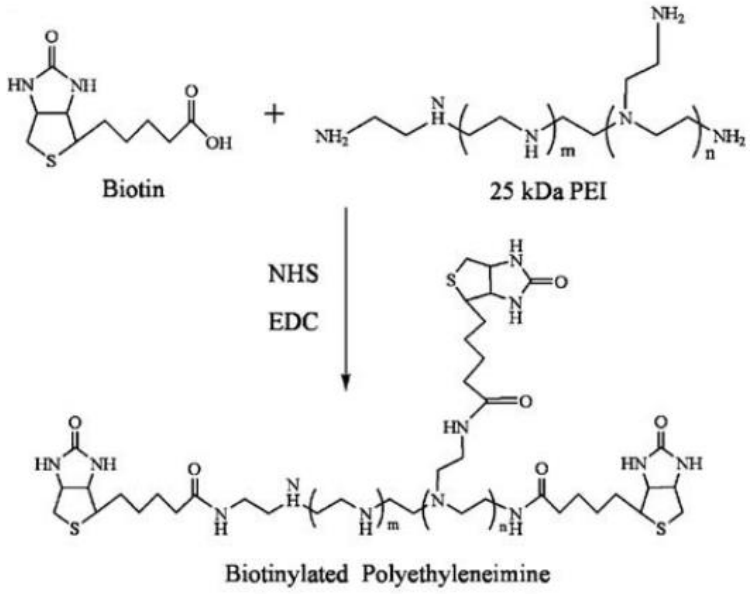

Figure A.2 – Synthesis of biotinylated polyethylenimine [A].

The commercial polyethylenimine usually has a branched structure and it is soluble in polar solvents such as water, ethanol, methanol and acetone and depending on the molecular weight, it is partially soluble in benzene and tetrahydrofuran [B]. The standard synthetic route to obtain b-PEI involves the electrophilic (or cationic) ring-opening polymerization of unsubstituted ethyleneimine with a protonic catalyst such

as Lewis acids and their salts, phenols or halogens, as shown in Figure A.3 [B]. This polymerization causes the formation of a secondary amino group in the polymer chain, which is more basic than the monomer. Therefore, chain transfer to the polymer takes place significantly and finally leads to branching.

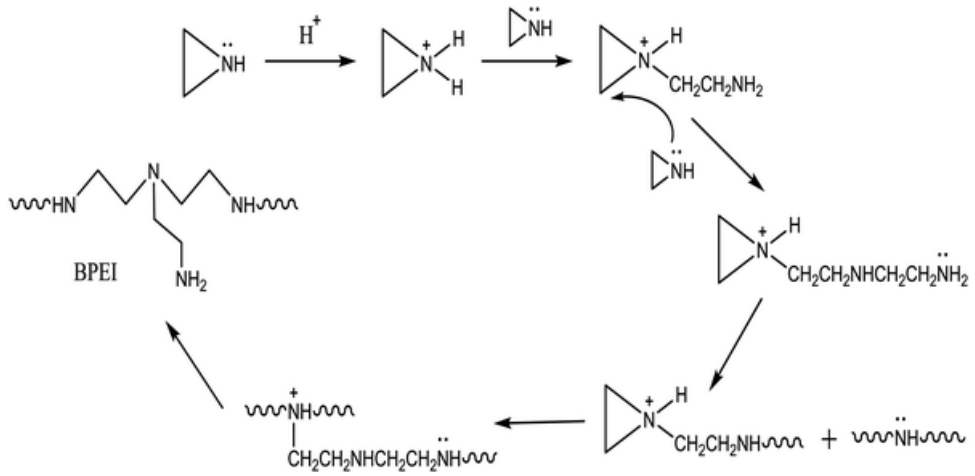

Figure A.3 – Standard synthetic way to produce branched-PEI via ring - opening polymerization of unsubstituted ethyleneimine [B].

In this work, specifically, two branched-polyethylenimine with different weight average molecular weights (i.e. Mw1 = 25'000 g/mol and Mw2 = 750'000 g/mol) were used to prepare the electrospinning feed solutions. First of all, different quantities of b-PEI with Mw = 25'000 g/mol were added to 0,5 mL of methanol at room temperature in order to check solubility at different concentrations and viscosity of solutions. Because of the good solubility of b-PEI in methanol, concentrations as high as 1'000 mg/mL (i.e. 500 mg of b-PEI in 0.5 mL of methanol) have been used.

The electrospinning solution was prepared by dissolving the weighted polymer powder in a set volume of methanol and letting it stirring for 4 h at room temperature. In this way, it was possible to produce clear solutions in a relatively short time.

The solutions of b-PEI are electrospun by using the same horizontal electrospinning setup that we employed for the electrospinning of PVA/BSA blends. Hence, electrospun fibers were collected on a microscope glass fixed to the metal collector through aluminum tape and analyzed using an optical microscope. The variation of experimental parameters such as concentration, viscosity of solution, applied voltage,

tip-to-collector distance and feed rate and their effects on the process efficiency have been extensively investigated. Results are reported in table A.1 and shown in Figure A.4.

Concentration (mg/mL)	Voltage (kV)	Feed Rate (ml/h)	Distance (cm)
200	13-16	0,01-0,5	13-18
400	11-17	0,01-0,7	13-18
600	14-18	0,3-0,7	13-22
800	16-22	0,2-0,7	13-15
1000	16-20	0,05-0,6	13-15

Table A.1 – Summary of the most striking parameters tested to electrospin solution of b-PEI and methanol.

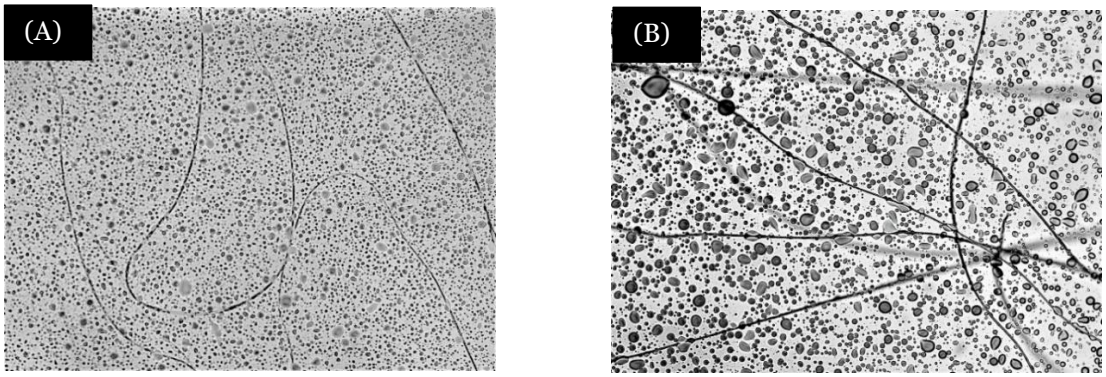

Figure A.4 – Optical microscope images of few electrospun b-PEI fibers obtained at (A) 400 mg/mL and (B) 600 mg/mL.

Looking at Figure A.4, it can be noticed that only few fibers result from the electrospinning, meaning that the yield of the process is almost zero. As stated in Chapter 1 there is an interplay among the variables of the electrospinning process; for instance, relatively high flow rates that result in ejection of droplets at the needle tip and occasionally in dripping at a given voltage, can be effective at higher voltages. Concerning the applied voltage, at values lower than 11 kV only droplets are visible at

optical microscope, whereas only few fibers are produced in the range of 14-17 kV. Around 18-22 kV continuous discharges from the syringe towards the diffusion pump are instead observed, hence no more increase of voltage has been tested.

Thus, in order to improve the efficiency of the process, different solutions have been tried:

(i) The use of other solvents such as water, ethanol, chloroform and tetrahydrofuran (THF);

(ii) The addition of salts to the feed solution (i.e. 1% of NaCl with respect to the weighted polymeric powder), which are used to vary the viscosity and the conductivity of solutions [C];

(iii) The addition of pyridine, which is commonly employed as an additive to improve the deposition of continuous fibers, increasing the conductivity of the feed solution. It is used in small amount (i.e. 50 and 100 ppm) as reported by *Lach et al.* [D].

(iv) The use of a b-PEI with higher molecular weight (Mw ~ 750'000 g/mol) [E].

However, none of the listed options led to an evident improvement. Hence, the idea of electrospinning pure b-PEI instead of PVA/BSA blends was put aside.

Appendix III

A.3.1 Materials

Poly(vinyl alcohol) 99+% hydrolyzed (Mw 89,000 – 98,000), poly(vinyl alcohol) 98-99% hydrolyzed (Mw 31,000 – 50,000), Bovine Serum Albumin – lyophilized powder ≥ 96%, Poly(ethyleneimine) solution 50 wt.% H_2O (Mw ~ 750,000), Atto 520 – Biotin, Glutaraldehyde aqueous solution 50%, hydrochloric acid min. 37%, acetone ≥ 99,5% and ammonium hydroxide solution (puriss. 30-33% NH_3 in H_2O) were purchased from Sigma Aldrich. The tryptophan employed in quenching test was purchased from TCI.

Thermo Scientific Pierce Coomassie Plus (Bradford) Protein Assay Kit was used during the Bradford protein assay.

A.3.2 Experimental Apparatus

- Electrospinning was performed by loading the feed solution in a 2,5 mL (or 5 mL) syringe with a 22 gauge needle (Hamilton Gastight model 1002 TLL), which was then placed on an infusion pump (KDS Scientific, model series 200). The electrospinning process was carried out using a horizontal setup. Voltage is applied to the needle by a High Voltage Power Supply (Spellman SL30P300).

- Optical images were taken with an Olympus microscope with the use of an INFINITY microscope camera.
- SEM images were taken at the Center for Nano Science and Technology (CNST) by means of a JEOL scanning electron microscope model JSM-6010LV, applying a potential of 3 to 5 kV. Diameter analysis was performed by taking 100 measurements with ImageJ software (Rasband, W.S., ImageJ, U. S. National Institutes of Health, Bethesda, Maryland, USA, http://imagej.nih.gov/ij/, 1997-2016).
- Bradford protein assays were performed at the Center for Nano Science and Technology (CNST), thanks to the assistance of Dr. Stefano Donini, using a Beckman Coulter DU730 Life Science UV-vis spectrophotometer, in semi-micro cuvettes in PMMA.
- Infrared spectra were recorded using a Nicolet 6700 FT-IR spectrometer. The resolution used is 4 cm^{-1} and 128 sample scans are acquired.
- PL and PLE spectra were collected at the National Research Council (laboratory of Dr. C. Botta (CNR), using a Fluorolog HORIBA spectrofluorometer.
- Measurements of fluorescence quantum yield (QY) have been done at the National Research Council (CNR), using an adapted Labsphere IS-060 (integrating sphere).
- UV-vis absorption spectra were recorded with a Varian Cary 5000 spectrophotometer with a scan rate of 150 nm/min, an average time of 0,4 s and a date interval of 1 nm.
- Spincoating was performed by use of a Laurell spincoater model ws-400B-6npp/lite.

Bibliography

[1] D. Natelson, "*Nanostructures and Nanotechnology*". Cambridge University Press, 2015.

[2] Kevin C. Honeychurch, "*Nanosensors for Chemical and Biological Applications*", Woodhead Publishing, 1st. Edition, 2014.

[3] Anthony P.F. Turner, *"Advancing in Biosensors: perspective in Biosensors",* Elsevier, vol.5, pp. 2-21, 2003.

[4] Powner E. and Yalcinkaya F., "*Intelligent sensors: structure and system*", Sensor Review, Vol. 15 No. 3, pp. 31-35, 1995.

[5] George S. Wilson and Michael A. Johnson, "*In-Vivo Electrochemistry: What can we learn about living Systems?*", Chem.Rev. , 108, 2462-2481, 2008.

[6] Reitzig M., Katzmann J., Schuster C., Härtling T., "Optical nanosensor technology – from basic research to industrial applications", Germany, 2015.

[7] Eggins B.R., "*Chemical Sensors and Biosensors*". John Wiley, Chichester, 2002.

[8] Hierold C., "*From micro - to nanosystems: mechanical sensors go Nano*", J. Micromech. Microengineering, 2004.

[9] Bellan LM, Wu D, Langer RS. "*Current trends in nanobiosensor technology*". Wiley Interdiscip. Rev. Nanomed. Nanobiotechnology; 3(3), pp. 229–246, 2011.

[10] Clark L.C., Lyons C., "*Electrode systems for continuous monitoring cardiovascular surgery*". Ann. N. Y. Acad. Sci., 102, pp. 29–45, 1962.

[11] Wilson J.S., "*Sensor Technology Handbook*". Elsevier, Amsterdam/Boston, 2005.

[12] P. T. Kissinger, "*Biosensors—a perspective*", Biosensors and Bioelectronics, vol. 20, no. 12, pp. 2512–2516, 2005.

[13] Grieshaber D., MacKenzie R., Janos V¨or¨os and Reimhult E., "*Electrochemical Biosensors – Sensor Principles and Architectures*", 2008.

[14] Bo T., Lihua C., Kehua X., Linhai Z., Jiechao G., Qingling L., "*A New Nanobiosensor for Glucose with High Sensitivity and Selectivity in Serum Based on Fluorescence Resonance Energy Transfer (FRET) between CdTe Quantum Dots and Au Nanoparticles*", Chem. Eur. J., 14, pp. 3637 – 3644, 2008.

[15] Weinberg R., "*The Biology of Cancer*". USA, Garland Science, 2013.

[16] Uludag Y., Tothill IE.,"*Cancer biomarker detection in serum samples using surface plasmon resonance and quartz crystal microbalance sensors with nanoparticle signal amplification*". Analytical Chem., UK, pp.5898–5904, 2012.

[17] Prime KL., Whitesides GM., "*Self-assembled organic monolayers: model systems for studying adsorption of proteins at surfaces*". J Am Chem. Soc., pp. 10714–10721, 1993.

[18] Ye Hu, H.Fine D., Tasciotti E., Ferrari M., "*Nanodevices in diagnostics*". Wiley Inter. Rev. Nanomed Nanobiotechnol., 2011.

[19] Shalini P., "*Nanobiosensors: the future for diagnosis of disease?*". USA, Nanobios. In disease diagnosis Journal, 2014.

[20] Campaña, A.L.; Florez, S.L.; Noguera, M.J.; Fuentes, O.P.; Ruiz Puentes, P.; Cruz, J.C.; Osma, J.F. "*Enzyme-Based Electrochemical Biosensors for Microfluidic Platforms to Detect Pharmaceutical Residues in Wastewater*". *Biosensors, 9*, 41, 2019.

[21] Maruvada P., Wang W., Wagner P. D., "*Biomarkers in molecular medicine: cancer detection and diagnosis*", USA, BioTechniques 38:S9-S15, 2005.

[22] James P. Chambers, Bernard P. Arulanandam, Leann L. Matta, Alex Weis, and James J. Valdes, "*Biosensor recognition elements*", Curr. Issues Mol. Biol., pp. 1–12, USA.

[23] Tothill IE., "*Biosensors for cancer markers diagnosis*". Semin. Cell Dev Biol., pp. 55–62, 2009.

[24] Koker T., Tang N., Tian C., Martel R., Pinaud F., "*Cellular imaging by targeted assembly of hot-spot SERS and photoacoustic nanoprobes using split-fluorescent protein scaffolds*", USA, 2018.

[25] May C. Morris, "*Progress in Molecular Biology and Translational science: Fluorescence – Based Biosensor*s", volume 113, 1st edition, Academic Press, 2013.

[26] May Morris, "*Fluorescent Biosensors for Cancer Cell imaging and Diagnostics*", Biosensors and Cancer, pp. 101-124, 2012.

[27] Wang H, Nakata E, Hamachi I., "*Recent progress in strategies for the creation of protein-based fluorescent biosensors*". Chem. BioChem., pp. 2560–2577, 10, 2009.

[28] Morris MC., "*Fluorescent biosensors of intracellular targets from genetically encoded reporters to modular polypeptide probes*". Cell Biochemical Biophysical, pp. 19–37, 56, 2010.

[29] Changqin D., Yang T., "*Gold nanocluster-based fluorescence biosensor for targeted imaging in cancer cells and ratiometric determination of intracellular PH*", Biosensors& bioelectronics, vol.65, pp. 183-190, 2015.

[30] "*The molecular Probes Handbook: A Guide to Fluorescence Probes and Labeling Technologies*", Eleventh Edition, Molecular Probes, Invitrogen, 2005.

[31] Kumar P., Kim K.-H., Bansal V., Lazarides T., Kumar N., "*Progress in the sensing techniques for heavy metal ions using nanomaterials*". J. Ind. Eng. Chem., vol. 54, pp. 30–43, 2017.

[32] Choi S.J., Persano L., Camposeo A., Jang J.S., Koo W.T., Kim S.J., Cho H.J., Kim I.D., Pisignano D., "*Electrospun Nanostructures for High Performance Chemiresistive and Optical Sensors*". Macromol. Mater. Eng., vol. 302, pp. 1–37, 2017.

[33] Terra I.A.A., Sanfelice R.C., Valente G.T., Correa D.S., "*Optical sensor based on fluorescent PMMA/PFO electrospun nanofibers for monitoring volatile organic compounds*". J. Appl. Polym. Sci., 2018.

[34] Anthony L. Andrady, "*Science and Technology of Polymer Nanofibers*". John Wiley & Sons, 2008.

[35] A. Greiner, Wendorff JH, "*Electrospinning: A Fascinating Method for the Preparation of Ultrathin Fibers*". Angewandte Chemie – Int. Ed., 2007.

[36] Jamil A. Matthews, David G. Simpson and Gary L. Bowlin, "*Electrospinning of Collagen Nanofibers*". Biomacromolecules, vol. 3, no. 2, pp. 232-238, 2002.

[37] A. Macagnano, E. Zampetti, and E. Kny, "*Electrospinning for High Performance Sensors"*. Cham: Springer International Publishing, 2015.

[38] C. Cleeton, A. Keirouz, N. Radacsi, "*Electrospun Nanofibers for Drug Delivery and Biosensing*", ACS Biomater. Sci. Eng., 5, pp. 4183–4205, 2019.

[39] A.L. Yarin, S. Koombhongse, D.H. Reneker, "*Taylor cone and jetting from liquid droplets in electrospinning of nanofibers*". J. Appl. Phys. 90, pp. 4836–4846, 2001.

[40] M. Yousefzadeh, "*Electrospun Nanofibers*", Woodhead Publishing S., pp. 277-301, 2017.

[41] A. Luzio, E. V. Canesi, C. Bertarelli, and M. Caironi, "*Electrospun polymer fibers for electronic applications*," Materials (Basel), vol. 7, no. 2, pp. 906–947, 2014.

[42] T.J. Sill, H.A. von Recum, "*Electrospinning: applications in drug delivery and tissue engineering*". Biomaterials 29(13), 2008.

[43] S. Agarwal, A. Greiner, Wendorff J.H., "*Functional materials by electrospinning of polymers*". Prog. Polym. Science, vol. 38, no.6, pp. 963–991, 2013.

[44] S. Ramakrishna, K. Fujihara, W.E. Teo, T.C. Lim and Z. Ma, "*Introduction to Electrospinning and Nanofibers*", World Scientific Publishing, 2005.

[45] S. R. Coles et al., "*A Design of Experiments (DoE) approach to material properties optimization of electrospun nanofibers*," J. Appl. Polym. Sci.,Vol. 117, no. 4, pp. 2251–2257, Aug. 2010.

[46] Z. Li and C. Wang, "*One-Dimensional nanostructures*". Berlin, Heidelberg: Springer Berlin Heidelberg, 2013.

[47] H. Belofsky, "*Plastics: Product Design and Process Engineering*". Hanser Publishers, 1995.

[48] G. R. Mitchell, "*Electrospinning*". Royal Society of Chemistry, 2015.

[49] L. Huang, NN. Bui, S.S. Manickam and J.R. McCutcheon, "*Controlling electrospun nanofiber morphology and mechanical properties using humidity*," J. Polym. Sci. Part B Polym. Phys., vol. 49, no. 24, pp. 1734–1744, Dec. 2011.

[50] Asmatulu R., Waseem S. Khan, "*Synthesis and Applications of Electrospun Nanofibers*", Chapter 9, Micro and Nano Tech., pp. 175-196, 2019.

[51] Idelma A.A. terra, Luiza A. Mercante, Rafaela S. Andre and Daniel S. Correa, "*Fluorescent and Colorimetric Electrospun Nanofibers for Heavy-Metal sensing*". 2017.

[52] Jose V., Marx S., Murata H., Koepsel R.R., Russell A.J., "*Direct electron transfer in a mediator-free glucose oxidase-based carbon nanotube-coated biosensor*". Vol. 50, pp. 4010–4020, 2012.

[53] Zhang N., Deng Y., Tai Q., Cheng B., Zhao L., Shen Q., He R., Hong L., Liu W., Guo S., et al. "*Electrospun TiO2 nanofiber-based cell capture assay for detecting circulating tumor cells from colorectal and gastric cancer patients*". Adv. Mater. Vol. 24, pp. 2756–2760, 2012.

[54] Jun J., Lee J.S., Shin D.H., Jang J., "*Aptamer-functionalized hybrid carbon nanofiber FET-type electrode for a highly sensitive and selective platelet-derived growth factor biosensor*". ACS Appl. Mater. Interfaces, vol. 6, pp. 3859–13865, 2014.

[55] E. González, L. M. Shepherd, L. Saunders, and M. W. Frey, "*Surface Functional Poly (lactic Acid) Electrospun Nanofibers for Biosensor Applications*," Materials (Basel)., vol. 9, no. 1, p. 47, Jan. 2016.

[56] A. Composeo, M. Moffa, L. Persano, "*Electrospun fluorescent nanofibers and their application in Optical Sensing*". In: Macagnano A., Zampetti E., Kny E., "*Electrospinning for high performance Sensors*", Nanosc. And Tech., Springer, 2015.

[57] D. Reneker H., A. Yarin L.,"*Electrospinning jets and polymer nanofibers*". Polymer 49, pp. 2387-2425, 2008.

[58] Dr. Shixuan C., Dr. Sunil K.B., Prof. Surinder K.B., "*Emerging Roles of electrospun Nanofibers in Cancer Research*", 2017.

[59] E. Petryayeva and W. R. Algar, "*Toward point-of-care diagnostics with consumer electronic devices: the expanding role of nanoparticles*," RSC Adv., vol. 5, no. 28, pp. 22256–22282, 2015.

[60] Luo C.J., Edirisinghe M., Nangrejo M., "*A novel method of selecting solvents for polymer electrospinning*", Polymer, UK, Vol. 51, 2010.

[61] Lehninger A.L., Nelson D.L. and Cox M.M., "*Principles of Biochemistry*". W. H. Freeman, Lehninger, 5th edition, 2000.

[62] H. Sang Y., T. Gyoung K., T. Gwan P., "*Surface-functionalized electrospun nanofibers for tissue engineering and drug delivery*", vol. 61, pp. 1033-1042, 2009.

[63] Weiser D., Németh C., Ender F., "*Electrospun Nanofibers for Entrapment of Biomolecules*", Ch. 8, 2018.

[64] Jiangbing X., You-Lo Hsieh, "*Ultra-high fibrous membranes from electrospinning of natural proteins: casein and lipase enzyme*", vol.38, pp. 2125-2133, 2003.

[65] Shahidul Md., Mohammad K., "*Fabrication and characterization of poly (vinylalchol)/alginate blend nanofibers by electrospinning method*". Colloids and Surfaces A: Physiochemical and Engineering Aspects, vol.366, 2010.

[66] Luu Y.K., K. Kim, B. S. Hsiao, B. Chu, and M. Hadjiargyrou, "*Development of a nanostructured DNA delivery scaffold via electrospinning of PLGA and PLA-PEG block copolymers*". J. Control. Release, vol. 89, no. 2, pp. 341–353, 2003.

[67] J. Hu, M. P. Prabhakaran, X. Ding, and S. Ramakrishna, "*Emulsion electrospinning of polycaprolactone: influence of surfactant type towards the scaffold properties*". J. Biomater. Sci. Polym. Ed., vol. 26, no. 1, pp. 57–75, 2015.

[68] Kwon I.K. and T. Matsuda, "*Co-Electrospun Nanofiber Fabrics of Poly (L -lactide-co- E -caprolactone) with Type I Collagen or Heparin*". Biomacromolecules, vol. 6, no. 4, pp. 2096–2105, 2005.

[69] Greiner A, Wendorff JH, Yarin AL, Zussman E., "*Biohybrid nanosystems with polymer nanofibers and nanotubes*". Applied Microbiology and Biotechnology, 2006.

[70] Walker HK., Hall WD., Hurst JW., "*Clinical Methods: the History, Physical, and Laboratory Examinations*". Chapter 101: "*Serum Albumin and Globulin*", third edition, 1990.

[71] Raoufinia R., Mota A., Keyhanvar N., Safari F., "*Overview of Albumin and its Purification Methods*". Vol. 6, pp. 495-507, 2016.

[72] Gelamo EL., Tabak M., "*Spectroscopic studies on the interaction of Bovine (BSA) and Human (HAS) serum albumins with ionic surfactants*". Vol. 11, pp. 2255-2271, 2000.

[73] Hsieh S.R., Reddy P.M., Chang C.J., Kumar A., "*Exploring the Behaviour of Bovine serum albumin in Response to Changes in the Chemical Composition of Responsive Polymers: Experimental and Simulation Studies*". Pp. 1-15, 2016.

[74] Xianyong Y., Ying Y., Shiyu L., Qing Y., "*The fluorescence spectroscopic study on the interaction between imidazo [2,1-b]thiazole analogues and bovine serum albumin*". Molecular and Biomol. Spectroscopy, Elsevier, 2011.

[75] Crouse H.F, Potoma J., F. Nejrabi, D. L. Snyder, B. S. Chohan, and S. Basu, "*Quenching of tryptophan fluorescence in various proteins by a series of small nickel complexes*," Dalt. Trans., vol. 41, p. 2720, 2012.

[76] Ni Y., Zhu R., Kokot S., "*Competitive binding of small molecules with biopolymers: a fluorescence spectroscopy and chemometrics study of the interaction of aspirin and ibuprofen with BSA*". Pp. 4794-4801, 2011.

[77] Dror Y., Makarov V., Wolf H., Admon A., Zussman E., "*Nanofibers Made of Globular Proteins*". Biomacromolecules, vol.9, pp. 2749-2754, 2008.

[78] Tang C., Ozcam AE., Stout B., "*Effect of PH on protein distribution in electrospun PVA/BSA composite nanofiber*s". Biomacromolecules, USA, pp. 1269-78, 2012.

[79] Wang C., Tong S.N., Tse Y.H., Wang M., "*Conventional Electrospinning vs. Emulsion Electrospinning: a Comparative study on the development of nanofibrous Drug/ Biomolecule delivery vehicles*". Adv. Mat. Research, Vol. 410, pp. 118-121, 2012.

[80] Kowalczyk T., Nowicka A., Elbaum D., "*Electrospinning of Bovine Serum Albumin. Optimization and the Use for production of Biosensors*". Biomacromolecules, pp. 2087-2090, 2008.

[81] Gaaz T.S., Sulong A.B., Akhtar M.N., Kadhum A.H., "*Properties and Applications of Polyvinyl Alcohol, Halloysite Nanotubes and their Nanocomposites*". Molecules, vol.20, pp. 22833-22847, 2015.

[82] Park J., Ito T., Kim K. *et al.,* "Electrospun poly (vinyl alcohol) nanofibers: effects of degree of hydrolysis and enhanced water stability". *Polym. J., vol.* 42, pp. 273–276, 2010.

[83] Gao Q., Takizawa J. and Kimura M., "Hydrophilic non-wovens made of cross-linked fully-hydrolyzed poly(vinyl alcohol) electrospun nanofibers". Polym., UK, vol. 54, no. 1, pp. 120–126, 2013.

[84] Fazel R., Torabi S.F., Ghasempour S., "*Electrospun poly (vinyl alcohol)/bovine serum albumin biocomposite membranes for HRP immobilization*". Enzyme and Microbial Tech., vol. 93-94, pp. 1-10, 2016.

[85] Moradzadegan A., Ranaei S.O., Ebrahim A., Jalili R., "*Immobilization of acetylcholinesterase in nanofibrous PVA/BSA membranes by electrospinning*". Eng.Life Sci., vol.10, pp. 57-64, 2010.

[86] Zeng J., A. Aigner, F. Czubayko, T. Kissel, J.H. Wendorff and A. Greiner, "*Poly (vinyl alcohol) nanofibers by electrospinning as a protein delivery system and the retardation of enzyme release by additional polymer coatings*". Biomacromolecules, vol. 6, no. 3, pp. 1484–1488, May 2005.

[87] Won J.J., R. Nirmala, R. Navamathavan, and H. Y. Kim, "*Electrospun core-shell nanofibers from homogeneous solution of poly (vinyl alcohol)/bovine serum albumin*". Int. J. Biol. Macromol., vol. 50, no. 5, pp. 1292–1298, 2012.

[88] "*Core-shell nanofibers as drug delivery systems*", Ata Pharm., vol.69, pp. 131-153, 2018.

[89] Aina A., Morris A., Gupta M., Sharma R., "*Dissolution behaviour of PVA in water and its effect on the physical morphologies of PLGA scaffolds*", UK J. of Pharm. And Bio., vol. 2, pp. 1-6, 2014.

[90] Nyflott A., Mericer C., Minelli M. et al., "*The influence of moisture content on the polymer structure of poly (vinyl alcohol) in dispersion barrier coatings and its effect on the mass transport of oxygen*". J. of Coatings Tech. and Research, vol. 14, pp. 1345-1355, 2017.

[91] Yao L., Haas T.W., A. Guiseppi-Elie, G. L. Bowlin, D. G. Simpson, and G. E. Wnek, "*Electrospinning and stabilization of fully hydrolyzed poly(vinyl alcohol) fibers*," Chem. Mater., vol. 15, no. 9, pp. 1860–1864, 2003.

[92] Van Stokkum IH., Linsdell H., Hadden JM., Haris PI., Chapman D., Bloemendal M., "*Temperature-induced changes in protein structures studied by Fourier transform infrared spectroscopy and global analysis*". Biochemistry, vol. 34, pp. 10508–10518, 1995.

[93] Rondeau P., Armenta S., Caillens H., Chesne S., Bourdon E., "*Assessment of temperature effects on beta-aggregation of native and glycated albumin by FTIR spectroscopy and PAGE: relations between structural changes and antioxidant properties".* Arch Biochem Biophys., vol.460, pp. 141–150, 2007.

[94] McKee M.G., Wilkes G.L., Colby R.H., Long T.E., "*Correlations of Solution Rheology with Electrospun Fiber Formation of Linear and Branched Polyesters*". Vol.37, pp. 1760-1767, 2004.

[95] Angammana C.J., Shesha H. J., "*Analysis of the Effects of Solution Conductivity on Electrospinning Process and Fiber Morphology*". Vol. 47, no.3, 2011.

[96] Risdian C., Nasir M., A. Rahma, and H. Rachmawati, "*The Influence of Formula and Process on Physical Properties and the Release Profile of PVA/BSA Nanofibers Formed by Electrospinning Technique*". J. Nano Res., vol. 31, pp. 103–116, 2015.

[97] Andrade G., E. Barbosa-Stancioli F., Piscitelli Mansur, W. L. Vasconcelos, and H. S. Mansur, "*Design of novel hybrid organic-inorganic nanostructured biomaterials for immunoassay applications*". Biomed. Mater., vol. 1, no. 4, pp. 221–234, 2006.

[98] Yurong L., Bolger B., Cahill P.A., McGuinness G.B., "*Water resistance photocrosslinked polyvinyl alcohol based fibers*". Material Let., 2008.

[99] Z. Tang et al., "*UV-cured poly(vinyl alcohol) ultrafiltration nanofibrous membrane based on electrospun nanofiber scaffolds*". J. Memb. Sci., vol. 328, no. 1–2, pp. 1–5, 2009.

[100] Zeytuncu B., M. H. Morcali, S. Akman, and O. Yucel, "*Influence of the amount of poly(vinyl alcohol) on the in situ production of photo-crosslinked thioamide functionalized nanofiber membranes*". J. Serbian Chem. Soc., vol. 80, no. 1, pp. 97–106, 2015.

[101] Ichimura K., S. Iwata, S. Mochizuki, M. Ohmi, D. Adachi, "*Revisit to the photocrosslinking behavior of PVA-SbQ as a water-soluble photopolymer with anomalously low contents of quaterized stilbazol side chains*". J. Polym. Sci. Part a Polym. Chem., vol. 50, no. 19, pp. 4094–4102, 2012.

[102] Miranda T.M.R., Gonçalves A.R., and Amorim M.T.P., "*Ultraviolet-induced crosslinking of poly(vinyl alcohol) evaluated by principal component analysis of FTIR spectra*". Polym. Int., vol. 50, no. 10, pp. 1068–1072, 2001.

[103] Tang C., C. D. Saquing, J. R. Harding, and S. A. Khan, "I*n situ cross-linking of electrospun poly(vinyl alcohol) nanofibers*". Macromolecules, vol. 43, no. 2, pp. 630–637, 2010.

[104] Nimni M.E., D. Cheung, B. Strates, M. Kodama, and K. Sheikh. "*Chemically modified collagen: a natural biomaterial for tissue replacement*". J. Biomed. Mater. Res. Vol. 21, pp. 741-771, 1987.

[105] Boyer R.F., "*Modern Experimental Biochemistry"*. Massachusetts: Addison-Wesley Publishing Co., 1986.

[106] Snyder J.C., Desborough S.L., "*Rapid estimation of potato tuber total protein content with Coomassie brilliant blue G-250*". Theor. Appl. Genet., vol. 52, pp.135-139, 1978.

[107] Berges J.A., Fisher A.E., Harrison P.J. "*A comparison of Lowry, Bradford and Smith protein assays using different protein standards and protein isolated from the marine diatom Thalassiosira pseudonana"*. Mar. Biol., vol. 115, pp. 187-193, 1993.

[108] Bradford M.M., "*A rapid and sensitive method for the quantitation of microgram quantities of protein utilizing the principle of protein-dye binding*". Anal. Biochem., vol. 72, no. 1–2, pp. 248–254, 1976.

[109] Guenzler H., Gremlich H.U., "*IR spectroscopy. An introduction*". Germany, Wiley-VCH, 2002.

[110] Georgiou C.D., K. Grintzalis, G. Zervoudakis and I. Papapostolou, "*Mechanism of Coomassie brilliant blue G-250 binding to proteins: A hydrophobic assay for 97 nanogram quantities of proteins*". Anal. Bioan. Chem., vol. 391, no. 1, pp. 391–403, 2008.

[111] M. Bonde, H. Pontoppidan, and D. S. Pepper, "*Direct dye binding-A quantitative assay for solid-phase immobilized protein*". Anal. Biochem., vol. 200, no. 1, pp. 195–198, Jan. 1992.

[112] X. Shan, Liu C., F. Li, C. Ouyang, Q. Gao and K. Zheng, "*Nanoparticles vs. nanofibers: a comparison of two drug delivery systems on assessing drug release performance in vitro*". Des. Monomers Polym., vol. 18, no. 7, pp. 678–689, 2015.

[113] A. Barth, "*Infrared spectroscopy of proteins*". Biochim. Biophys. Acta - Bioenerg., vol. 1767, no. 9, pp. 1073–1101, Sep. 2007.

[114] Militello V., Casarino M., A. Emanuele, A. Giostra, F. Pullara and M. Leone, "*Aggregation kinetics of bovine serum albumin studied by FTIR spectroscopy and light scattering*". Biophys. Chem., vol. 107, no. 2, pp. 175–187, 2004.

[115] Tian J., Liu J., X. Tian, Z. Hu and X. Chen, "*Study of the interaction of kaempferol with bovine serum albumin*". J. Mol. Struct., vol. 691, no. 1–3, pp. 197–202, 2004.

[116] Jia Y.T., J. Gong, X. H. Gu, H. Y. Kim, J. Dong, and X. Y. Shen, "*Fabrication and characterization of poly (vinyl alcohol)/chitosan blend nanofibers produced by electrospinning method*". Carbohydr. Polym., vol. 67, no. 3, pp. 403–409, 2007.

[117] Mansur H.S., C. M. Sadahira, A. N. Souza and A. A. P. Mansur, "*FTIR spectroscopy characterization of poly (vinyl alcohol) hydrogel with different hydrolysis degree and chemically crosslinked with glutaraldehyde*". Mater. Sci. Eng. C, vol. 28, no. 4, pp. 539–548, 2008.

[118] Castagna R., Colnago P., Donini S., Serafini A., Parisini E., Bertarelli C., "*Biohybrid Electrospun Membrane for the Filtration of Ketoprofen Drug from Water*". ACS Omega, vol. 4, 2019.

[119] Wang D., Liang N., Kawashima Y., Yan F., Sun S., "*Biotin-modified bovine serum albumin nanoparticles as a potential drug delivery system for paclitaxel*". J. Mat. Scien., vol. 54, pp. 8613-8626, 2019.

[120] Anandakumar S., V. S. Rani, S. Oh, B. L. Sinha, M. Takahashi and C. Kim, "*Translocation of bio-functionalized magnetic beads using smart magnetophoresis*". Biosens. Bioelectron., vol. 26, no. 4, pp. 1755–1758, 2010.

[121] Ghisaidoobe A.B.T., S. J. Chung, "*Intrinsic tryptophan fluorescence in the detection and analysis of proteins: A focus on Forster resonance energy transfer techniques*". Int. J. Mol. Sci., vol. 15, no. 12, pp. 22518–22538, 2014.

[122] Banerjee s., Both A., Sarkar M., "*Probing the Aggregation and Signaling Behavior of Some twisted 9,9'-Bianthryl Derivatives: Observation of Aggregation-Induced Blue-Shifted Emission*". ACS Publ., 2018.

[123] Ju E.; Yang, X.; Lin, Y.; Pu, F.; Ren, J.; Qu, X., "*Exonucleaseaided amplification for label-free and fluorescence turn-on DNA detection based on aggregation-induced quenching*". Chem. Commun., vol. 48, pp. 11662–11664, 2012.

[124] Buschmann V., Weston K.D., Sauer M., “Spectroscopic Study and evaluation of Red-absorbing Fluorescent dyes”. 2003.

[125] Marmè N., Knemeyer J., Sauer M., Wolfrum J., “*Inter- and Intramolecular Fluorescence Quenching of organic Dyes by Tryptophan*”. 2003.

[126] Marmè N., Knemeyer J., “*Sensitive bioanalysis-combining single-molecule spectroscopy with monolabeled self-quenching probes*”. Anal. And Bioanal. Chem., 2007.

[127] Nueweiler H., Schulz A., Variana A.C., Smith C., Wolfrum J., Sauer M., “*Detection of Individual p53-Autoantibodies by using quenched peptide-Based molecular probes*”. Angew. Chem. Int. Ed., n.24, vol.41, 2002.

[A] Zeng X., Sun Y.X., Zhang X.Z., Cheng S.X., “*A potential Targeting Gene vector based on Biotinylated Polyethyleneimine/Avidin Bioconjugates*”. Pharm. Research., vol.26, n.8, 2009.

[B] Virgen-Ortiz J., Berenguer A., Santos J., Barbosa O., “*Polyethylenimine: A very useful ionic polymer in the design of immobilized enzyme biocatalysts*”. J. of Mat. Chem., vol.5, 2016.

[C] Mazari A., Jirsak O., “*Effect of sodium chloride on electrospinning of poly (ethylene oxide) fibers*”. Vol 19, 2001.

[D] Lach A., Morris H., Martins J., Carr A., “*Pyridine as an additive to improve the deposition of continuous electrospun filaments*”. 2019.

[E] Eminoglu E., Beypinar F., Kahraman M., Durmus A., “*Fabrication of photo-crosslinked polyethylenimine-based barriers for CO2 capture*”. Polym. Adv. Technol., vol.26, pp. 1053-1058, 2015.